

DIODE-PUMPED TWO MICRON SOLID-STATE LASERS

by

Ian F. Elder

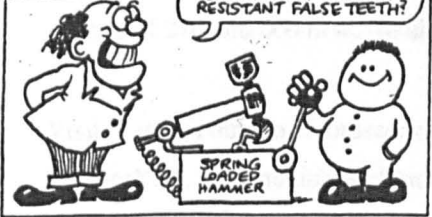
**Department of Physics and Applied Physics,
University of Strathclyde**

A thesis submitted in fulfilment of the requirements for the degree of Ph.D

January 1997

The copyright of this thesis belongs to the author under the terms of the United Kingdom Copyrights Act as qualified by University of Strathclyde Regulation 3.49. Due acknowledgement must always be made of the use of any material contained in, or derived from, this thesis.

professor
Piehead



Viz, no. 57, 32 (1992)

Abstract

This thesis presents an investigation of diode-pumped two micron solid-state lasers, concentrating on a comparison of the cw room temperature operation of Tm:YAP, Tm,Ho:YAP and Tm,Ho:YLF. Dopant concentrations in YAP were 4.2% thulium and 0.28% holmium; in YLF they were 6% thulium and 0.4% holmium.

Thermal modelling was carried out in order to provide an insight into the thermal lensing and population distributions in these materials.

Laser operation was achieved utilising an end-pumping geometry with a simple two mirror standing wave resonator. The pump source for these experiments was a 3 W laser diode. Maximum output power was achieved with Tm:YAP, generating 730 mW of laser output, representing 42% conversion efficiency in terms of absorbed pump power. Upper bounds on the conversion efficiency of Tm,Ho:YAP and Tm,Ho:YLF laser crystal of 14% and 30% were obtained, with corresponding output powers of 270 and 660 mW. In all three cases, the output beam was TEM₀₀ in nature.

Visible upconversion fluorescence bands in the green and red were identified in Tm,Ho:YAP and Tm,Ho:YLF, with additional blue emission from the latter, all assigned to transitions on holmium. The principal upconversion mechanisms in these materials all involved the holmium first excited state. Upconversion in Tm:YAP was negligible.

The spectral output of Tm:YAP consisted of a comb of lines in the range 1.965 to 2.020 μm . For both the double-doped crystals, the laser output was multilongitudinal mode on a single transition, wavelength 2.120 μm in YAP, 2.065 μm in YLF.

In the time domain the output of Tm:YAP was dominated by large amplitude spiking, unlike both of the double-doped laser crystals. The long lifetime of the thulium upper laser level (4.4 ms) provided very weak damping of the spiking. Excitation sharing between thulium and holmium, with a measured characteristic lifetime in YAP of 11.9 μs and YLF of 14.8 μs , provided strong damping of any spiking behaviour.

Acknowledgements

First and foremost, I would like to thank my supervisor at DRA Malvern Dr. John Payne for initiating this project, and providing continued encouragement throughout combined with a high degree of technical expertise. I am also indebted to him for providing an environment conducive to good research for me to work in, despite the mountain of bureaucracy burdening the organisation. Thanks also to Professor Allister Ferguson, my supervisor at Strathclyde University, for his continual support and advice during the extended duration of this project.

Throughout the course of this project it was a great pleasure to work with fellow members of the section - the self-styled Solid-State Hard Men JK, Henry, Jonny, Phil and Kenny. Their sharing of expertise and apparatus played a significant part in the completion of this thesis.

Many thanks also to Phil Harding and his workshop boys, especially Jerry, Dave and Ian, for managing to decipher my back-of-the-fag-packet scrawls to manufacture the excellent mechanical components which formed the basis of all the experiments. The laser crystals used in this work were grown by Brian Cockayne, Mick Crosbie and Leslie Taylor; cutting and polishing of the samples was performed by Roy Vivien and Steve Aldridge - many thanks to all for their expertise on this front.

I would like to thank the members of The Groin Strains five-a-side team, and also the Mountainbiking Madskulls, for providing essential, if only temporary, relief from the madhouse in the form of lunchtime sporting pursuits.

Thanks to my fellow Catbells flatmates for ensuring the phone and gas were never disconnected, and also to the assorted members of the Malvern/Worcester posse, too numerous to mention by name, for providing a wide range of entertainment of an evening (most of it legal).

Finally, a big thank you to my parents for emphasising the importance of a good education, and providing the necessary support to encourage me down this path.

Contents

Chapter 1 : Introduction

1.1	Introduction	1
1.2	Thesis outline	1
1.3	Historical review	3
1.4	References	6

Chapter 2 : Diode-pumping of two micron solid-state lasers

2.1	Introduction	9
2.2	Advantages of diode-pumped solid-state lasers	9
2.3	Spectroscopy of two micron solid-state laser materials	12
2.4	Conclusions	24
2.5	References	25

Chapter 3 : Thermal modelling

3.1	Introduction	27
3.2	Thermal effects in solid-state lasers	28
3.3	Temperature distributions	32
3.4	Thermal lensing	42
3.5	Thermal fracture limit	48
3.6	Population distributions	51
3.7	Excitation sharing	56
3.8	Conclusions	60
3.9	References	62

Chapter 4 : Laser performance

4.1	Introduction	63
4.2	Optical pumping scheme	64
4.3	Laser experiments	72
4.4	Conclusions	90
4.5	References	93

Chapter 5 : Pump absorption effects

5.1	Introduction	94
5.2	Investigation of pump absorption effects	96
5.3	Rate equation analysis of pump beam transmission	110
5.4	Conclusions	117
5.5	References	119

Chapter 6 : Upconversion processes

6.1	Introduction	120
6.2	Visible emission spectra of thulium and holmium	122
6.3	Measurement of visible upconversion spectra	130
6.4	Determination of visible upconversion excitation mechanisms	135
6.5	Near infrared upconversion processes	140
6.6	Conclusions	145
6.7	References	148

Chapter 7 : Relaxation oscillations

7.1	Introduction	151
7.2	Laser temporal behaviour	153
7.3	Relaxation oscillation analysis	157
7.4	Conclusions	164
7.5	References	165

Chapter 8 : Conclusions

8.1	Summary of the achievements of this work	166
8.2	Prospects for future work	170

Appendix A : Thulium and holmium energy levels	173
-------------------------------------------------------	------------

Introduction

1.1 Introduction

To date neodymium (Nd^{3+}) has been the most commonly used dopant ion in laser diode-pumped solid-state lasers, the favoured host lattice being yttrium aluminium garnet (YAG). The success of diode-pumping Nd^{3+} :YAG can be attributed to its spectroscopic properties which include a large stimulated emission cross-section, and a relatively simple pumping scheme. The 1.064 μm laser transition operates as a four-level laser, with the laser diode effectively pumping the upper laser level directly.

Solid-state lasers operating around two microns are the subject of much interest, as this is an eye-safe waveband which offers the possibility of atmospheric propagation for applications such as rangefinding, coherent laser radar and atmospheric sensing. There are also medical applications because liquid water has strong absorption bands in this wavelength region. Two micron lasers are also required as pump sources for optical parametric oscillators generating three to five micron mid infrared (MIR) radiation. The principal ions of interest are the rare earths thulium (Tm^{3+}) and holmium (Ho^{3+}) in glass or crystalline hosts.

The widespread availability since the early 1980s of reliable high power semiconductor laser diodes as pump sources for all-solid-state lasers has led to a revolution in solid-state laser technology. This new class of diode-pumped solid-state laser now allows miniaturisation of efficient laser sources. The ever increasing wavelength range covered by laser diodes means that more and more solid-state gain media are becoming amenable to diode-pumping^{1,2}.

1.2 Thesis outline

The work described in this thesis details development in the field of diode-pumped two micron solid-state lasers, concentrating on cw room temperature operation of the three

laser crystals Tm:YAP, Tm,Ho:YAP and Tm,Ho:YLF. Investigation of their laser performance has revealed several general characteristics common to this class of laser.

The remainder of this chapter outlines the format of this thesis and sets out a historical background to this work with a brief review of the history of diode-pumped two micron solid-state lasers. Chapter 2 provides an introductory overview of the rapidly expanding field of diode-pumped solid-state lasers, describing the physical process of diode-pumping and the important advantages offered by this approach. Basic spectroscopic properties of rare earth doped crystalline hosts are introduced, concentrating on the properties most relevant to lasing in thulium and holmium.

An understanding of thermal effects in the gain medium is essential in order to fully characterise the operation of a solid-state laser, particularly in the case of thulium and holmium lasers. In Chapter 3, thermal modelling of this class of laser is investigated. The absorption of pump light in a solid-state laser medium leads to heat deposition setting up temperature gradients in the gain medium. The first sections of this chapter deal with calculation of the steady state temperature distributions, followed by an analysis of the accompanying thermal lensing along with consideration of the thermal fracture limit of gain media of interest. In addition to these thermal issues, the effects of temperature on the terminal laser level population, hence laser threshold, of thulium and holmium, as well as the excitation sharing between thulium and holmium, need to be considered. The final sections of Chapter 3 cover these topics.

Chapter 4 contains the bulk of the experimental work, which centred around the comparison of the laser performance of Tm:YAP, Tm,Ho:YAP and Tm,Ho:YLF under identical experimental conditions. Characterisation of the laser diode pump source and optics is followed by comparison of the output power performance of the three laser crystals, their temperature sensitivity of operation, and finally their longitudinal and transverse mode behaviour.

Chapters 5 to 7 examine in more detail three aspects of laser behaviour forthcoming from the work of Chapter 4. Chapter 5 investigates pump beam absorption effects in both the single-doped thulium and double-doped thulium and holmium laser crystals. A simple computer program was written to model the effects of pump saturation in single-doped Tm:YAP. Reasonable agreement between theory, based on rate equation analysis, and experiment was obtained. In Chapter 6, the spectral content of the visible upconversion produced by both Tm,Ho:YAP and Tm,Ho:YLF is examined in detail. A

mechanism producing this fluorescence is proposed from the experiments performed. Upconversion processes are a potentially major loss mechanism for the two micron holmium laser transition(s), particularly in YAP. Chapter 7 investigates the markedly different temporal behaviour of Tm:YAP and Tm,Ho:YAP. Using a modified version of the standard rate equation analysis for relaxation oscillations, an explanation for the far superior temporal stability of the double-doped laser crystal is proposed in terms of the excitation sharing between thulium and holmium.

Finally Chapter 8 summarises the main achievements of this work and outlines some potential future developments in the area of diode-pumped two micron solid-state lasers.

1.3 Historical review

Several excellent review articles³⁻⁶ have been written detailing developments in diode-pumping from the first reported use of semiconductor sources by Newman⁷ in 1963, who used GaAs LEDs to pump Nd:CaWO₄, to the present day, principally concerning themselves with neodymium lasers. In this section the history of two micron solid-state lasers is briefly reviewed.

Holmium lasers have been reported as early as 1962 by Johnson *et al.*⁸, the host lattice here being liquid nitrogen cooled CaWO₄. Cooling was required because of the temperature dependent nature of the laser transition (as detailed in the following chapter). Within the next ten years work was carried out on a range of multi-doped laser hosts, either pulsed (flashlamp-pumped)⁹ or cw (arclamp-pumped)¹⁰.

The first report of a diode-pumped two micron laser was by Allen *et al.*¹¹ using multi-doped holmium in YAG, closely followed by Hemmati's¹² demonstration of lasing of holmium in YLF. Both these lasers operated at 77 K, but with the advent of more powerful pump sources room temperature operation was soon possible^{13,14}. In subsequent years there has been considerable effort in the field of diode-pumped two micron lasers.

Kintz *et al.*¹⁵ reported 2.02 μm emission with a 56% slope efficiency at room temperature from a diode-pumped Tm:YAG laser. High power cw operation of Tm:YAG has also been demonstrated¹⁶, 2.3 W being generated using 10 W of pump power. The long fluorescence lifetimes of thulium and holmium offer the prospect of

efficient Q-switched lasers. Suni and Gates¹⁷ reported 15% optical-to-optical conversion in Tm:YAG using a single 3 W laser diode, generating 2.5 mJ pulses at 50 Hz when the rod was held at -40°C. Pulse energies fell to 1 mJ when operated at room temperature. Q-switching in Tm,Ho:YLF has also been investigated; Budni *et al.*¹⁸ used 6 W of pump power to produce 1.75 mJ, 10 ns pulses at 1 kHz, representing a conversion efficiency of 29% (laser rod cooled to 77 K), whilst room temperature operation has reported¹⁹ using more modest pump powers of 500 mW. In this case optical-to-optical conversion was 5.5%, with 22 ns pulses of energy 220 μ J. Kubo and Kane²⁰ presented results comparing cw and Q-switched operation of Tm:YAG and Tm,Ho:YAG. They concluded that for the laser configuration under investigation the single-doped thulium gave the greatest output in both modes of operation, and the output was less temperature sensitive; best results 19.5% optical-to-optical conversion cw with 1.18 W output, 3.9% conversion Q-switched with 1.5 mJ pulses (in both cases the rod temperature was -38°C).

The results quoted above have been for lasers utilising the laser diodes in an end or longitudinal pumping geometry. Power scaling can be achieved in a side or transverse pumping geometry using centimetre bar diode arrays. Bowman *et al.*²¹ used 126 centimetre bars, each of 60 W peak power, to pump a water-cooled Cr,Tm,Ho:YAG laser. Multiple Q-switch pulses were obtained, a burst of sixteen 24 mJ pulses for each pump pulse, representing a 5% optical-to-optical conversion efficiency. 30 mJ Q-switched pulses at 10 Hz have been demonstrated with a side-pumped Tm,Ho:YLF laser operating at room temperature²². Power scaling in the longitudinal pumping geometry can be achieved by using a lens duct to deliver the output of a stack of centimetre bar arrays onto the end of a laser rod. Utilising such a technique, 51 W of cw output power have been generated in Tm:YAG with a 24% slope efficiency²³.

The standard laser diodes used for pumping two micron solid-state lasers are GaAlAs devices. Recently, the use of GaInAsSb laser diodes emitting at 1.9 μ m to pump single-doped Ho:YAG has been reported²⁴. A diode pump power of 4 W produced 0.7 W of laser output at 2.1 μ m. YAG and YLF are the two most common crystalline hosts for doping with thulium and/or holmium. Comparison of diode-pumping of Tm:YAG with Tm:LYAG and Tm:LAG (where L represents lutetium) has been reported²⁵, all showing similar optical conversion efficiencies, but with substitution of lutetium for yttrium shifting the laser wavelength and greatly improving its atmospheric transmission. Diode-pumping of Tm,Ho:LAG has also been reported, with 35.6% conversion efficiency, when the laser rod was cooled to 77 K²⁶.

Single frequency lasers operating at eye-safe wavelengths are a topic of interest, in particular for laser radar applications. Reports of such devices in the literature, for the case of diode-pumped two micron lasers, include 58 mW from a Tm,Ho:YAG laser containing intracavity etalons to ensure single frequency operation²⁷, 27 mW from a Tm:YAG monolithic non-planar ring oscillator (NPRO)²⁰, and 6 mW from a monolithic Tm,Ho:YLF laser²⁸. To date, the highest power reported from a single frequency diode-pumped two micron laser is 2.5 W, using Tm,Ho:YLF cooled to -35°C in a ring resonator geometry, pumping with 14 W from a fibre-coupled centimetre bar array²⁹.

Waveguide structures allow confinement of the pump and generated optical beams, offering the prospect of lower thresholds and higher gains than in bulk crystals. Laser diode-pumped optical fibre lasers have been investigated. Operation both at 2.3 μm , with a threshold at 4 mW of launched pump power³⁰, and at 1.97 μm ³¹, has been reported in thulium-doped fluorozirconate fibres, as well as the demonstration of a double-doped thulium,holmium silica fibre laser³². Efficient lasing in a liquid phase epitaxy grown Tm:YAG planar waveguides generated 102 mW at 2.012 μm with a pump power of 360 mW³³.

To date, there has been only one report in the open literature of diode-pumped mode-locked two micron lasers (unlike the case with neodymium lasers), where a thulium fibre laser generated 190 fs pulses with 1 mW mean power³⁴. Mode-locking of bulk lasers has been restricted to Ti:sapphire pumping of Tm:YAG, which produced 35 ps pulses with a mean power of 70 mW (11.5% optical-to-optical conversion)³⁵, while use of a krypton ion pump source laser produced 45 ps pulses from Cr,Tm:YAG and 800 ps pulses from Cr,Tm,Ho:YAG³⁶.

1.4 References

- [1] C. A. Wang & S. H. Groves, 'New materials for diode laser pumping of solid-state lasers', IEEE J. Quantum Electron., vol. 28, no. 4, 942 (1992)
- [2] J. G. Endriz *et al.*, 'High power laser diode arrays', IEEE J. Quantum Electron., vol. 28, no. 4, 952 (1992)
- [3] R. L. Byer, 'Diode laser-pumped solid-state lasers', Science, vol. 239, 742 (1988)
- [4] T. Y. Fan & R. L. Byer, 'Diode laser-pumped solid-state lasers', IEEE J. Quantum Electron., vol. 24, no. 6, 895 (1988)
- [5] G. P. A. Malcolm & A. I. Ferguson, 'Diode-pumped solid-state lasers', Contemporary Physics, vol. 32, no. 5, 305 (1991)
- [6] D.W. Hughes & J. R. M. Barr, 'Laser diode pumped solid state lasers', J. Phys. D: Appl. Phys., vol. 25, 563 (1992)
- [7] R. Newman, 'Excitation of the Nd^{3+} fluorescence in $CaWO_4$ by recombination radiation in $GaAs$ ', J. Appl. Phys., vol. 34, 437 (1963)
- [8] L. F. Johnson, J. E. Geusic & K. Nassau, 'Optical maser characteristics of Ho^{3+} in $CaWO_4$ ', Proc. IRE, vol. 50, 87 (1962)
- [9] R. L. Remski, L. T. James, K. H. Goen, B. Di Bartolo & A. Linz, 'Pulsed laser action in $LiYF_4:Er^{3+}, Ho^{3+}$ at 77K', IEEE J. Quantum Electron., vol. 5, 214 (1969)
- [10] E. P. Chicklis, C. S. Naiman, R. C. Folweiler, D. R. Gabbe, H. P. Jenssen & A. Linz, 'High efficiency room temperature 2.06 μm laser using sensitised $Ho^{3+}:YLF$ ', Appl. Phys. Lett., vol. 19, no. 4, 119 (1971)
- [11] R. Allen, L. Esterowitz, L. Goldberg, J. Weller & M. Storm, 'Diode-pumped 2 μm holmium laser', Electron. Lett., vol. 22, no. 18, 947 (1986)
- [12] H. Hemmati, 'Efficient holmium:yttrium lithium fluoride laser longitudinally pumped by a semiconductor laser array', Appl. Phys. Lett., vol. 55, 564 (1987)
- [13] G. Kintz, L. Esterowitz & R. Allen, 'CW diode pumped $Tm^{3+}, Ho^{3+}:YAG$ 2.1 μm room temperature laser', Electron. Lett., vol. 23, no. 12, 616 (1987)
- [14] H. Hemmati, '2.07 μm cw diode-laser-pumped $Tm, Ho:YLiF_4$ room temperature laser', Opt. Lett., vol. 14, no. 9, 435 (1989)
- [15] G. J. Kintz, R. Allen & L. Esterowitz, 'Continuous wave laser emission at 2.02 μm from diode-pumped $Tm^{3+}:YAG$ at room temperature', in *Digest of Conference on Lasers & Electro-Optics*, (OSA, Washington, DC), paper FB2 (1988)
- [16] G. J. Kintz, T. Baer, P. Gooding, M. Kierstead, D. Head & J. Cole, 'High power cw 2 μm laser', in *Digest of Conference on Advanced Solid-State Lasers*, (OSA, Washington, DC), paper WA1 (1992)

- [17] P. J. M. Suni & G. H. Gates, 'Damage free operation of a 2.5 mJ Tm:YAG laser pumped by a 3 W room-temperature diode laser', in *Digest of Conference on Lasers & Electro-Optics*, (OSA, Washington, DC), paper CPDP12 (1991)
- [18] P. A. Budni, M. G. Knights, E. P. Chicklis & H. P. Jenssen, 'Performance of a diode-pumped high PRF Tm, Ho:YLF laser', *IEEE J. Quantum Electron.*, vol. 28, no. 4, 1029 (1992)
- [19] B. T. McGuckin, R. T. Menzies & H. Hemmati, 'Efficient energy extraction from a diode-pumped Q-switched Tm, Ho:YLiF₄ laser', *Appl. Phys. Lett.*, vol. 59, no. 23, 2926 (1991)
- [20] T. S. Kubo & T. J. Kane, 'Diode-pumped lasers at five eye-safe wavelengths', *IEEE J. Quant. Electron.*, vol. 28, no. 4, 1033 (1992)
- [21] S. R. Bowman *et al.*, 'High average power operation of a Q-switched diode-pumped holmium laser', *Opt. Lett.*, vol. 18, no. 20, 1724 (1993)
- [22] M. G. Jani, N. P. Barnes, K. E. Murray & G. E. Lockard, 'Diode-pumped, long pulse length Tm, Ho:YLiF₄ laser at 10 Hz', in *OSA Proceedings on Advanced Solid-State Lasers*, (OSA, Washington, DC), vol. 24, 362 (1995)
- [23] R. J. Beach, S. B. Sutton, E. C. Honea, J. A. Skidmore & M. A. Emanuel, 'High power 2 μm diode-pumped Tm:YAG laser', *SPIE*, vol. 2698, 168 (1996)
- [24] C. D. Nabors, J. Ochoa, T. Y. Fan, A. Sanchez, H. Choi & G. Turner, 'Ho:YAG laser pumped by 1.9 μm diode lasers', *IEEE J. Quantum Electron.*, vol. 31, no. 9, 1603 (1995)
- [25] J. D. Kmetec, T. S. Kubo, T. J. Kane & C. J. Grund, 'Laser performance of diode-pumped thulium-doped Y₃Al₅O₁₂, (Y,Lu)₃Al₅O₁₂, and Lu₃Al₅O₁₂ crystals', *Opt. Lett.*, vol. 19, no. 3, 186 (1994)
- [26] V. Kushawaha, Y. Chen, Y. Yan & L. Major, 'High-efficiency continuous-wave diode-pumped Tm, Ho:LuAG laser at 2.1 μm', *Appl. Phys. B*, vol. 62, 109 (1996)
- [27] S. W. Henderson & C. P. Hale, 'Tunable single-longitudinal-mode diode laser pumped Tm:Ho:YAG laser', *Appl. Opt.*, vol. 29, no. 12, 1716 (1990)
- [28] G. J. Koch, J. P. Deyst & M. E. Storm, 'Single-frequency lasing of monolithic Ho, Tm:YLF', *Opt. Lett.*, vol. 18, no. 15, 1235 (1993)
- [29] A. Finch, J. H. Flint & D. M. Rines, '2.5 Watts single-frequency cw Tm, Ho:YLF ring laser', in *OSA Trends in Optics & Photonics, "Advanced Solid-State Lasers"*, vol. 1, 312 (1996)
- [30] R. Allen & L. Esterowitz, 'CW diode-pumped 2.3 μm fibre laser', *Appl. Phys. Lett.*, vol. 55, 721 (1989)
- [31] J. N. Carter, R. G. Smart, D. C. Hanna & A. C. Tropper, 'CW diode-pumped operation of 1.97 μm thulium doped fluorozirconate fibre laser', *Electron. Lett.*, vol. 26, 599 (1990)
- [32] C. Ghisler, W. Lüthy, H. P. Weber, J. Morel, A. Woodtli, R. Dändliker, V. Nueman, H. Berthou & G. Kotrotsios, 'A Tm³⁺ sensitised Ho³⁺ silica fibre laser at 2.04 μm pumped at 809 nm', *Opt. Comm.*, vol. 109, 279 (1994)

- [33] C. Borel, A. Rameix, P. Thony, B. Ferrand, D. P. Shepherd, A. C. Large, T. J. Warburton, A. C. Tropper, D. C. Hanna, S. Guy, M. F. Joubert & B. Jacquier, '*Growth by liquid phase epitaxy and laser performance at 2.012 μm of a Tm:YAG planar waveguide*', in *OSA Proceedings on Advanced Solid-State Lasers*, (OSA, Washington, DC), vol. 24, 37 (1995)
- [34] R. C. Sharp, D. E. Spock, N. Pan & J. Elliot, '*190-fs passively mode-locked thulium fibre laser with a low threshold*', *Opt. Lett.*, vol. 21, no. 12, 881 (1996)
- [35] J. F. Pinto, L. Esterowitz & G. H. Rosenblatt, '*Continuous-wave mode-locked 2 μm Tm:YAG laser*', *Opt. Lett.*, vol. 17, no. 10, 731 (1992)
- [36] F. H. Heine, E. Heumann, G. Huber & K. L. Schepler, '*Mode locking of room-temperature cw thulium and holmium lasers*', *Appl. Phys. Lett.*, vol. 60, no. 10, 1161 (1992)

Diode-pumping of two micron solid-state lasers

2.1 Introduction

This chapter provides a background to the field of diode-pumped two micron solid-state lasers, highlighting the basic principles of these devices and the important advantages they offer. The first section deals with the advantages of diode-pumped lasers as compared with conventional lamp-pumped solid-state lasers and direct use of the diode lasers themselves. The bulk of this chapter is contained within the second section, which discusses the crystalline hosts employed then details the basic spectroscopic features of the rare earths, concentrating on thulium and holmium.

2.2 Advantages of diode-pumped solid-state lasers

Solid-state lasers offer intrinsic stability advantages over gas and liquid lasers, which can exhibit hydrodynamic instabilities. However they have been limited in their applications due to low efficiencies, thermal problems and large size (lamp-pumped solid-state lasers), or alternatively due to low powers combined with limited spatial and spectral properties (laser diodes). Diode-pumping of solid-state lasers offers major advantages over both lamp-pumping schemes and the direct use of laser diodes as sources of coherent radiation. Therefore it is instructive to make a comparison between these various types of laser source.

2.2.1 Comparison with lamp-pumping

Laser diodes efficiently emit optical radiation into a narrow spectral band. When this emission band lies within an excitation band of the active ion of the solid-state laser medium, laser diode optical pumping can be very efficient with little excess heat generation. Flashlamps, although they convert electrical energy to optical energy more efficiently (80% rather than 30-50%)¹, do so over a wide spectral band, and so the

absorption efficiency is very much lower, because much of the flashlamp radiation lies outside strong absorption lines. The substantial UV content of lamp light can lead to degradation of the pump cavity and coolant, and solarisation of the laser rod, problems which are eliminated with laser diode pump sources. A good spectral match between pump wavelength and laser medium absorption band(s) also significantly reduces the amount of waste heat generated in the laser medium. For example, with diode-pumped Nd:YAG, crystal heating is reduced by a factor of three compared with a flashlamp-pumped system².

A significant advantage of laser diode pumping compared with lamp-pumping is system lifetime and reliability. Laser diode arrays have exhibited lifetimes in excess of 20,000 hrs in cw and 10^{10} shots in pulsed mode³; lamp life is of the order 400 hrs cw and 10^7 shots in pulsed operation^{1,4}.

Flashlamps require large high voltage supplies, storage capacitors and trigger circuits, and so are bulky and inherently more dangerous than the relatively compact low power drivers which could even be powered by battery packs. Higher powers can presently be obtained from lamp-pumped systems. However, scaling to higher average powers in diode-pumped systems is on the increase, with improvements in diode fabrication and thermal management technology. Another hindrance is cost, with laser diode arrays being much more expensive than lamps, but prices are on a downward trend as sales volumes increase.

Perhaps the greatest advantage of diode-pumping over conventional techniques is the reduction in noise which can be achieved. The cooling requirements of lamp-pumped systems combined with poor mode-matching results in thermal fluctuations in the gain medium which cause frequency instabilities in the laser output. The reduced densities of waste heat in the efficient diode-pumping process, combined with intrinsically more stable solid-state pumps, results in improvements in noise performance of several orders of magnitude. Diode-pumped lasers have been demonstrated to yield sub 1 Hz linewidths⁵ compared to around 100 kHz for flashlamp-pumped lasers⁶.

2.2.2 Comparison with laser diodes

In a laser diode, the p-n junction provides the active medium. Light emission occurs by recombination of electron-hole pairs in this region. Laser action can occur if a population inversion is achieved by generating sufficient electron-hole pairs, optical

feedback being provided by the cleaved facets of the semiconductor. The laser diode is essentially a cw device with low energy storage capability due to its short upper level lifetime, whereas the solid-state laser can store energy in the long-lived metastable ion levels, leading to enhanced peak powers through Q-switching. The high peak power pulses produced can then be used to generate radiation at new wavelengths by intensity dependent processes including optical parametric oscillation.

The geometry of the edge-emitting diode laser, where the radiation originates from a very small facet area, leads to a highly divergent output beam. The emitting aperture is typically rectangular, leading to differing divergences in the two orthogonal directions. The output spectrum is typically several nanometres wide and is temperature dependent. By using the diode light to optically excite a solid-state laser medium, a diffraction-limited high brightness beam can be generated from the solid-state laser. The fundamental linewidth of the diode-pumped solid-state laser is several orders of magnitude smaller than that of the diode laser.

The most severe drawback of current generations of laser diode is that they operate at power levels very close to the damage threshold of their facets. Therefore, for any application requiring pulsed operation the peak power may not greatly exceed the average output power from the diode.

Finally, diode-pumped solid-state lasers offer the possibility of operation in wavelength regions where laser diodes either perform poorly or are not yet available.

2.3 Spectroscopy of two micron solid-state laser materials

2.3.1 Laser host crystals

The two crystalline hosts investigated in this work are yttrium aluminium perovskite (YAP or YAIO) and yttrium lithium fluoride (YLF). Throughout this work, the former crystal is referred to as YAP. In both cases the triply ionised rare earth dopant laser ion substitutes for the trivalent yttrium in the host lattice, thus avoiding the need for charge compensation.

YAP (chemical formula $YAlO_3$) is a biaxial crystal with the orthorhombic D_{2h}^{16} space group, the yttrium ions in sites of C_s (monoclinic) symmetry⁷. It is derived from the same Y_2O_3 - Al_2O_3 system as the more common laser host yttrium aluminium garnet (YAG, chemical formula $Y_3Al_5O_{12}$). However, although YAG is a mechanically robust oxide host, it has a cubic structure, which leads to thermal birefringence and subsequent depolarisation losses when thermally loaded. The natural birefringence of YAP dominates any thermally induced birefringence which, combined with similar mechanical properties to YAG, makes it a potentially useful laser host. Figure 2.1 shows the room temperature absorption spectrum of a slice of Tm,Ho:YAP measured in a Perkin Elmer Lambda 9 spectrophotometer.

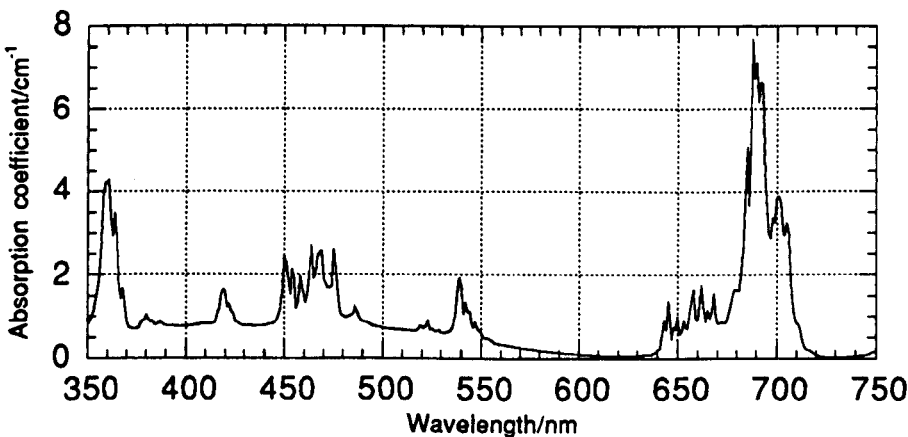


Figure 2.1 Visible absorption spectrum of 4.2% Tm, 0.28% Ho:YAP

The discrete spectral features are due to the thulium and holmium dopants, while the broad absorption peaking at approximately 450 nm and extending to 600 nm is due to colour centres in the crystal. This broad absorption gives the YAP crystals a distinctive amber tint. Colour centre formation can be a problem if broadband lamp sources are used to optically excite the YAP crystal, but for the case of excitation with

near infrared laser diodes the presence of colour centres does not affect laser performance. The corresponding absorption spectrum of YLF (and also of YAG) shows no sign of colour centre formation and indeed to the eye thulium and/or holmium doped crystals appear colourless. Given the mass density of YAP, 5.35 g cm^{-3} , combined with its chemical formula, YAlO_3 , the number density of yttrium sites is calculated to be $1.965 \cdot 10^{22} \text{ cm}^{-3}$.

YLF (chemical formula YLiF_4) is a uniaxial crystal with the tetragonal C_{4h}^{64} space group, the yttrium ions in sites of S_4 (tetragonal) symmetry⁷. It too is a naturally birefringent material, minimising the effects of any thermally induced birefringence. Being a fluoride host, YLF is less mechanically robust than the harder oxide YAP host. The number density of yttrium sites is $1.398 \cdot 10^{22} \text{ cm}^{-3}$ (mass density 3.99 g cm^{-3}).

Both YAP and YLF are grown by the Czochralski technique, whereby a boule is grown from a single crystal seed by pulling it from a high temperature melt containing the pertinent starting materials.

2.3.2 General spectroscopic features of the rare earths

In the fifth period of the periodic table after the element lanthanum (no. 57) the filling of the 4f shell takes place, from cerium with an outer configuration $5s^25p^64f^15d^16s^2$ to ytterbium with configuration $5s^25p^64f^{13}5d^16s^2$. These are the lanthanide or rare earth elements⁸.

It has been known since the early days of the Bohr theory that the 4f, 5d and 6s electrons in the rare earths have very nearly the same energy. In the triply charged lanthanide ions the 5d and 6s electrons are removed. The energy levels of the incompletely filled $4f^n$ shell spread over the order of 40000 cm^{-1} resulting in many levels being separated by up to $10\text{-}20000 \text{ cm}^{-1}$ which give rise to transitions from the near infrared to the blue.

The spectra of the triply ionised rare earths in transparent materials consist of a series of sharp lines that more closely resemble free ion, atomic, or molecular spectra than other solid-state ion spectra, which generally have a broad structure. The invention of crystal-field theory by Bethe (1929) and the application of group theory to impurity ion spectroscopy by Bethe (1930) and Kramers (1930) paved the way for a more

complete understanding of the spectra⁹. This early work indicated that in most cases transitions were due to forced electric dipole transitions, and to a lesser extent by magnetic dipole transitions. Electric dipole transitions between the states of the $4f^n$ electron configuration of an isolated rare earth ion (RE^{3+}) are prohibited by the parity selection rule, which states that the only allowed electric dipole transitions are those resulting in a change of parity, which involves an angular momentum quantum number change of ± 1 . Van Vleck¹⁰ showed that this could be more or less be avoided due to the noncentrally symmetric interactions of the RE^{3+} ions with the surroundings, which mix states of opposite parity. Examples of these interactions in a crystalline environment are both static and dynamic, the former involving pure electronic transitions in noncentrally symmetric centres, the latter noncentrally symmetric vibrations of the surroundings that induce electronic vibrational (vibronic) transitions.

In the rare earths, the inner unfilled and optically active $4f^n$ shell is compressed and shielded by the outer filled $5s^2$ and $5p^6$ shells. Hence the lattice vibrations act only as a small perturbation i.e. the electron-phonon coupling strength is low, as contrasted with the transition metal ions chromium (Cr^{3+}) and titanium (Ti^{3+}). Hence the static portion of the noncentrally symmetric interaction is the main contributor to the observed RE^{3+} spectra in crystalline environments. Because of this weak interaction with the lattice, the spectra resemble those of the corresponding free ion and moreover the gross features of the spectra are essentially independent of the particular host lattice being studied.

In the free ion case, the outer electrons are considered to be in a centrally symmetric field produced by the nucleus surrounded by the inner filled electron shells. The electrostatic electron interaction creates terms that are characterised by certain total orbital and spin angular moments (L and S). The spin-orbit interaction partially reduces the $(2L+1)(2S+1)$ multiple term degeneracy, and forms a multiplet structure of free-ion spectra, the term values being determined by Hund's Rules¹¹ - these are the gross spectral features alluded to earlier.

When placed in a crystalline environment, the ion is regarded as being surrounded by ligands which act only as a source of electric potential. Since the ion no longer experiences a spherically symmetric potential, the orbital $(2L+1)$ -fold degeneracy is partially or completely removed, depending on the symmetry of the lattice. In the weak crystal field regime being considered here, this produces Stark splittings, leading to the creation of energy level manifolds. These Stark levels correspond to the

irreducible representations of the site symmetry group as required by group theory. The Stark splittings within individual manifolds, produced by the interaction with the lattice, are small compared to the manifold separations, determined principally by the spin-orbit coupling.

2.3.2 Spectroscopic properties of thulium and holmium

For laser operation in the two micron spectral region, the principal ions of interest are thulium (Tm^{3+}) and holmium (Ho^{3+}). These have ten and twelve 4f electrons respectively with corresponding ground states $^3\text{H}_6$ and $^5\text{I}_8$, according to Hund's Rules. Figure 2.2 is a generic diagram depicting the low-lying energy level manifolds of thulium and holmium.

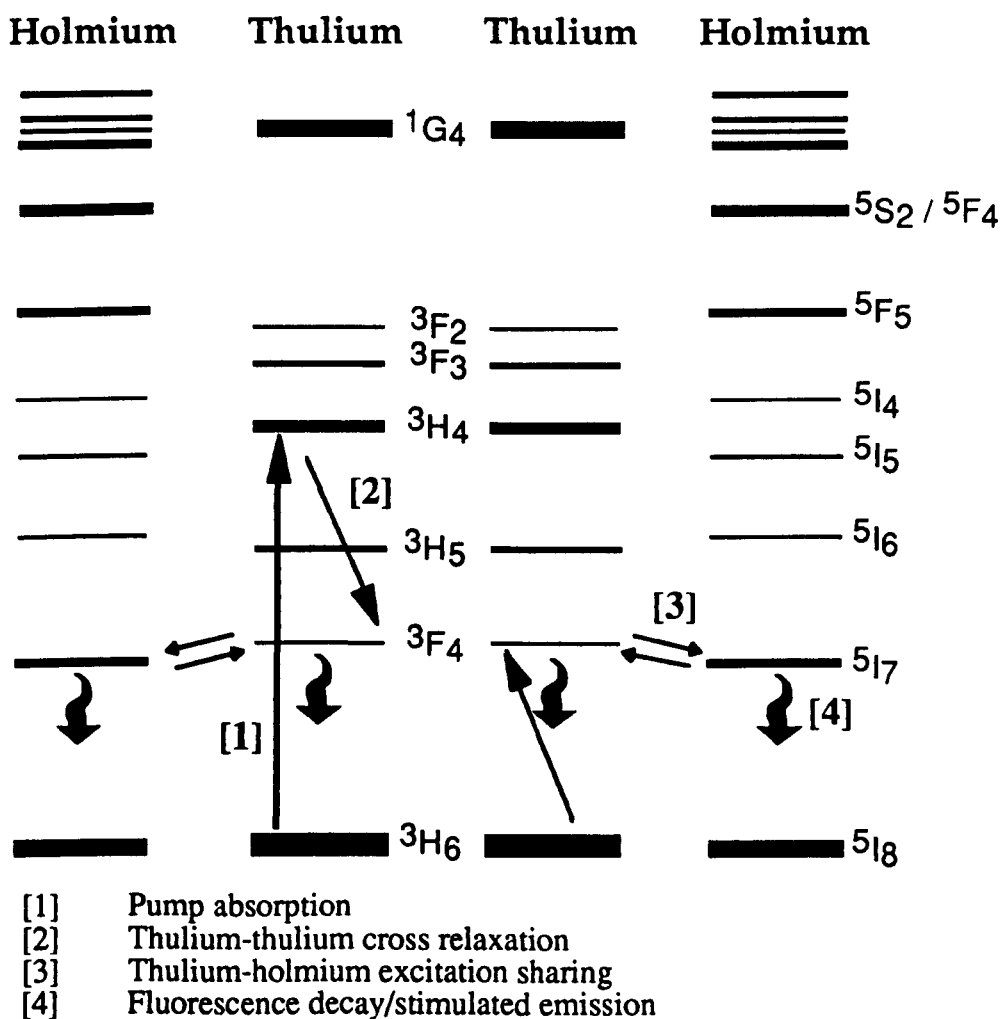


Figure 2.2 Low-lying energy level manifolds of the rare earth ions thulium and holmium

The widths of the manifolds indicate the effect of broadening induced by the weak crystal field interaction. Individual Stark splittings are omitted for simplicity, and also because their exact nature varies from host to host. Several features are immediately apparent.

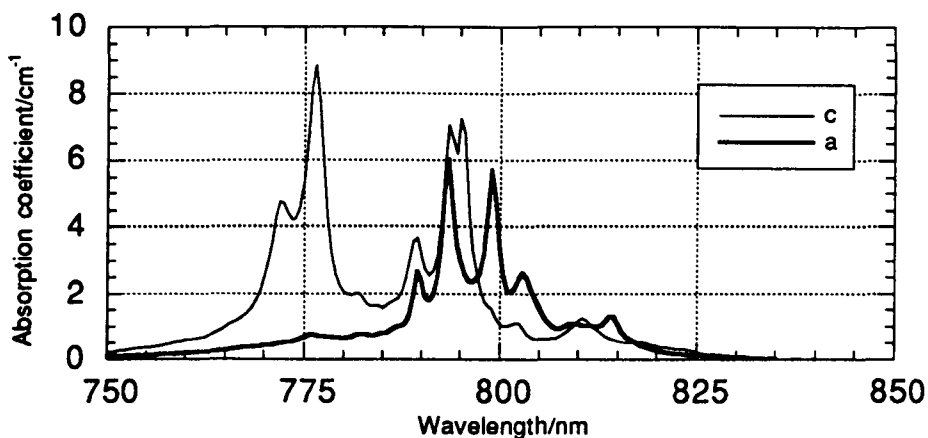


Figure 2.3 Room temperature pump band absorption spectrum of 4.2% Tm:YAP

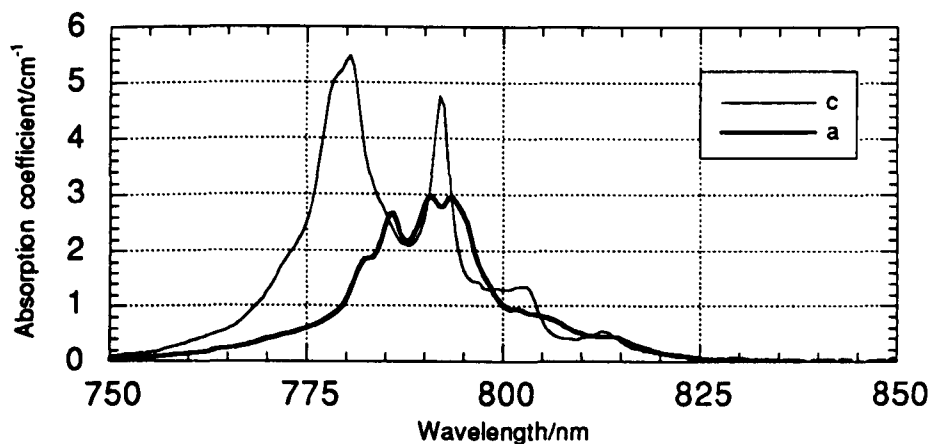


Figure 2.4 Room temperature pump band absorption spectrum of 6% Tm:YLF

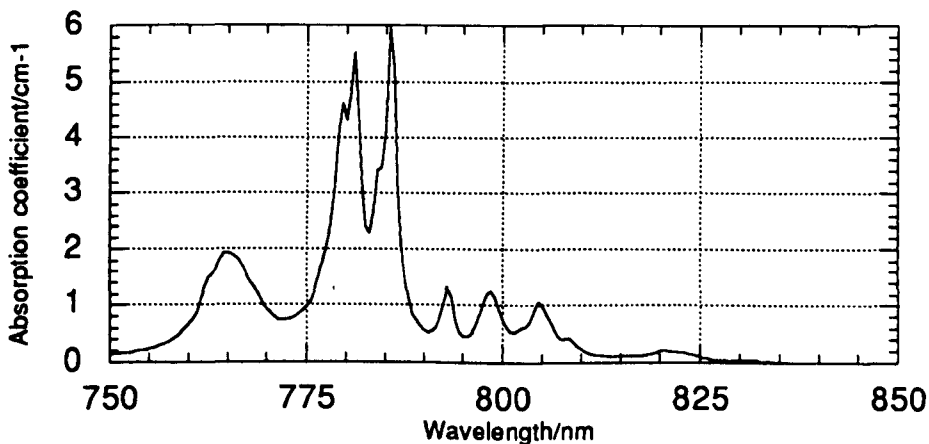


Figure 2.5 Room temperature pump band absorption spectrum of 6% Tm:YAG

Thulium possesses an absorption band (3H_4) at around 12500 cm^{-1} , corresponding to an absorption wavelength of 800 nm, which is accessible by commercially available high power GaAs/AlGaAs laser diodes, unlike holmium which possesses no absorption bands amenable to excitation by such pump sources. Figures 2.3 to 2.5 are the absorption spectra of the thulium 3H_6 to 3H_4 transition in YAP, YLF and, for the purposes of comparison, YAG.

In order to obtain these absorption spectra, polished spectroscopic samples of Tm:YAP, Tm:YLF and Tm:YAG were measured in a Perkin Elmer Lambda 9 spectrophotometer. A thin film infrared polariser was also introduced into the sample chamber in order that the orientation-dependent absorption spectra of the birefringent materials could be determined. The absorption spectra were measured at room temperature, taken to be 20°C (293 K). For Tm:YAP and Tm:YLF, the principal absorption peaks are at 795 and 792 nm respectively (looking at the c-axis absorption in both cases), wavelengths which can be accessed by temperature tuning of one laser diode. The principal absorption peaks for Tm:YAG are at 781 and 786 nm, wavelengths too far removed from that of YAP and YLF to be accessed by the same laser diode. Therefore both Tm:YAG and Tm,Ho:YAG are not included in the laser experiments reported here.

In order to predict spectroscopic parameters, an accurate knowledge of the energy levels of the active ion in the host is required. Hence there has been extensive work carried out in theoretically and experimentally determining these levels. Appendix A tabulates the energy levels of the two lowest lying manifolds of thulium and holmium, as well as the thulium 3H_4 pump band, in the crystalline hosts of interest, YAP and YLF.

The lasing transition(s) of both thulium and holmium in the two micron wavelength region occur from low-lying Stark levels in the first excited manifold to high-lying levels in the ground state manifold (no greater than 600 cm^{-1} above the bottom Stark level). This means that such lasers possess a significant lower level thermal (temperature-dependent) population. Because of this terminal laser level population these lasers are termed as being "quasi-three level", as opposed to ruby, where the terminal laser level is also the ground state of the system, and so exhibits true three level operation.

2.3.3.1 Basic lasing dynamics

The principal characteristics of this class of laser stem from two major features, namely the long wavelength of operation and the possibility of inter-ionic excitation exchange due to the existence of energy level pairs with comparable energy differences.

The long wavelength implies that the energy level difference on the laser transition is small, with the consequence that nonradiative processes will not be negligible. In general these act as alternative routes for quenching the upper laser level, and so detract from the laser operation.

The large number of possible resonant energy transfer processes in thulium and holmium allows the excitation energy of short wavelength pump photons to generate a number of excitation quanta on the lasing initial state. This can be seen by referring back to figure 2.2, which indicates a single pump photon from a laser diode exciting a thulium ion to the 3H_4 manifold. Cross-relaxation between adjacent ions (one excited, the other in the ground state) leads to population of the 3F_4 manifold containing the upper laser level. By this process two quanta of laser excitation are created by one pump photon. This process can be thought of as the interaction between two dipoles, representing the 3H_4 - 3F_4 and 3H_6 - 3F_4 transitions respectively. Hence this "two for one" process is very dependent on the separation of the thulium ions i.e. on their concentration (both Stoneman¹² and Noginov¹³ quote that at least 4% Tm doping is required to make this process efficient in YAG, which corresponds to a thulium doping density of $5.6 \cdot 10^{20} \text{ cm}^{-3}$), as well as on the degree of overlap of the emission and absorption spectra. There is rapid energy migration^{14,15} amongst the thulium ions, and if holmium is also present, resonant energy transfer to the 5I_7 manifold can occur, de-exciting the thulium ion to the ground state. This is a reversible process, leading to a thermal equilibrium distribution of excitation between the two ions under steady-state conditions. Although in this way quantum (number) efficiencies greater than unity are readily achievable, the resonant processes can act also to inhibit laser action through upconversion of excitation to energy levels not available for lasing at two microns.

As stated in the previous section, the upper and lower laser levels of thulium and holmium are Stark splittings of energy level manifolds containing many such splittings. Each energy level manifold is independently in thermal equilibrium, which

means that within each manifold the population of the Stark splittings is determined by a Boltzmann distribution, which itself depends on temperature and the detailed nature of the levels within the manifold. Redistribution of population within each energy level manifold takes place very rapidly, typically on a subpicosecond timescale, much faster than any other processes adding or removing population from the manifold, including the stimulated emission rate on the laser transition, thus maintaining the Boltzmann distribution.

Figure 2.6 depicts the scenario. The energy level manifolds shown represent the ground and first excited states of either thulium or holmium, with the exact nature of the splittings not critical here. For clarity, only the lower and upper levels of each manifold are shown. In general, lasing occurs from the bottom level of the first excited state energy level manifold to a high-lying level in the ground state energy level manifold. The higher lying this terminal level, the smaller the level population is, reducing the magnitude of the lasing threshold. Therefore the laser will tend to oscillate on the longest wavelength possible. The following chapter provides a more detailed analysis of the population distributions within these energy level manifolds, and their bearing on laser threshold calculations.

Co-doping laser crystals separates the functions of diode pump beam absorption and stimulated emission on the two micron laser transition. Relatively high concentrations of thulium are used to provide efficient absorption of the pump light, with excitation sharing transferring excited state population to holmium (see figure 2.2). Low concentrations of the lasing species are used to aid in minimising the laser threshold. A balance has to be struck between keeping the holmium concentration low to reduce laser threshold, but keeping it sufficiently high so as to increase the fraction of the excited state population residing on the holmium.

Because of the quasi-three level nature of the thulium and holmium two micron laser transitions, high brightness pump sources are required in order to achieve laser thresholds. Tight focussing of the pump beam increases the pump intensity, but at the expense of reduced depth of focus of the optics train. Short length, highly doped laser crystals can effectively absorb the pump light in a small volume which, when properly mode-matched in the end-pumped geometry to the two micron laser resonator mode, can efficiently excite operation on the fundamental transverse mode.

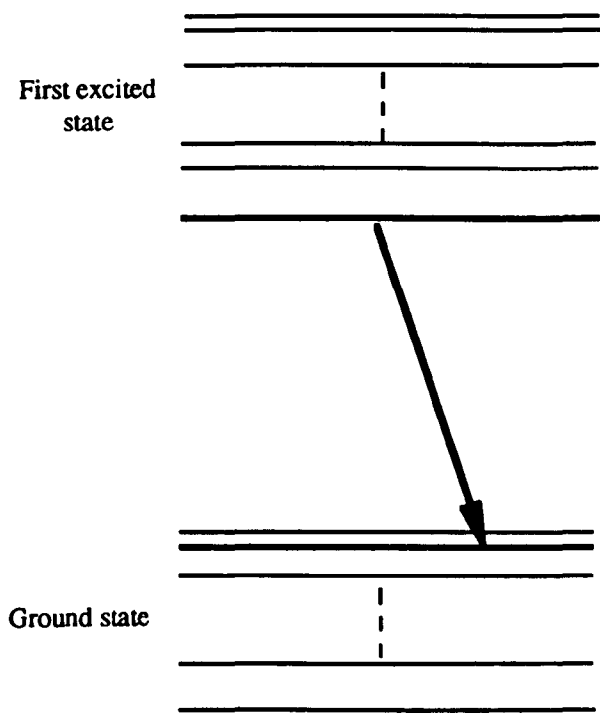


Figure 2.6 Two micron lasing transition in thulium or holmium

2.3.3.2 Stimulated emission cross-sections

An important spectroscopic parameter in understanding the performance of a lasing species is the magnitude of the stimulated emission cross-section of the lasing transition. The definitive method of determining the emission cross-section involves measurements of gain in the laser material under investigation, by probing the excited gain medium with a low intensity beam to obtain a value for the small signal gain.

The method used here to determine the stimulated emission cross-section of thulium and holmium involved measurement of the absorption spectrum of the lasing species in the wavelength region of the lasing transition, utilising the fact that the lower laser level is thermally populated. In order to obtain the relevant absorption spectra, polished spectroscopic samples of Tm:YAP, Ho:YAP and Ho:YLF were measured in a Perkin Elmer Lambda 9 spectrophotometer, in a similar fashion to the diode pump band absorption spectra measurements of section 2.3.3. The following three graphs depict the absorption spectra which were measured at room temperature.

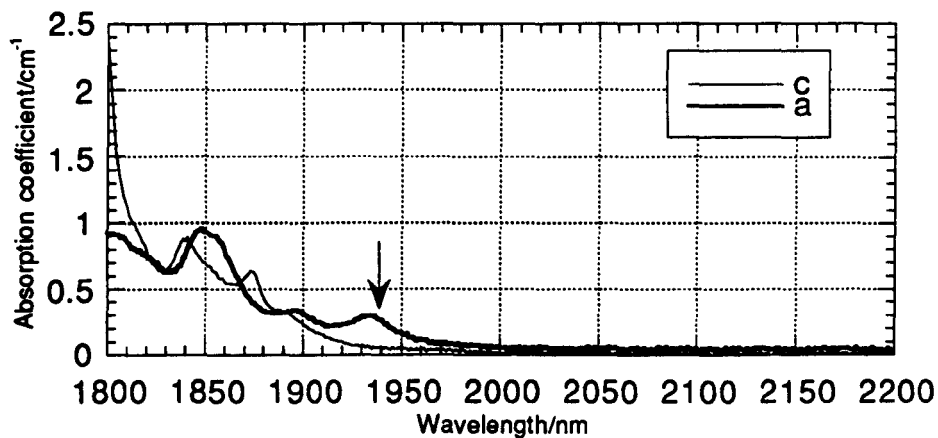


Figure 2.7 Room temperature absorption spectrum of 4.2% Tm:YAP

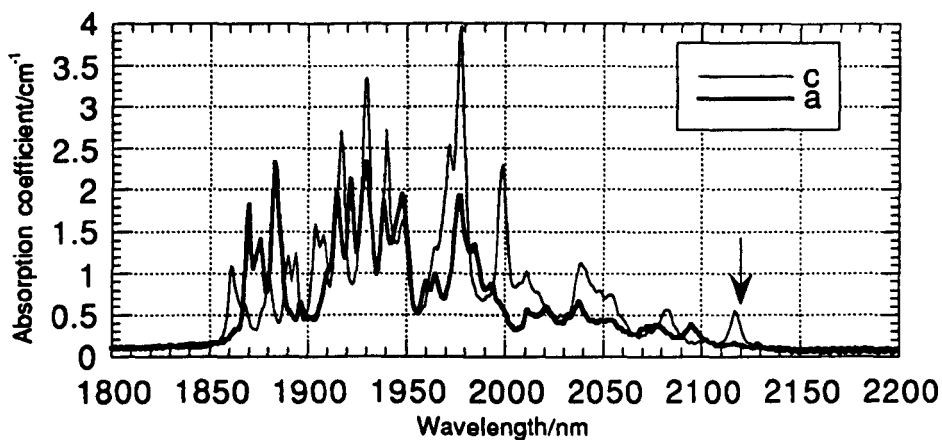


Figure 2.8 Room temperature absorption spectrum of 1.5% Ho:YAP

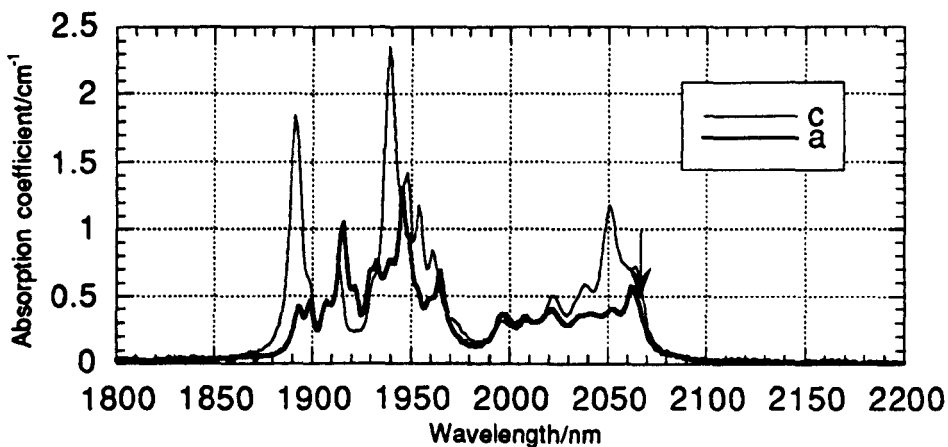


Figure 2.9 Room temperature absorption spectrum of 1.5% Ho:YLF

The arrows indicate the wavelength, and the polarisation relative to the crystallographic axes, of the laser transitions investigated in this work. The absorption cross-section is given by

$$\sigma_{abs} = \frac{\alpha_l}{N_l} \quad 2-1$$

where α_l is the absorption coefficient at the laser wavelength, and N_l is the population density residing in the lower laser level, which is a temperature-dependent fraction of the total ground state population density. Absorption measurements made by the spectrophotometer involve probing the samples with a weak beam, therefore the ground state population can be assumed to equal the total doping density of the rare earth ion. The emission cross-section is related to the absorption cross-section by the expression

$$\sigma_{em} = \frac{g_l}{g_u} \sigma_{abs} \quad 2-2$$

where g_u and g_l are the degeneracies of the upper and lower laser levels respectively. The degeneracy terms are obtained from knowledge of the energy levels of the rare earth ion in the crystalline host (see Appendix A), as is the fractional occupation of the lower laser level. Tabulated below are the derived emission cross-section values of the laser transitions investigated in this work.

Lasing ion	$\lambda/\mu\text{m}$	Polarisation axis	g_l/g_u	Measured σ_{em} (10^{-20} cm^2)	Published σ_{em} (10^{-20} cm^2) ¹⁶
Tm ³⁺ in YAP	1.940	a	0.50	0.6	0.5
Ho ³⁺ in YAP	2.120	c	0.50	7.5	8.2
Ho ³⁺ in YLF	2.065	a	0.67	3.7	-

Table 2.1 Measured stimulated emission cross-sections of thulium and holmium

There is good agreement between the measured values and corresponding published figures. In the case of Tm, Ho:YLF, the published data is for the 2.050 μm transition. Using figure 2.9 and Appendix A, the measured value for the emission cross-section at this wavelength is $1.9 \cdot 10^{-20} \text{ cm}^2$, in reasonable agreement with the published value of $1.84 \cdot 10^{-20} \text{ cm}^2$. Therefore we can have some confidence in the measured emission cross-section values. Identical measurements were also carried out with different concentrations of thulium and holmium, yielding similar results to the

tabulated values of emission cross-section, confirming that these results were not concentration dependent.

It is immediately apparent from table 2.1 that holmium possesses a significantly higher emission cross-section than thulium (indeed Payne *et al.*¹⁶ contains a more comprehensive table of cross-section values which clearly illustrates this trend), and so for a given population inversion density would offer higher gain than thulium. This is one of the principal reasons of going to the additional complexity of co-doping crystals with both thulium and holmium, with lasing occurring on the holmium, rather than relying on lasing in thulium alone.

2.3.3.3 Fluorescence decay lifetimes

Allied to the stimulated emission cross-section measurement is consideration of the fluorescence decay lifetime of the first excited state energy level manifold. This is another important parameter in characterising laser performance. Excitation with a laser diode provides a method of determining the lifetime of the thulium 3F_4 level. 4.2% Tm:YAP was measured to have a fluorescence lifetime of 4.4 ms, 5% Tm:YLF a lifetime of 8 ms. A suitable excitation source was not available for performing similar measurements on single-doped holmium crystals. As detailed in chapter six, the fluorescence decay from the first excited state of double-doped thulium and holmium crystals is strongly affected by various upconversion processes taking place, resulting in the measured fluorescence decay not being a simple single exponential decay. A search through the open literature reveals the fluorescence decay lifetime of the first excited state of singly doped thulium or holmium crystals is in the range 5 to 20 ms depending on the host crystal¹⁶⁻¹⁸.

2.4 Conclusions

In this chapter the relative merits of diode-pumped solid-state lasers versus both lamp-pumped solid-state lasers and the direct use of laser diodes have been discussed.

The two laser host crystals investigated in this work, YAP and YLF, were introduced, before a treatment of the general spectroscopic features of the triply ionised rare earth ions. The optically active $4f^n$ electron shell is shielded from the surrounding environment, therefore the crystal field is a small perturbation only, and the gross spectral features resemble those of the free ion.

The principal rare earth ions of interest for two micron lasers are thulium and holmium. Only thulium has an absorption band to match the spectral output of high power commercially available AlGaAs laser diodes. The presence of nearly equally spaced sets of energy levels in both thulium and holmium accounts for many of their properties, including the efficient cross-relaxation process in thulium which populates the first excited state from which two micron laser emission occurs. Excitation sharing takes place between the first excited states of thulium and holmium, allowing lasing on the latter.

Using the principle of reciprocity, values for stimulated emission cross-sections were determined from absorption measurements at the appropriate wavelengths. Stimulated emission cross-sections of $6 \cdot 10^{-21} \text{ cm}^2$, $3.7 \cdot 10^{-20} \text{ cm}^2$ and $7.5 \cdot 10^{-20} \text{ cm}^2$ were calculated for the principal laser transitions of thulium in YAP, holmium in YLF and holmium in YAP respectively.

Two micron laser emission in both thulium and holmium occurs into a high-lying Stark level of the ground-state energy level manifold. Therefore the temperature distribution within the gain medium will have an important role to play in laser operation. The next chapter describes thermal modelling of diode-pumped two micron solid-state lasers.

2.5 References

- [1] T. Y. Fan, 'Diode-pumped solid state lasers', Lincoln Lab. Journal, vol. 3, no. 3, 413 (1990)
- [2] T. S. Chen, V. L. Anderson & O. Kahan, 'Measurement of heating and energy storage in diode-pumped Nd:YAG', IEEE J. Quantum Electron., vol. 26, no. 1, 6 (1990)
- [3] J. G. Endriz, M. Vikili, G. S. Browder, M. DeVito, J. M. Haden, G. L. Harnagel, W. E. Plano, M. Sakamoto, D. F. Welch, S. Willing, D. P. Worland & H. C. Yao, 'High power laser diode arrays', IEEE J. Quantum Electron., vol. 28, no. 4, 952 (1992)
- [4] T. Gray & C. Frederickson, 'Pumping Nd:YAG lasers : lamp or diode array?', Lasers & Optronics (November 1990)
- [5] D. Shoemaker, A. Brilliet, C. N. Man, O. Cregut & G. Kerr, 'Frequency-stabilised laser diode-pumped Nd:YAG laser', Opt. Lett., vol. 13, 111 (1988)
- [6] K. C. Peng, L. A. Wu & H. J. Kimble, 'Frequency-stabilised Nd:YAG laser with high output power', Appl. Opt., vol. 24, 938 (1985)
- [7] R. J. Pressley, 'CRC Handbook of Lasers with Selected Data on Optical Technology', Ohio: CRC Press (1971)
- [8] B. Henderson & G. F. Imbusch, 'Optical spectroscopy of inorganic solids', Oxford : Clarendon (1989)
- [9] K. A. Gschneidner, Jr & L. Eyring (Editors), 'Handbook on the physics and chemistry of rare earths', vol. 5, Amsterdam : North-Holland Publishing Company (1982)
- [10] J. H. Van Vleck, 'The puzzle of rare-earth spectra in solids', J. Phys. Chem., vol. 41, 67 (1937)
- [11] P. W. Atkins, 'Molecular quantum mechanics', 2nd edition, Oxford : University Press (1983)
- [12] R. C. Stoneman & L. Esterowitz, 'Intracavity-pumped 2.09 μm Ho:YAG laser', Opt. Lett., vol. 17, no. 10, 736 (1992)
- [13] M. A. Noginov, A. M. Prokhorov, G. K. Sarkisyan, V. A. Smirnov & I. A. Shcherbakov, 'Cross-relaxation deactivation of the ground state of ions of rare-earth elements in crystals', Sov. J. Quantum Electron., vol. 21, no. 9, 945 (1991)
- [14] V. A. French & R. C. Powell, 'Laser-induced grating measurements of energy migration in Tm,Ho:YAG', Opt. Lett., vol. 16, no. 9, 666 (1991)
- [15] S. A. Payne, L. K. Smith, W. L. Kway, J. B. Tassano & W. F. Krupke, 'The mechanism of Tm to Ho transfer in LiYF₄', J. Phys. Condens. Matter, vol. 4, 8525 (1992)
- [16] S. A. Payne, L. L. Chase, L. K. Smith, W. L. Kway & W. F. Krupke, 'Infrared cross-section measurements for crystals doped with Er³⁺, Tm³⁺ and Ho³⁺', IEEE J. Quantum Electron., vol. 28, no. 11, 2619 (1992)

- [17] M. Falconieri & G. Salvetti, '*Effects of co-dopant concentrations and excitation conditions on the 2 μm fluorescence dynamics in Tm,Ho:YLF crystals*', Appl. Phys. A, vol. 59, 253 (1994)
- [18] J. A. Caird, L. G. DeShazer & J. Nella, '*Characteristics of room-temperature 2.3 μm laser emission from Tm³⁺ in YAG and YAlO₃*', IEEE J. Quantum Electron., vol. 11, no. 11, 874 (1975)

Thermal modelling

3.1 Introduction

In order to fully characterise the operation of a solid-state lasers, an understanding of thermal effects in the gain medium is essential. Heat deposition produces thermally induced strains which can lead to phenomena such as thermal birefringence and lensing, and ultimately to fracture of the solid-state gain medium. For the particular case of the quasi-three level thulium and holmium lasers of interest here, temperature dependent population distributions determine the laser threshold and excitation sharing between thulium and holmium, further increasing the requirement for thermal modelling of this class of laser.

In the longitudinal or end-pumping geometry employed in this work, the output from the laser diode is collected and beam-shaped before being focussed down to form a pump spot on the laser crystal. This technique allows good mode-matching between the spot size of the solid-state laser resonator mode and the pump spot size in the gain medium. The gain media employed in end-pumped geometries are usually of short length with high doping to give efficient absorption of the pump beam. This geometry, with potentially high heat deposition in a small volume, enhances the thermal effects in the gain medium.

The first sections of this chapter investigate the steady-state temperature distribution and associated thermal lensing in the laser crystals of interest, followed by a treatment of the thermally induced fracture limit. Subsequent sections analyse the temperature dependence of the population distributions, with particular regard to their effects on laser threshold and excitation sharing between thulium and holmium.

Computer modelling was carried out using THINKPascal™ software installed on a Macintosh Powerbook 180 laptop.

3.2 Thermal effects in solid-state lasers

3.2.1 Introduction

Thermal effects in solid-state lasers are due to the combined actions of heat generation by absorption of pump light and heat flow induced by cooling processes. In the case of continuous wave (cw) operation a steady state condition will be reached. Heating and cooling of the laser gain medium leads to the formation of temperature profiles within the material.

Diode-pumped solid-state lasers in an end-pumped geometry offer the prospect of efficient laser sources, as the pump and laser modes can be made to overlap to a high degree. However it is necessary to investigate the thermal effects brought about by adopting this type of pumping geometry, as these will in turn affect the optical performance of the solid-state laser.

One important effect, thermal lensing, results from a combination of temperature induced phenomena in the gain medium. In order to calculate these changes, the heat flow equation must first be solved to obtain the temperature distribution within the gain medium.

The ultimate limit on pumping of a laser crystal is the possibility of thermal fracture, caused by excessive heat deposition. As the heat load in the laser crystal increases, there is a resultant increase in the thermally induced stresses finally leading to fracture of the crystal at the maximum stress point.

For the particular case of thulium and holmium lasers, the temperature distribution is also important when calculating laser threshold and related parameters. These ions operate as quasi-three level lasers, with the lower laser level a high-lying Stark splitting of the ground state energy level manifold. Population within this manifold is thermally distributed according to Boltzmann statistics, hence the temperature can have a critical effect on the threshold, through the lower laser level thermal population.

The following analysis first deals with calculation of the temperature distribution within an optically pumped gain medium, then with derivation of the corresponding thermal lens. Two cases are considered, namely Gaussian and top-hat pump profiles,

as these are considered the cases closest to typical laser diode focussed pump beam profiles.

As discussed in the previous chapter, the two laser crystals studied in this work are yttrium lithium fluoride (YLF) and yttrium orthoaluminate (YAP). Below are tabulated the values of the relevant physical properties of these crystals. Note that for the birefringent hosts YLF and YAP all the properties tabulated below are anisotropic, but despite a thorough literature search only the values appearing here could be found¹. For comparison purposes the corresponding parameters for the common laser host yttrium aluminium garnet (YAG) are also included in Table 3.1. The initial analysis concerning temperature distributions and thermal lensing will also include results for YAG.

	YAP	YLF	YAG
Thermal Conductivity K ($W\ mm^{-1}\cdot K^{-1}$)	0.011	0.006	0.013
Thermal Expansion Coefficient α_0 ($10^{-6}\ K^{-1}$)	a: 9.5 b: 4.3 c: 10.8	a: 13 c: 8	7.5
dn/dT ($10^{-6}\ K^{-1}$) *	8.1	-4.3	7.3
Young's Modulus E ($10^6\ N\ cm^{-2}$)	22	6.9	27.8
Tensile strength σ_T ($N\ cm^{-2}$)	15800	3300	18100
Poisson's Ratio **	0.3	0.33	0.3
Refractive Index ($\lambda = 2\ \mu m$)	a: 1.93 b: 1.92 c: 1.90	a: 1.44 c: 1.46	1.80

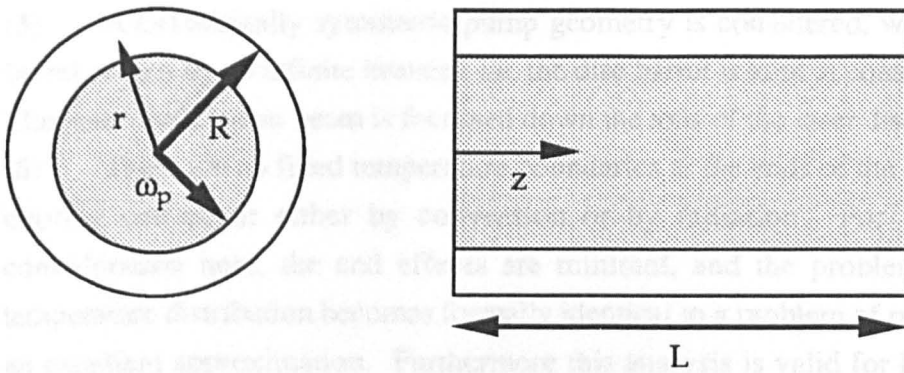
* Values for a wavelength of one micron, and temperatures close to ambient.

** Poisson's ratio for YAP taken to equal that of YAG, in the absence of a known value (the value of this parameter does not vary greatly over a wide range of materials).

Table 3.1 Thermal and mechanical parameters of laser host crystals

3.2.2 The end-pumping geometry

End-pumped two micron lasers are characterised by gain media of short length (less than 5 mm), utilising the high absorption of thulium around 790 nm. The following diagram portrays end and side views of the end-pumping geometry under consideration. The gain medium takes the form of a laser disc of length L and radius R , optically excited by a pump beam of radius ω_p .



Shaded area represents pumped region of gain medium

Figure 3.1 End-pumping geometry

The following points are central to the analysis :

- (1) The physical properties of the gain media, including the value of the absorption coefficient, are taken to be constant over the range of temperatures under consideration.
- (2) Heating of the gain medium is produced solely by absorption of the pump beam, and so the heat deposition profile will have the same shape as the pump beam. Absorption of the pump beam in thulium is followed by a cross-relaxation process (then excitation sharing if co-doped with holmium) resulting in two quanta at two microns from a single pump photon - the so-called "2-for-1" process. Assuming this to be 100% quantum efficient the energy efficiency of the pumping is approximated by $2 \times 0.79 \mu\text{m} / 2 \mu\text{m}$ i.e. 80%. The remaining 20% manifests itself as nonradiative decay into the host lattice. According to T.S Chen *et al.*², in diode-pumped Nd:YAG approximately half the stored energy is converted to heat. More recent work by McInnes and Richards³ determined the fractional heat load to be 0.29 under conditions of lasing, 0.36 when not lasing. These later results provide closer agreement with the quantum defect in neodymium lasers. For the two micron lasers being investigated here, the excitation mechanisms populating the upper laser level are more complicated than with neodymium lasers. At each stage nonradiative decay occurs to some degree. Taking this into account a figure of 50% for the percentage of absorbed pump light converted to heat is considered appropriate to serve as an upper limit for the fractional heat load.
- (3) The pump beam is assumed to have zero divergence i.e. the pump beam has a fixed diameter throughout the gain medium.
- (4) Absorption of the pump beam occurs according to Beer's Law, and so any saturation effects have been ignored.

(5) A cylindrically symmetric pump geometry is considered, with the laser disc barrel cooled by an infinite heatsink i.e. the disc barrel is kept at constant temperature. The laser diode pump beam is focussed down the axis of the laser disc.

(6) There are no fixed temperature boundaries at the ends of the laser disc, where cooling can occur either by convection or by radiation. For the cases under consideration here, the end effects are minimal, and the problem for the *mean* temperature distribution becomes formally identical to a problem of radial heat flow to an excellent approximation. Furthermore this analysis is valid for laser rods of any aspect ratio (length/radius).

(7) The condition $\omega_p \alpha \ll 1$ holds. This implies that radial temperature gradients are much greater than axial temperature gradients, further confirming that the heat flow equation can be solved for radial variations only (to a first approximation).

3.3 Temperature distributions

3.3.1 Heat equation

In the steady state the heat flow equation takes the form⁴ (in cylindrical polar coordinates)

$$\begin{aligned}\nabla \cdot \underline{H}(r, z) &= \frac{1}{r} \frac{\partial}{\partial r} (rH) + \frac{\partial H}{\partial z} = Q(r, z) \\ Q(r, z) &= \frac{\partial P_a(r, z)}{\partial V}\end{aligned}\tag{3-1}$$

where \underline{H} is the heat flux and Q is the power deposited as heat (P_a) per unit volume. Note that as radially symmetric cases are under investigation, the angular component of the dot product has been neglected. The heat flux is related to the corresponding temperature distribution within the gain medium by

$$\underline{H}(r, z) = -K \nabla T(r, z)\tag{3-2}$$

where K is the thermal conductivity of the gain medium being pumped.

Referring to the approximations made in section 3.2.2, equations 3-1 and 3-2 can be simplified by ignoring the axial (z dependent) terms. Therefore the governing equations for radial heat flow are

$$\frac{1}{r} \frac{d}{dr} \{rH(r, z)\} = Q(r, z)\tag{3-3}$$

and

$$H(r, z) = -K \frac{dT(r, z)}{dr}.\tag{3-4}$$

3.3.2 Finite element analysis

The end-pumping geometry lends itself to dividing the laser disc into a series of slices, then considering heat deposition and temperature profiles in each slice individually. Using this technique, variations of the peak temperature along the length of the laser rod can be investigated. The temperature of the pumped region affects the laser threshold of the quasi-three level systems under consideration here. Sections 3.3.3 and 3.3.4 detail this finite element analysis for top-hat and Gaussian pump beam profiles.

3.3.3 Top-hat pump beam profile

Here the combination of a zero divergence pump beam with a top-hat profile leads to Q being a constant. Rearranging the above equations yields the differential equation governing the temperature distribution

$$\frac{1}{r} \frac{d\{r dT/dr\}}{dr} + \frac{Q}{K} = 0. \quad 3-5$$

Dividing the rod into a series of slices, we now consider the n^{th} slice, thickness Δz , a distance z (equal to $(n-1)\Delta z$) from the pumped face of the laser rod. There are two distinct regions to consider within the gain medium, namely inside and outside the pumped region. In the former case solution of equation 3-5 reveals a parabolic temperature profile peaking at the rod centre, with a logarithmic decay of temperature outside the pumped region. Thus the self-consistent solution to 3-5 for the radial temperature gradient $\Delta T(r,z)$ is

$$\Delta T(r,z) = T(r,z) - T_0 = \frac{P_{ph}(1 - \exp(-\alpha\Delta z))}{4\pi K\Delta z} \exp(-\alpha z) \times \begin{cases} 2 \ln\left(\frac{R}{\omega_p}\right) + 1 - \left(\frac{r}{\omega_p}\right)^2, & r \leq \omega_p \\ 2 \ln\left(\frac{R}{r}\right), & r > \omega_p \end{cases} \quad 3-6$$

where P_{ph} is the fraction of the incident pump power contributing to heat deposition.

In the cases under consideration the $\alpha\Delta z$ term is sufficiently small to allow $\exp(-\alpha\Delta z)$ to be expanded as a power series. Now equation 3-6 reads as

$$\Delta T(r,z) = \frac{\alpha P_{ph}}{4\pi K} \exp(-\alpha z) \times \begin{cases} 2 \ln\left(\frac{R}{\omega_p}\right) + 1 - \left(\frac{r}{\omega_p}\right)^2, & r \leq \omega_p \\ 2 \ln\left(\frac{R}{r}\right), & r > \omega_p. \end{cases} \quad 3-7$$

3.3.4 Gaussian pump beam profile

Equation 3-3 can be integrated over a disc of thickness Δz

$$\int_z^{z+\Delta z} \int_0^r H(r',z') 2\pi r' dr' dz' = \int_z^{z+\Delta z} \int_0^r \frac{dP(r',z')}{dV} 2\pi r' dr' dz' \quad 3-8$$

Now the power per unit volume can be defined as

$$\frac{dP}{dV} = \alpha I_h(r,z) \quad 3-9$$

where α is the pump absorption coefficient and $I_h(r,z)$ is the intensity of the incident pump light that contributes to heating of the gain medium. If the pump beam is Gaussian the intensity profile will be given by

$$I_h(r, z) = I_{0h} \exp\left(-2r^2/\omega_p^2\right) \exp(-\alpha z) \quad 3-10$$

where I_{0h} is the peak value of the incident intensity. Here the $\exp(-\alpha z)$ term takes account of absorption in the gain medium. Substituting 3-9 and 3-10 into 3-8 and integrating yields

$$2\pi r \Delta z H = \int_z^{z+\Delta z} \int_0^r \alpha I_{0h} \exp\left(-2r'^2/\omega_p^2\right) \exp(-\alpha z') 2\pi r' dr' dz'. \quad 3-11$$

Solution of this equation gives the heat flux as

$$H = \frac{I_{0h} \omega_p^2}{4\Delta z} (1 - \exp(-\alpha \Delta z)) \exp(-\alpha z) \left(\frac{1 - \exp\left(-2r^2/\omega_p^2\right)}{r} \right). \quad 3-12$$

Using a standard definition for Gaussian beams

$$P_{ph} = \frac{1}{2} \pi \omega_p^2 I_{0h} \quad 3-13$$

and also performing a series expansion of the $\exp(-\alpha \Delta z)$ term (as in section 3.3.3) we obtain

$$H(r, z) = \left(\frac{\alpha P_{ph}}{2\pi K} \right) \exp(-\alpha z) \left(\frac{1 - \exp\left(-2r^2/\omega_p^2\right)}{r} \right). \quad 3-14$$

Substituting this final equation into 3-4, and integrating to the crystal boundary R we obtain the following expression for the radial temperature gradient $\Delta T(r, z)$

$$\int_r^R H dr' = -K \int dT$$

$$\Delta T(r, z) = \frac{\alpha P_{ph}}{2\pi K} \exp(-\alpha z) \left[\ln\left(\frac{R}{r}\right) - \int_r^R \frac{\exp\left(-2r'^2/\omega_p^2\right)}{r'} dr' \right]. \quad 3-15$$

The final term in this temperature profile can be expressed in terms of standard exponential integrals, or alternatively it can be evaluated numerically using Simpson's Rule.

In equation 3-15 the exponential integral term falls rapidly to zero when r is greater than ω_p . Hence for both types of pump beam profile (comparing equations 3-7 and 3-15) the radial temperature gradient outside the pumped region behaves as

$$\Delta T(r, z) = \frac{\alpha P_{ph}}{2\pi K} \exp(-\alpha z) \ln\left(\frac{R}{r}\right). \quad 3-16$$

This is the intuitively correct result, as we would expect the temperature profile far from the pumped region to be independent of the shape of the pump beam. It is also worthwhile to note that the temperature difference between the disc axis and barrel is independent of the heatsink temperature for both top-hat and Gaussian pump beam profiles (as long as the temperature differences are not sufficient to significantly alter the thermal properties of the gain medium).

3.3.5 Mean temperature distribution

Calculation of the mean temperature distribution is important as the basis for thermal lens calculations. As opposed to the finite element analysis detailed previously, we now consider absorption, and the consequent heat deposition, along the entire length of the laser rod. Formally, this is achieved by integration of the finite element analysis equations over the rod length L . Sections 3.3.6 and 3.3.7 outline the solutions for top-hat and Gaussian pump beam profiles.

3.3.6 Top-hat pump beam profile

The radial heat equation can be solved in identical fashion to section 3.3.3, but now considering the rod length L as opposed to a slice of thickness Δz . The resulting equation for the mean radial temperature gradient $\Delta T(r)$ is

$$\Delta T(r) = \frac{P_a}{4\pi KL} \times \begin{cases} 2 \ln\left(\frac{R}{\omega_p}\right) + 1 - \left(\frac{r}{\omega_p}\right)^2 & , \quad r \leq \omega_p \\ 2 \ln\left(\frac{R}{r}\right) & , \quad r > \omega_p \end{cases} \quad 3-17$$

where

$$Q = \frac{P_a}{\pi\omega_p^2 L} \quad 3-18$$

$$P_a = P_{ph}(1 - \exp(-\alpha L)).$$

As defined previously, P_{ph} is the fraction of the incident pump power available to contribute to heat deposition.

3.3.7 Gaussian pump beam profile

In this case, equation 3-3 is now integrated over the length L of the laser disc

$$\int_0^L \int_0^r H(r', z') 2\pi r' dr' dz' = \int_0^L \int_0^r \frac{dP(r', z')}{dV} 2\pi r' dr' dz'. \quad 3-19$$

Following through the finite element analysis of section 3.3.4, but now with the new integral limits, yields the following expression for the heat flux

$$H(r) = \frac{I_{0h}\omega_p^2}{4L}(1 - \exp(-\alpha L)) \left(\frac{1 - \exp\left(-2r^2/\omega_p^2\right)}{r} \right). \quad 3-20$$

The corresponding mean radial temperature gradient is

$$\Delta T(r) = \frac{P_{ph}}{2\pi KL}(1 - \exp(-\alpha L)) \left(\ln\left(\frac{R}{r}\right) - \int_r^R \frac{1 - \exp\left(-2r'^2/\omega_p'^2\right)}{r'} dr' \right). \quad 3-21$$

3.3.8 Modelling results

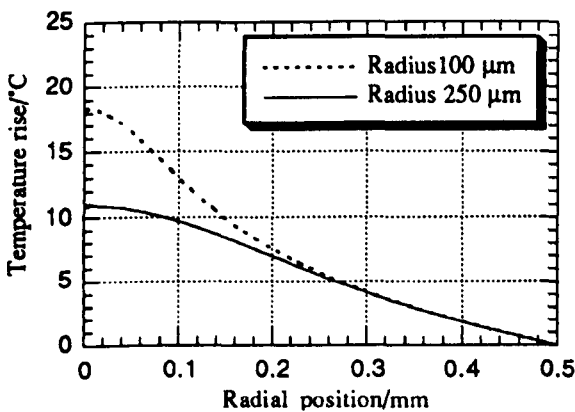
Four pieces of Pascal code were written, two each for the finite element analysis and mean temperature distribution problems, separately considering top-hat and Gaussian pump beam profiles. With the finite element analysis, the gain medium is divided up into 200 μm thick slices. For each slice the amount of pump light absorbed is calculated taking into account any pump beam absorption prior to it. The mean temperature distribution uses the total amount of pump power absorbed by the gain medium. In both cases, the radial temperature profile is determined by stepping out radially from the centre of the laser disc to its barrel in 200 increments. After each increment the corresponding temperature is calculated. In this fashion the radial temperature profile is obtained.

In this section temperature distributions are calculated for cases of practical interest. As detailed in chapter four, the experimental work was carried out using a 3 W cw laser diode focussed to a spot with a full width at half maximum (FWHM) in the range of order 50 to 500 μm , depending on the arrangement of the pump optics. Typically the optics train transmitted 80-90% of the diode output. Therefore the maximum power incident on a laser disc pumped by a single 3 W laser diode was of order 2.5 W.

It is instructive to make comparisons between Gaussian and top-hat profile beams. As a basis for comparison, consider the case of both profiles having the same peak intensity, and also containing the same power. In order for these conditions to hold the radius of the Gaussian profile has to be $\sqrt{2}$ that of the top-hat profile.

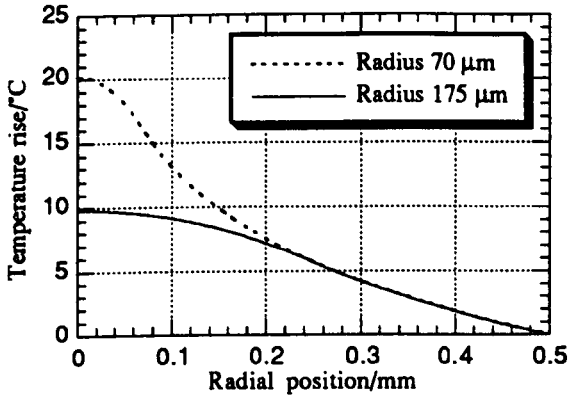
As listed in table 3.1, the principal crystalline laser hosts of interest are YAP and YLF, with YAG included for the purposes of comparison. The laser diode pumping bands of thulium (in standard concentrations) around 790 nm in these hosts possess absorption coefficients α of 6.5 cm^{-1} and 4.5 cm^{-1} respectively (5.5 cm^{-1} for YAG). Experimental work was undertaken using 3 mm thick laser discs, with diameters ranging from 1 to 5 mm. The following figures are derived using these parameters, thus allowing real scenarios to be modelled.

Figures 3.2 and 3.3 serve to illustrate the radial variation of the mean temperature rise (above the heatsink temperature) in a YLF laser rod in order to compare the temperature profiles induced by Gaussian and top-hat pump beam profiles. Both graphs clearly illustrate the similarity between the temperature distributions produced by the different pump beam shapes, and how the temperature profiles converge away from the rod axis (region of greatest pumping). The peak temperature rise for corresponding Gaussian and top-hat beam radii agree to within 10% of each other, confirming the expected result.



YLF laser rod ; 1 mm disc diameter ; 2.5 W incident pump power

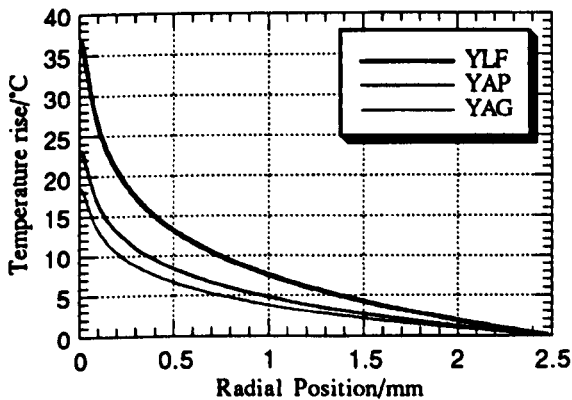
Figure 3.2 Mean temperature distributions induced by Gaussian pump beam profiles



YLF laser rod ; 1 mm disc diameter ; 2.5 W incident pump power

Figure 3.3 Mean temperature distributions induced by top-hat pump beam profiles

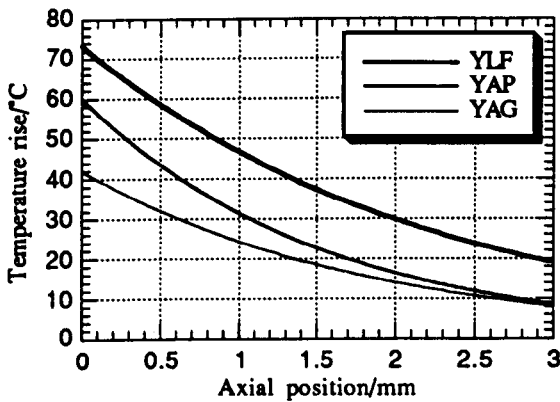
In order to compare temperature rises in the different host crystals the mean temperature distribution with 2.5 W incident power was determined for each host in turn. The predicted profiles are depicted in figure 3.4, for the extreme case of pumping a small region (Gaussian pump beam of radius of 50 μm) of a 5 mm diameter YLF laser disc.



2.5 W incident power ; 50 μm radius Gaussian pump beam ; 2.5 mm radius laser disc

Figure 3.4 Mean temperature distributions in laser hosts of interest

It is also of interest to compare the axial temperature variations in the three host crystals being studied here. The finite element analysis outlined in sections 3.3.2 to 3.3.4 was used to generate the data in figure 3.5, with parameters identical to those used above.



2.5 W incident power ; 50 μm radius Gaussian pump beam ; 2.5 mm radius laser disc

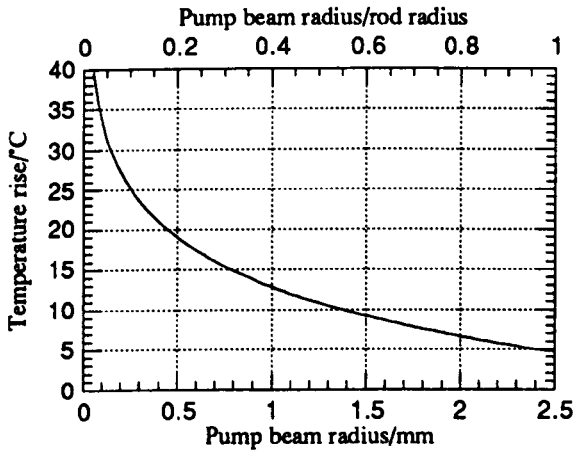
Figure 3.5 Axial temperature variations in laser hosts of interest

Figure 3.5 clearly illustrates that for a zero divergence pump beam the maximum temperature rise occurs at the pumped face (the region of maximum pump beam absorption, hence heat deposition). As outlined in section 3.2.2 this axial temperature variation is not strictly correct, as no account has been taken of end-cooling effects, nor of axial thermal conduction in the laser rod. The location of the highest temperature will, in reality, be shifted in from the pumped face by an amount determined by the magnitude of the cooling effect at the pumped face (note that a similar effect will be present at the opposite end of the laser rod, although it will inherently be of smaller magnitude due to the rod temperature being closer to ambient at this face). In the cases under consideration here end-cooling effects (either by convection or radiation) are sufficiently small as to make little difference to the analytically calculated axial temperature variation⁵. Hence the results generated here give a good estimate of the peak temperature rises, which in turn allow effects on laser threshold to be determined to a fair degree of accuracy.

The previous two figures highlight the fact that due to its poorer thermal conductivity the induced temperature rises in YLF are the greatest of the three, even though the lower absorption coefficient produces the least heat deposition. The slightly poorer thermal conductivity, allied with higher absorption, combine to produce greater temperature rises in YAP than in YAG.

Returning to the mean temperature distribution, the variation in the peak temperature rise as a function of pump spot radius (at fixed pump power) is investigated in figure 3.6 for a 3 mm long, 2.5 mm radius YLF disc ; the Gaussian pump beam radius varies

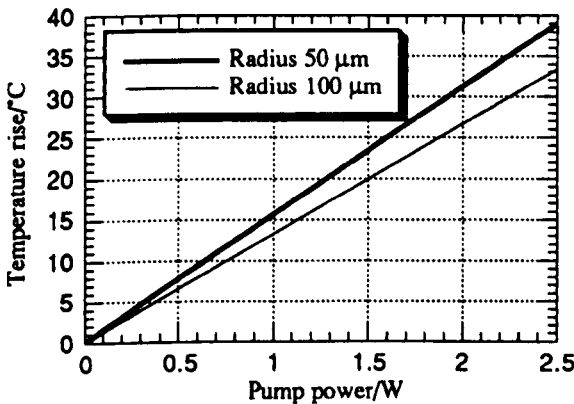
from 0.05 to 2.5 mm. In fact it is the *ratio* of the pump beam radius to the disc radius, with all other parameters (pump power, absorption coefficient and rod length) fixed in value, that determines the peak temperature rise, and hence this is also included as an axis of the graph. This means that the results graphed here can be generalised to any YLF disc radius.



YLF laser disc ; 2.5 W incident power

Figure 3.6 Variation of peak temperature rise with pump spot size for fixed pump power

Keeping pump and rod sizes constant, the variation of peak temperature with pump power can be investigated. The results are shown here in figure 3.7, for the particular case of a 2.5 mm radius YLF disc. The graph clearly illustrates the linear dependence of the peak temperature rise with pump power.



YLF disc ; 2.5 mm radius ; Gaussian pump beam radii 50 and 100 μm

Figure 3.7 Variation of peak temperature rise with pump power

The behaviour depicted in the previous two graphs (temperature rise determined by ratio of pump beam to rod radius for fixed pump power ; temperature rise proportional

to pump power for fixed pump beam to rod radius ratio) can be confirmed by studying the mean temperature profile equations 3-17 and 3-21. The latter equation, for a pump beam with a Gaussian intensity profile, does not show the behaviour predicted by figure 3.6 explicitly, but was verified by running the computer code with a range of pump beam and laser crystal radii, keeping the ratio of the two constant.

3.4 Thermal lensing

3.4.1 General theory

The phase change associated with passage through a lens is given by the following⁶

$$\Delta\phi_f = -\frac{kr^2}{2f} \quad 3-22$$

where f is the effective focal length, k is the wave number of the incident radiation and r is the radial coordinate i.e. a parabolic variation in phase describes a spherical lens (in the paraxial limit). The total phase change $\Delta\phi$ on a single pass through the gain medium of length l is

$$\Delta\phi(r) = \int_0^l k\Delta n(r, z) dz \quad 3-23$$

where $\Delta n(r, z)$ is the change in refractive index arising from temperature effects. There are three temperature dependent effects to consider⁷:

- (i) Variations due to dn/dT
- (ii) Thermal deformation of the laser crystal ends
- (iii) Thermally induced strain birefringence

This last effect is not trivial to calculate, and has been omitted from the following analysis (it also has the smallest magnitude of the three contributions). The remaining two contributions to the thermal lensing can be calculated by considering the heat deposition in the crystal as a whole i.e. in effect using the mean temperature distribution.

The variation of refractive index with temperature yields the expression

$$\Delta n_r(r, z) = \Delta T(r, z) \frac{dn}{dT}. \quad 3-24$$

Heat deposition in the gain medium causes distortions in the flatness of the laser disc ends, due to the thermally induced stresses and strains in the gain medium. A radially varying thermally induced strain produces curvature of the laser disc ends, thus producing a lensing effect. The phase change associated with this effect is⁸

$$\Delta\phi = k\Delta L(n_0 - 1) = kL\varepsilon_z(n_0 - 1) \quad 3-25$$

where ε_z is the mean axial strain in the laser disc. The strain distribution follows closely the temperature profile, assuming that mechanical constraining effects are small in comparison, and so the ΔT term in 3-24 can be used in 3-25 to obtain the phase change, hence the induced thermal lens focal length. As equation 3-25 stands, there is no upper limit on the relative expansion of adjacent planes of ions in the crystal produced by the radial temperature gradient. In reality, the expansion of adjacent

planes is restricted to a small fraction of the interionic separation, beyond which the material will fracture. This places an upper bound on the applicability of equation 3-25.

3.4.2 Top-hat pump beam profile

In the case of end-pumping the pump spot typically does not fill the laser disc diameter, and so the temperature profile is only parabolic over a small region. This implies that any spherical lens type behaviour is restricted to this small area of the disc. In order to evaluate thermal lensing, we need to assume that only the distortions over the pumped area are of interest i.e. the two micron laser mode has a beam radius no greater than the pump spot radius. This is not entirely unreasonable, as usually the pump and laser mode are made to have comparable diameters in order to maximise excitation of the fundamental transverse mode.

Within the pumped volume of the gain medium, the radial variation of the refractive index is described by⁷

$$\Delta n_r(r) = -\frac{Q}{4K} \frac{dn}{dT} r^2. \quad 3-26$$

The associated phase change over a length L is given by

$$\begin{aligned} \Delta\phi &= kL\Delta n_r \\ &= -kL \frac{Q}{4K} \frac{dn}{dT} r^2. \end{aligned} \quad 3-27$$

Comparison of 3-27 with 3-22, and using the relationship between P_a and Q in 3-18, reveals the focal length induced by the temperature dependent refractive index f_T to be

$$f_T = \frac{2\pi\omega_p^2 K}{P_a} \left(\frac{dn}{dT} \right)^{-1}. \quad 3-28$$

The effects of laser disc end-face curvature can be evaluated using 3-25. The radially varying portion of the axial strain is

$$\varepsilon_z = -\frac{\alpha_0 P_a}{4\pi\omega_p^2 K L} (1 + \nu) r^2 \quad 3-29$$

where α_0 is the thermal expansion coefficient and ν is Poisson's ratio for the gain medium material. Substituting for ε_z in 3-25, then comparing with 3-22 reveals the focal length induced by laser disc end-face curvature to be

$$f_C = \frac{2\pi\omega_p^2 K}{P_a} \left(\alpha_0 (1 + \nu) (n_0 - 1) \right)^{-1}. \quad 3-30$$

Thus the combined thermal effects result in the gain medium behaving as a lens with focal length

$$f = \left(\frac{1}{f_T} + \frac{1}{f_C} \right)^{-1} = \frac{2\pi\omega_p^2 K}{P_a} \left(\frac{dn}{dT} + \alpha_0(1+\nu)(n_0 - 1) \right)^{-1}. \quad 3-31$$

3.4.3 Gaussian pump beam profile

The $\Delta T(r,z)$ term derived previously (equation 3-15) contains an exponential integral component. From a book of tables of mathematical functions⁹, this can be written as a power series in (r/ω_p) . Referring to equations 3-22 to 3-25 it is the quadratic term in ΔT that is of interest in calculating the thermally induced phase change. Extracting this term yields

$$\Delta n_T(r,z) = -\frac{\alpha P_{ph} \exp(-\alpha z) \frac{dn}{dT} 2r^2}{4\pi K \omega_p^2}. \quad 3-32$$

Inserting this term into equation 3-23 and integrating gives the phase change associated with thermal lensing. Using equation 3-22 the effective focal length f_T can then be written as

$$f_T = \frac{\pi\omega_p^2 K}{P_a} \left(\frac{dn}{dT} \right)^{-1}. \quad 3-33$$

The thermally induced end-face curvature effects are assumed to be similar to the top-hat profile case, but now with ω_p as the $1/e^2$ radius of the pump beam. As in the top-hat profile case, the axial strain distribution follows that of the temperature. Again it is the quadratically varying term that is of interest. Extracting this from the expression for ϵ_z leads to an end-face curvature focal length of

$$f_C = \frac{\pi\omega_p^2 K}{P_a} \left(\alpha_0(1+\nu)(n_0 - 1) \right)^{-1}. \quad 3-34$$

Hence the combined focal length of the gain medium can be written as

$$f = \frac{\pi\omega_p^2 K}{P_a} \left[\frac{dn}{dT} + \alpha_0(1+\nu)(n_0 - 1) \right]^{-1}. \quad 3-35$$

3.4.4 Modelling results

As with the temperature distribution calculations, separate pieces of code were written to investigate thermal lensing induced by top-hat and Gaussian pump beam profiles. After the initial parameters (choice of gain medium, disc thickness and radius, absorption coefficient, beam radius and incident optical power) have been input, the thermal lens is calculated as described in the theory sections previously (sections 3.4.2

and 3.4.3). The laser diode and pumping geometry considered here are identical to the ones described in section 3.3.8.

Inspection of equations 3-31 and 3-35 reveals that the only difference between the expressions for focal lengths induced by top-hat and Gaussian pump beams is a factor of two. As a consequence identical focal lengths are produced when we compare Gaussian pump beam profiles with $\sqrt{2}$ the radius of top-hat pump beam profiles. This behaviour reflects the temperature profile results in section 3.3.8.

The thermally induced lens has a focal length proportional to the square of the pump beam radius, and is also inversely proportional to the pump power, hence heat deposited. This dependency immediately suggests making the pump beam as large as possible in order to minimise the focussing power. However in order to maximise laser efficiency it is desirable to match the pump beam size to the mode size of the two micron laser resonator containing the gain medium. Therefore a large pump beam implies a large mode size which will raise the laser threshold, impacting severely on the overall efficiency. If the mode size is a significant fraction of the laser disc diameter, diffraction losses also start to become significant, with the disc acting as a limiting aperture in the resonator, clipping the wings of the laser mode.

We can also note that the thermally induced lens is independent of the disc radius R . This result can be derived by looking at the equations for the mean temperature profiles (equations 3-17 and 3-21). Within the pump beam radius ω_p the temperature difference $T(r=0) - T(r=\omega_p)$ is independent of R for both types of pump beam shape, all other parameters being fixed in value, with commensurate behaviour of the thermal lens.

Calculated thermal lenses are tabulated in table 3.2, using data from table 3.1. The dependence of focal length on pump beam size and power is clearly highlighted.

Pump parameters	YAP	YLF	YAG
Pump radius 50 μm Incident power 2.5 W	a: 4.2 b: 6.1 c: 3.9	a: 14.6 c: 104.3	6.7
Pump radius 50 μm Incident power 1.5 W	a: 7.0 b: 10.2 c: 6.5	a: 24.3 c: 173.8	11.2
Pump radius 50 μm Incident power 0.5 W	a: 21.0 b: 30.5 c: 19.5	a: 73.0 c: 521.5	33.5
Pump radius 100 μm Incident power 2.5 W	a: 16.8 b: 24.4 c: 15.6	a: 58.4 c: 417.2	26.8
Pump radius 100 μm Incident power 1.5 W	a: 28.0 b: 40.7 c: 26.0	a: 97.3 c: 695.3	44.7
Pump radius 100 μm Incident power 0.5 W	a: 84.0 b: 122.0 c: 78.0	a: 292.0 c: 2086.0	134.0

Gaussian pump beam profiles

Table 3.2 Thermal lens focal lengths (in millimetres)

An interesting point to note from the data in table 3.1 is that the dn/dT value for YLF is negative around room temperature. This means that the two terms contributing to the thermal lens act in opposition, reducing the focussing power, but still producing a positive lens. Inspection of the focal lengths in table 3.2 confirms that the focussing in YLF is noticeably weaker than in either YAP or YAG, particularly for polarisation parallel to the YLF c-axis, this despite the greater temperature rise in YLF due to its lower thermal conductivity. Such behaviour needs to be taken in conjunction with the different absorption coefficient of thulium in the three hosts - the lower absorption coefficient in YLF also contributes to weaker focussing, in the case of incomplete absorption of the pump beam being considered here .

It is also important to note that the birefringent materials will produce an astigmatic thermal lens, as illustrated by the sample data in the table. However incomplete knowledge of the values of the relevant parameters in all crystallographic directions means that the calculated focal lengths can only be used as an approximation to the expected lensing behaviour of these laser materials.

A major advantage of naturally birefringent host crystals is that any thermally induced birefringence caused by heat deposition is by comparison very small, and so can be ignored. However for cubic YAG this is not the case. Thermally induced birefringence can have an extremely deleterious effect on the performance of lasers utilising isotropic gain media⁷. However as stated earlier calculation of thermally induced birefringence in an end-pumped geometry is a complex matter, and so has had to be omitted from the present analysis. It makes only a small contribution to the thermal lensing relative to the other two mechanisms, and so its omission from the analysis does not invalidate the results for YAG.

Table 3.2 indicates the possibility of generating very short (of the order one centimetre) focal length lenses in laser diode end-pumped two micron lasers. This has a significant impact on the design of such lasers, where the resonator has to support these strong thermal lenses. The short focal length of the thermally induced lens also means that aberrations associated with this lensing can be severe, a further problem to address during resonator design. As long as the thermally induced focal length (or lengths in the case of birefringent materials) is significantly greater than the resonator length at all pump powers used then any changes in the strength of the lens (or lenses) will only be a minor perturbation to the resonator mode size.

In practice, the end-pumped geometry employed in this work, using tightly focussed diode pump beams, makes experimental measurement of the thermal lensing a nontrivial task. This issue is addressed in more detail in the following chapter.

3.5 Thermal fracture limit

3.5.1 Theory

The ultimate limit on pumping of a laser crystal is the possibility of thermal fracture, caused by excessive heat deposition. As the heat load in the laser crystal increases, there is a resultant increase in the thermal stresses finally leading to fracture of the crystal at the maximum stress point. In general the compressive stresses at the (pumped) crystal axis are greater than the maximum tensile stresses which occur at the barrel of the crystal. However, since most materials are stronger in compression than in tension, stress fracture is typically initiated at the position of maximum tensile stress, in this case the outer edge of the crystal. In the end-pumped geometry being investigated here, the maximum stress occurs along the circumference of the crystal on the pump entrance face ; furthermore, the tangential (hoop) stress has the largest value^{7,10}. It is evident that determination of the fracture limit cannot be performed using analytically calculated, axially averaged quantities ; rather, numerical evaluation is required. From the literature, notably Cousins' paper⁸, we can compare analytically and numerically evaluated results to find an estimate of the thermal fracture limit, as outlined here.

The analytical value of the mean axial stress at the laser rod boundary is given by

$$\sigma_{\theta} = \frac{\alpha_0 E P_a}{4 \pi K L} \left(1 - \frac{1}{2} \frac{\omega_p^2}{R^2} \right) \quad 3-36$$

where E is the Young's modulus of the gain medium. The expression is valid for the condition that the pump beam radius ω_p is smaller than the laser crystal radius R. Insertion of the tensile strength σ_T for σ_{θ} allows the maximum heat deposition to be determined. Comparison of this value with numerically calculated data for the tangential stress at the boundary of the pumped face reveals that the maximum heat deposition allowed is overestimated by a factor of two using the analytical method. Hence a rule of thumb for the thermal fracture limit is given by

$$P_{a_{max}} = \frac{2 \pi K L \sigma_T}{\alpha_0 E} \left(1 - \frac{1}{2} \frac{\omega_p^2}{R^2} \right)^{-1} \quad 3-37$$

where $P_{a_{max}}$ is the maximum heat that can be deposited in a beam of radius ω_p without inducing thermal fracture of the laser crystal. It must be emphasised that this expression can only be used to give a rough estimate of the permissible thermal loading.

3.5.2 Results

As part of a literature search for material and thermal parameters a value for the tensile strength of YLF was found¹; corresponding values for YAP and YAG were derived from data in Koechner⁷ (see table 3.1).

Using equation 3-36 values for the maximum heat deposition as a function of the ω_p/R ratio can be determined. Typical results are tabulated below, for 3 mm thick discs.

ω_p/R	YAP	YLF	YAG
0.02	a: 15.9 b: 34.6 c: 13.8	a: 4.2 c: 6.8	21.3
0.1	a: 16.0 b: 34.8 c: 13.9	a: 4.2 c: 6.8	21.4
0.5	a: 18.2 b: 40.0 c: 15.8	a: 4.8 c: 7.7	24.3
1	a: 31.8 b: 69.3 c: 27.6	a: 8.3 c: 13.5	42.6

Table 3.3 Maximum heat deposition values (in Watts)

Inspection of the tabulated data reveals that YLF will reach its thermal fracture limit at low powers compared to both YAP and YAG. This is not surprising, as the latter two materials have superior thermal and mechanical properties. For the birefringent gain media the thermal fracture limit is determined by the "weakest" crystallographic direction i.e. the direction that reaches its fracture limit at the lowest heat load.

The thermal fracture limit is not a strong function of the ω_p/R ratio, but we can see that the maximum heat deposition allowed remains almost constant until the pump beam radius reaches one half the rod radius. This behaviour immediately suggests pumping as large a volume of the gain material as possible to reduce the risk of thermal fracture. However as discussed in the context of thermal lensing such a pumping scheme is usually not desirable. Rather it would be preferable to reduce the value of R. For a given pump spot size this reduces the temperature rise between the centre of the laser crystal and its circumference, which in turn reduces the magnitude of the thermally induced stresses and strains.

The thermal loading determined by equation 3-37 allows laser design to be carried out such that the thermal fracture limit of the gain medium is never exceeded. Using a single 3 W cw laser diode the thermal fracture limit will not be exceeded for the laser

crystals investigated here, assuming good contact between the barrel of the laser disc and the heatsink.

In practice, fracture stress in laser crystals depends also on the surface finish of any pumped surfaces. The size and number of any microcracks will contribute to the actual strength of the laser crystal and the heat load it will withstand. Assuming a good laser quality polished finish to the laser crystal faces, the thermal fracture limit will be dominated by the tangential stress calculated in equation 3-36.

3.6 Population distributions

The previous sections of this chapter have dealt with the calculation of temperature distribution, thermal lensing and thermal fracture limit due to absorption of light and subsequent heat generation in a solid-state laser host. These are important considerations in understanding laser operation in any solid-state laser host where heat is generated in the gain medium.

In the case of two micron thulium and holmium lasers a further consideration is the quasi-three level nature of their operation. The lower laser level is in general a high-lying Stark splitting of the ground state energy level manifold, typically between 300 and 600 cm^{-1} from the bottom of the ground state, resulting in a significant lower laser level population.

This section follows on from the basic lasing dynamics outlined in chapter two to develop an understanding of the population distributions within the energy level manifolds containing the laser levels, drawing on the earlier work of this chapter concerning temperature distributions.

Each energy level manifold is independently in thermal equilibrium. Therefore the distribution of population amongst the levels of each manifold will be described by a Boltzmann distribution, which is of course temperature dependent. Furthermore, the distribution of population within each manifold takes place on a very rapid (subpicosecond) timescale, far faster than any other processes occurring in the system, including the stimulated emission rate on the laser transition. Therefore as excitation is either added or removed from a particular energy level manifold, the remaining population always maintains a Boltzmann distribution, which is determined by temperature and the detailed nature of the splittings within the energy level manifold.

Let the fraction of the first excited energy level manifold population residing in the upper laser level be f_u , and the fraction of the ground state energy level manifold residing in the lower laser level be f_l . Appendix A tabulates the relevant energy levels of thulium and holmium. Taken in conjunction with a particular value of temperature, partition functions of the Boltzmann population distributions can be determined leading to values for the temperature dependent fractional populations f_u and f_l .

Because the lower laser level is populated, a certain fraction of the ground state population has to be excited before a population inversion on the laser transition can be created - the inversion threshold. Making the assumption that the entire population is shared between the ground and first excited state energy level manifolds only, the fraction F of the dopant population that needs to be excited to reach inversion threshold is given by

$$F = \frac{f_l}{f_u + f_l} \quad 3-38$$

Pascal code was generated which calculated the partition functions of the ground and first excited state energy level manifolds in order to yield values of f_l and F , using the known energy level values and taking temperature as an input parameter. A simple looping structure was implemented to allow the temperature to be varied over a suitable range.

Figures 3.8 to 3.13 are derived from the computer generated data and illustrate first the temperature variation of the lower laser level population f_l of thulium in YAP, holmium in YAP and holmium in YLF, followed by the temperature dependence of the fractional inversion threshold F for the same three combinations of lasing ion and host crystal lattice.

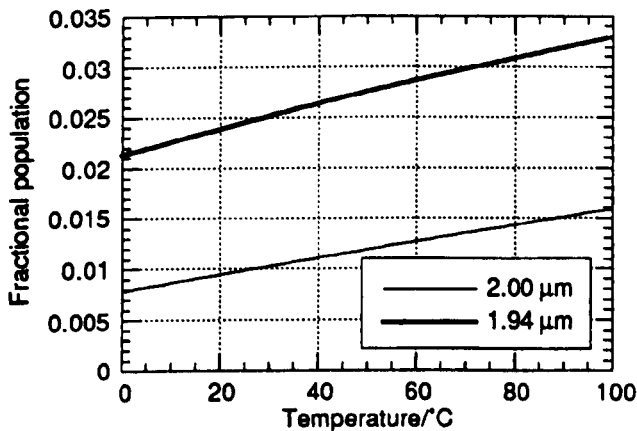


Figure 3.8 Lower laser level population of thulium in YAP

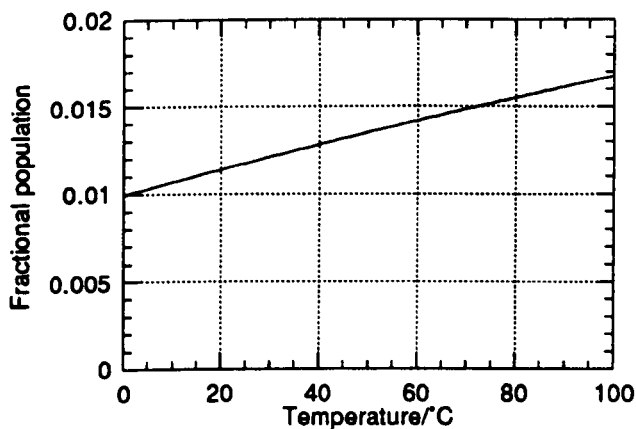


Figure 3.9 Lower laser level population of holmium in YAP

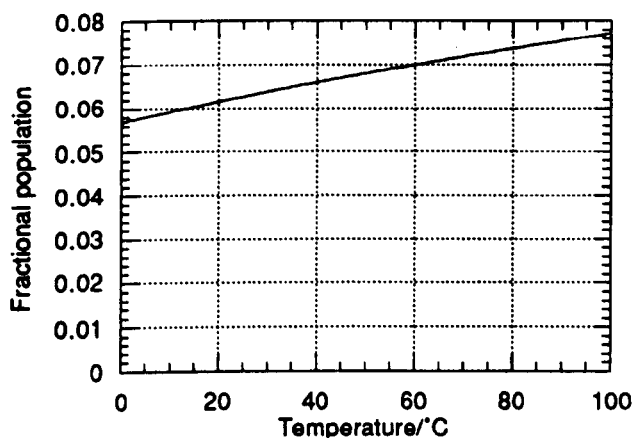


Figure 3.10 Lower laser level population of holmium in YLF

Depending on which particular wavelength lases in Tm:YAP, the fractional lower laser level population can vary by a factor of three for a fixed crystal temperature. From figures 3.4 and 3.5 the most severe temperature rise in YAP, under the typical experimental conditions detailed in the next chapter, was calculated to be 50°C. Also from the following chapter, a heatsink temperature of 15°C was employed, leading to a peak temperature at the centre of the pumped region (and therefore the laser mode) of order 65°C. Inspection of figure 3.8 reveals that the fractional lower laser level population varies from 1.3 to 2.9%.

Using similar temperature values for Ho:YAP, the 2.12 μm laser transition will have a fractional lower laser level population of 1.5%, by inspection of figure 3.9.

Carrying out a similar analysis for the 2.067 μm transition on Ho:YLF, figures 3.4 and 3.5 reveal that the maximum temperature rise will be just under 70°C, in turn

yielding from figure 3.10 a fractional lower laser level population of 7.5%. This is a significantly higher value than for either thulium or holmium in YAP, and is simply a measure of the much reduced splitting in YLF compared to YAP as clearly illustrated in the tabulated energy level values of Appendix A.

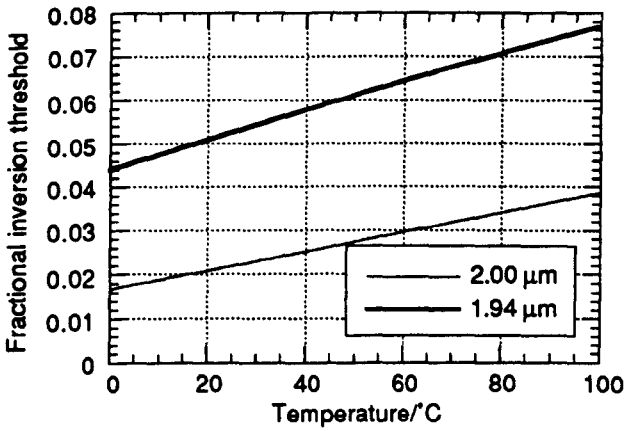


Figure 3.11 Fractional inversion threshold of thulium in YAP

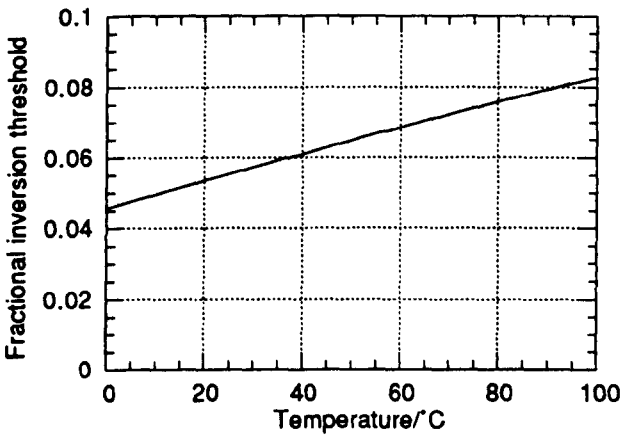


Figure 3.12 Fractional inversion threshold of holmium in YAP

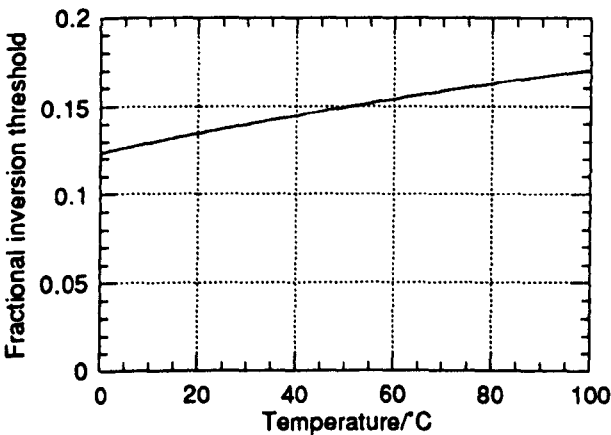


Figure 3.13 Fractional inversion threshold of holmium in YLF

Using the same temperature values as for the fractional lower laser level populations previously, the fraction of the ground state population that needs to be excited in order to create a population inversion threshold varies from 3.1% to 6.6% in Tm:YAP, depending on the exact laser wavelength. The corresponding values for Ho:YAP and Ho:YLF are 7.0% and 16.5% respectively. Once again, holmium in YLF suffers from having relatively small energy level manifold widths compared to the other two laser crystals of interest. The temperature rises used here in the calculation of lower laser level populations and fractional inversion thresholds are the maximum temperature rises predicted in section 3.3, and thus serve to illustrate the worst case scenario.

The fractional inversion threshold is a more temperature sensitive quantity than the fractional lower laser level population since it depends on both the fractional populations of the upper and lower laser levels. As the temperature decreases (increases), the value of f_u increases (decreases), the value of f_l decreases (increases), with the resultant value of F decreasing (increasing). This is one of the principal advantages of running such lasers at low temperatures, as it minimises the inversion threshold contribution to the lasing threshold.

3.7 Excitation sharing

In order to take advantage of high power AlGaAs laser diodes as pump sources combined with the greater stimulated emission cross-section of holmium versus thulium, laser crystals are often co-doped with both thulium and holmium, the former allowing absorption of the diode pump radiation, the latter providing the two micron laser transition. Excitation sharing between the thulium 3F_4 and holmium 5I_7 energy level manifolds provides the mechanism for lasing to occur on the holmium. This section details how excitation is shared between these two excited states.

Consider two pairs of energy levels 1 and 2 depicted in figure 3.14. Each level has a characteristic energy E_{ij} and population number density n_{ij} .

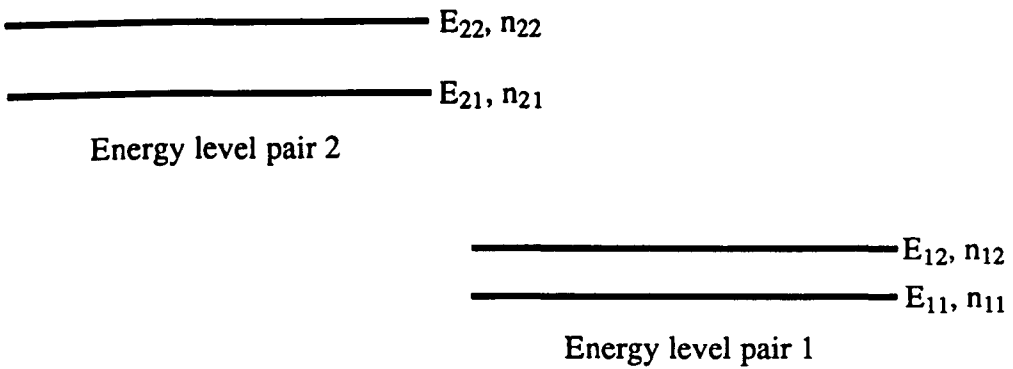


Figure 3.14 Energy level pairs

Initially, consider the energy level pairs separately, with both independently in thermal equilibrium. From the Boltzmann distribution, the mean energy of pair 1 is

$$\bar{E}_1 = \frac{E_{11} + \alpha E_{12}}{Z_1} \quad 3-39$$

where

$$\alpha = \exp\left(\frac{-(E_{12} - E_{11})}{kT}\right) \quad 3-40$$

and

$$Z_1 = 1 + \alpha \quad 3-41$$

is the partition function of the system.

Similarly for energy level pair 2

$$\bar{E}_2 = \frac{E_{21} + \beta E_{22}}{Z_2} \quad 3-42$$

where

$$\beta = \exp\left(\frac{-(E_{22} - E_{21})}{kT}\right) \quad 3-43$$

and

$$Z_2 = 1 + \beta. \quad 3-44$$

Consider the two pairs of levels now as being coupled together. In the case where the transfer rate of population between the coupled levels is fast compared to their fluorescence decay rates, then the coupled levels can be considered as one system in thermal equilibrium.

In order to calculate the relative population number density in each of the pairs of the coupled system, the total population density N is required

$$N = n_{11}Z_1 + n_{21}Z_2. \quad 3-45$$

The fraction of the total population f_1 residing in energy level pair 1 is

$$\begin{aligned} f_1 &= \frac{n_{11}Z_1}{N} \\ &= \frac{1}{1 + \frac{Z_2}{Z_1} \gamma} \end{aligned} \quad 3-46$$

where

$$\gamma = \exp\left(\frac{-(E_{21} - E_{11})}{kT}\right). \quad 3-47$$

This assumes the concentration of the energy level pairs 1 and 2 is equal. Labelling the respective concentrations c_1 and c_2 the final equation is

$$f_1 = \frac{1}{1 + \frac{c_2 Z_2}{c_1 Z_1} \gamma}. \quad 3-50$$

This result can be generalised to energy level manifolds containing many individual levels e.g. the thulium 3F_4 and holmium 5I_7 first excited state energy level manifolds. The critical parameters are the relative concentrations of the two species, the partition functions of the energy level manifolds which is a measure of the distribution of population within each manifold, and the splitting between the bottom levels of the manifolds through the γ term.

Inspection of the energy levels listed in Appendix A reveals that in general the holmium 5I_7 energy level manifold lies at lower energies than the thulium 3F_4

manifold. Therefore in the generalised treatment outlined here energy level pair 1 corresponds to holmium and energy level pair 2 to thulium.

This calculation yields the excitation sharing between the thulium and holmium coupled energy level manifolds. It is the steady state solution to the excitation sharing phenomenon, taking no account of the magnitude of the transfer rate of excitation between the thulium and holmium, and the corresponding reverse process. It is also an upper bound on the fraction of excitation that resides on the holmium, corresponding to the condition of low excited state population densities. For the materials investigated here the thulium concentration is over an order of magnitude greater than the holmium concentration, therefore as the excited state population density rises, excitation residing in thulium 3F_4 as a result of diode-pumping can diffuse rapidly among the thulium ions, but will find it increasingly difficult to locate ground state holmium ions to transfer to as the level of total excitation rises (French and Powell¹¹ measured the average "hopping time" between ions in 6% thulium doped YAG to be 43.5 ns, six orders of magnitude shorter than the fluorescence decay lifetime of the 3F_4 manifold). This is more typical of the situation in laser operation where the excited state population densities can be relatively high under intense pumping. In this scenario, the fraction of excitation resident on holmium will saturate as the thulium excited state population density continues to rise, thus breaking the thermal equilibrium between the thulium and holmium. However the simple thermal equilibrium analysis outlined here serves as a useful tool in determining approximately how excitation is shared between the coupled energy level manifolds of thulium and holmium, an important parameter in understanding laser operation in these double-doped materials.

Figure 3.15 illustrates the results of Pascal code written to calculate the fraction of excitation residing on holmium under steady-state pumping conditions. In a similar fashion to the previous section, the program uses the tabulated energy levels of Appendix A in order to calculate the partition functions, then uses equation 3-48 to determine the excitation sharing. By means of a simple loop structure this calculation can be performed over a wide range of temperatures.

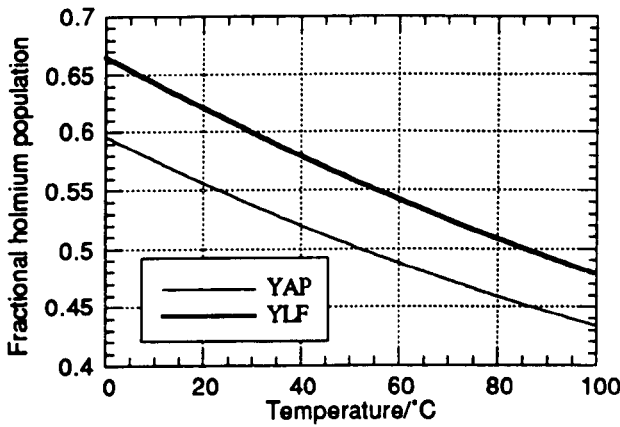


Figure 3.15 Fraction of excited state population residing on holmium in double-doped YAP and YLF

Concentrations employed here were 4.2% thulium, 0.28% holmium in YAP, and 6% thulium, 0.4% holmium in YLF; for both crystals these were equivalent to doping densities of $8.3 \cdot 10^{20} \text{ cm}^{-3}$ for thulium and $5.5 \cdot 10^{19} \text{ cm}^{-3}$ for holmium.

Using the same temperature rises as in section 3.6, the fraction of the excited state population residing on holmium in YAP is 0.48, whilst for YLF it is 0.50. Therefore in both cases approximately half the excited state population resides in the holmium 5I_7 first excited state manifold. Operation at lower temperatures increases the fractional occupation of the holmium at the expense of thulium, as the holmium levels form the lower portion of the coupled system. Therefore in double-doped crystals, lower laser crystal temperature not only has the benefit of lower inversion threshold contribution to the overall laser threshold, it also favours enhanced population of the holmium.

As in section 3.6, the temperature rises used are the maximum temperature rises occurring at the pumped face of the laser crystal, and so the corresponding temperature-dependent parameters calculated give the worst case scenarios. The variation of these quantities over a temperature range encompassing the typical experimental conditions encountered is illustrated in figures 3.8 to 3.15, allowing appropriate values for particular experimental conditions to be easily obtained.

3.8 Conclusions

In this chapter, steady-state thermal modelling has been described for several aspects of laser operation of thulium and holmium doped laser crystals. The end-pumped geometry employed can lead to severe temperature gradients which impact significantly on laser performance.

Analytical modelling of the temperature distribution produced by heat deposition on absorption of pump light in the gain medium was possible by assuming a cylindrically symmetric scenario with radial heat flow only. This assumption effectively reduced the problem to that of one dimensional heat flow. Two distinct types of solution were obtained, namely for the mean temperature distribution in the gain medium, and also for the axial variation of temperature along the gain medium length. The former has an exact analytical solution independent of the dimensions of the gain medium; the latter involved dividing the gain medium into a series of slices, then solving the radial heat equation for each slice independently. Using this technique, no account was taken of end effects, nor of axial heat conduction. However these were sufficiently small compared to the radial heat flow that their effect could be neglected to a first approximation.

Top-hat and Gaussian pump beam profiles were both investigated. Self-consistency of the radial heat equation solutions obtained for both these beam shapes was verified by the similarity of the mean temperature profiles generated by a Gaussian beam with $\sqrt{2}$ the radius of a top-hat beam.

The lower thermal conductivity of YLF compared to both YAP and YAG leads to steeper temperature gradients in the former for a given heat load. Even taking into account the weaker pump light absorption in YLF the peak temperature rise can reach 70°C, with a corresponding mean temperature rise of order 40°C, compared to a peak rise of 50°C in YAP with a corresponding mean temperature rise of order 25°C. These temperature rises were generated by simulating a 3 W laser diode as the pump source in the calculations.

Knowledge of the mean temperature distribution allowed thermal lensing effects to be evaluated. The two contributions to thermal lensing considered here were the change of refractive index with temperature and end-face curvature effects. Thermally induced stress birefringence also contributed to the lensing, but was been omitted due

to the complexity of the calculation for end-pumped geometries. Even in isotropic hosts such as YAG, its contribution to the total lensing is small, and so its omission did not invalidate the results derived here.

According to the modelling, thermally induced lenses with focal lengths of the order of one centimetre can be generated in YAP by pump beams of diameter of order 100 μm . In YLF the change of refractive index with temperature is negative, which counteracts the end-face curvature effects and thus reduces the focussing power. Therefore even though steeper temperature gradients are generated in YLF thermal lensing is weaker by comparison, reduced by a factor of three for light polarised parallel to the YLF a-axis and by over an order of magnitude for light polarised parallel to the YLF c-axis. Design of a two micron laser resonator will be influenced by the magnitude of the thermal lensing in the gain medium.

The ultimate limit on pumping of a laser rod is the possibility of thermal fracture. A rule of thumb for estimating the maximum thermal loading in an end-pumped geometry was proposed, by comparison of analytically and numerically derived data in the literature. The maximum heat deposition in short length laser rods is of the order 5 W for YLF and 15 W for YAP, for cases where the pump beam to laser crystal radius ratio ω_p/R is less than or equal to one half. Using only a single 3 W laser diode as the pump source thermal fracture is not a serious problem even for YLF, as long as adequate heatsinking of the laser crystal is employed.

In quasi-three level lasers such as thulium and holmium, the distribution of population within an energy level manifold in the steady state is determined by Boltzmann statistics. Therefore the lower laser level population is a temperature-dependent quantity. Using the calculated temperature distributions, the dependence of lower laser level population and inversion threshold has been investigated for the laser crystals used in this work. Holmium in YLF exhibits the greatest temperature sensitivity due to the relatively small width of the ground state energy level manifold.

A further temperature-dependent parameter which characterises the performance of double-doped laser crystals is the excitation sharing between the coupled first excited state energy level manifolds of thulium and holmium. Using similar thermal equilibrium arguments as previously, a simple expression for the fraction of excitation residing on holmium was presented, which represents an upper bound for this parameter. For both the Tm,Ho:YAP and Tm,Ho:YLF laser crystals procured for this

work, approximately one half of the excited state population resides on the holmium at the temperatures typically encountered experimentally.

The good thermomechanical properties of YAP combined with its natural birefringence which dominates any thermally induced birefringence, allied to the high stimulated emission cross-section of holmium in this host, suggest Tm,Ho:YAP to be a potentially powerful two micron laser source when optically excited by AlGaAs laser diodes.

3.9 References

- [1] M. J. Weber, '*CRC Handbook of Laser Science and Technology*', Volume IV Part 2 (1986) & Volume V Part 3 (1987), Florida: CRC Press, Inc.
- [2] T. S. Chen, V. L. Anderson & O. Kahan, '*Measurement of heating and energy storage in diode-pumped Nd:YAG*', IEEE J. Quantum Electron., vol. 26, no. 1, 6 (1990)
- [3] A. McInnes & J. Richards, '*Thermal effects in a coplanar-pumped folded-zigzag slab laser*', IEEE J. Quantum Electron., vol. 32, no. 7, 1243 (1996)
- [4] H. S. Carslaw and J. C. Jaeger, '*Conduction of Heat in Solids*', 2nd edition, Oxford: Clarendon, 1986
- [5] U. O. Farrukh, A. M. Buoncristiani & C. E. Byvik, '*An analysis of the temperature distribution in finite solid-state laser rods*', IEEE J. Quantum Electron., vol. 24, no. 11, 2253 (1988)
- [6] H. Kogelnik, '*Imaging of optical modes - resonators with internal lenses*', Bell System Technical Journal, vol. 44, 455 (1965)
- [7] W. Koechner, '*Solid-state Laser Engineering*', 2nd edition, New York: Springer-Verlag (1988) - principally chapter 7
- [8] A. K. Cousins, '*Temperature and thermal stress scaling in finite-length end-pumped laser rods*', IEEE J. Quantum Electron., vol. 28, no. 4, 1057 (1992)
- [9] M. Abramowitz & I. A. Stegun, '*Handbook of Mathematical Functions*', New York: Dover Publications, Inc (1965)
- [10] B. A. Boley & J. H. Weiner, '*Theory of Thermal Stresses*', New York: Wiley (1960)
- [11] V. A. French & R. C. Powell, '*Laser-induced grating measurements of energy migration in Tm,Ho:YAG*', Opt. Lett., vol. 16, no. 9, 666 (1991)

Laser performance

4.1 Introduction

It is of interest to compare the performance of a range of laser crystals under identical experimental conditions, in order to obtain an idea of their relative merits as gain media. In this chapter results of laser experiments using a 3 W cw laser diode as the pump source are presented. Laser crystals of 4.2% Tm:YAP, 4.2% Tm, 0.28% Ho:YAP and 6% Tm, 0.4% Ho:YLF were used in turn in this set-up, and their room temperature performance compared. The concentrations quoted here yield the same number density of thulium and holmium ions in the two crystalline hosts. Diode-pumped Tm,Ho:YLF has been relatively widely reported in the open literature¹⁻⁶, and so here serves as a benchmark against which to compare the other two laser crystals. To date, there have been no publications in the open literature concerning diode-pumping of either single-doped thulium or double-doped thulium and holmium in YAP. The most recent paper used a Ti:sapphire laser to pump Tm:YAP⁷, with publications prior to that solely concerned with lamp-pumping of these laser crystals e.g. the work of Weber *et al.*⁸ and Ivanov *et al.*⁹.

The first section is concerned with characterisation of the laser diode and the pump optics used as the optical excitation scheme for the laser experiments. Subsequent sections detail the comparisons made between the output power behaviour and temperature sensitivity of the three laser crystals, as well as measurements of their spectral and spatial output.

4.2 Optical pumping scheme

4.2.1 Characterisation of laser diode

The laser diode used in these experiments was an SDL-23-S-93A9-P1 device, a forerunner of the SDL-2380-P1 series "high brightness" laser diodes¹⁰. Details of the particular architecture employed in these devices were not forthcoming from the manufacturer. However it is known that these are partially coherent broad area emitters, with a total aperture width of 500 μm . Because of its short wavelength of operation, the particular laser diode used here was derated in maximum output power from 4 to 3 W. P1 package laser diodes have a built-in thermoelectric cooler for temperature control of the heatsink onto which the laser chip is bonded. An SDL-820 driver provided both the current source to power the laser diode and the electrical input and temperature sensing for the thermoelectric cooler. For the purposes of the experiments carried out during the course of this work, the laser diode was bolted to a finned heatsink, using thermal grease to ensure a good thermal contact.

Using a large area Gentec TPM-330 power meter, the laser diode optical output power was measured as a function of the drive current (the L/I characteristic), for four diode heatsink temperatures.

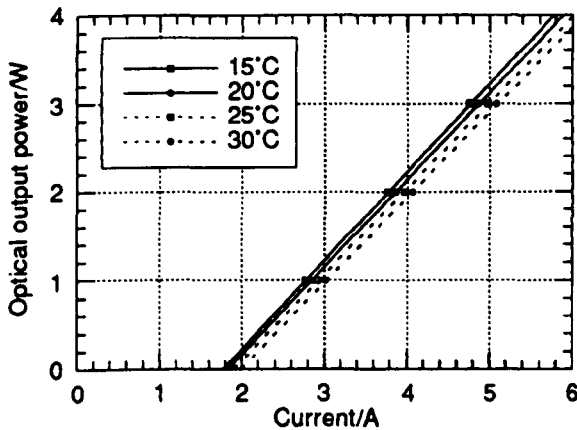


Figure 4.1 *L/I characteristic of laser diode as a function of temperature*

The laser threshold currents for the four heatsink temperatures of 15°C, 20°C, 25°C and 30°C are 1.77 A, 1.82 A, 1.90 A and 1.98 A respectively, with corresponding slope efficiencies of 1 W/A, 0.99 W/A, 0.97 W/A and 0.96 W/A. Higher temperatures of operation degrade the conversion to optical output power due to

changes in the thermal distribution of electrons and holes in the conduction and valence bands.

The temperature dependence of the laser threshold current is given by an expression of the form

$$\frac{I_{th}(T_2)}{I_{th}(T_1)} = \exp\left(\frac{T_2 - T_1}{T_0}\right) \quad 4-1$$

where T_0 is a device parameter relating to the temperature sensitivity of laser threshold. From the SDL catalogue, T_0 for the laser diode used here is approximately 160 K. Using the 15°C and 30°C threshold currents, the left hand side of equation 4-1 yielded the value 1.12, in close agreement with the theoretical value of 1.10 yielded by the right hand side of equation 4-1. Therefore it was concluded that the laser diode was operating as specified by the manufacturer. An electrical-to-optical conversion efficiency of 30% is quoted for this type of laser diode.

Because of the temperature dependence of the laser diode output power, a more useful plot than the L/I curves of figure 4.1 is the variation in drive current with temperature in order to maintain a fixed laser output power. The results for output powers of 1, 2 and 3 W are shown in figure 4.2.

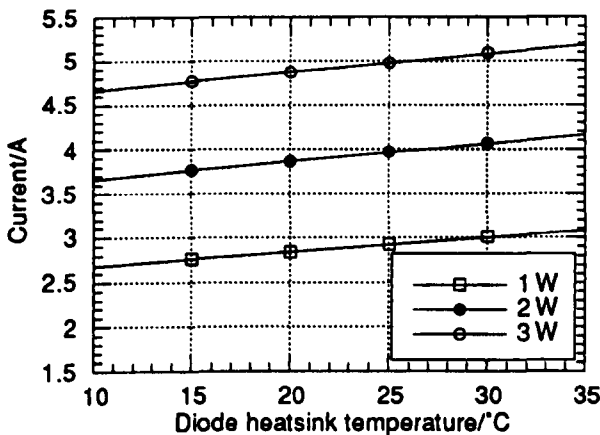


Figure 4.2 Variation of drive current with heatsink temperature

Not only does the optical output power of the laser diode depend on the heatsink temperature, the output wavelength also varies with temperature. A x10 microscope objective lens was used to capture and partially collimate as much of the diode output as possible. A Bentham M300HRA monochromator provided wavelength

discrimination, with a silicon photodiode behind the output slit to detect the transmitted light. A slit width of $50\ \mu\text{m}$ provided a resolution of $0.25\ \text{nm}$.

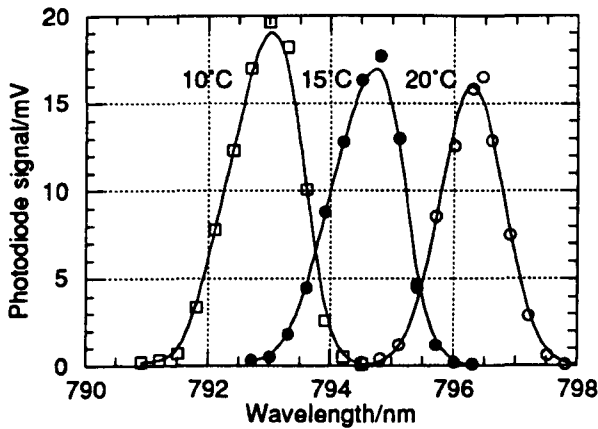


Figure 4.3 Variation of output wavelength with heatsink temperature

The results in figure 4.3 were obtained at the maximum diode output power of $3\ \text{W}$. The peak wavelength tuned at a rate of $0.33\ \text{nm}/^\circ\text{C}$, with a full width at half maximum (FWHM) spectral linewidth of $1.3\ \text{nm}$. The principal mechanism producing this temperature dependent wavelength tuning is narrowing of the bandgap with increasing temperature, shifting the output to longer wavelengths. A smaller effect on the spectral output is due to the fact that as large numbers of charge carriers are injected into the active region, the refractive index, hence the resonator length, undergoes change in turn modifying the longitudinal mode structure.

It is important to note that with the heatsink temperature fixed, as the drive current, hence the optical output power, is varied, the heat load in the active medium is altered. As a consequence the temperature gradient between the active region and the heatsink varies, resulting in the output wavelength changing. For a fixed heatsink temperature in the range 10 to 20°C , the peak of the spectral output was measured to vary as $0.9\ \text{nm}/\text{W}$. As the output power was reduced from 3 to $1\ \text{W}$, at a fixed heatsink temperature, the spectral linewidth was measured to reduce from $1.1\ \text{nm}$ to $0.8\ \text{nm}$.

4.2.2 Characterisation of the pump optics

The laser diode used here has an output facet of dimension 500 by $1\ \mu\text{m}$. Therefore the laser light is highly divergent and elliptical in cross-section as it diffracts from this small rectangular aperture. Values of divergence of 12° by 34° are given in the manufacturer's catalogue, corresponding to the 500 and $1\ \mu\text{m}$ dimensions. The latter,

in the plane perpendicular to the diode p-n junction, is essentially a diffraction-limited beam, unlike in the plane of the p-n junction where the beam is of very low quality, being of order 100 times diffraction-limited. The output of the laser diode is linearly polarised in the plane of the p-n junction, which with the experimental arrangement used here resulted in the diode output being horizontally polarised.

Optics were required to transform this output into a form suitable for end-pumping a two micron solid-state laser. Ideally what was required was a circular cross-section pump beam with a smooth intensity profile which could be focussed to a spot size which overlapped well with the fundamental mode of the two micron laser. Basic calculations using the rate equations governing lasing in thulium and holmium indicated that at room temperature a pump intensity in the range 5 to 10 kW cm⁻² would be required in order reach lasing threshold. This places an upper bound on the pump spot size, given the diode output power of 3 W, of order 200 μm. Therefore a pump optics train which could focus the diode output to a spot size smaller than 200 μm needed to be designed.

Off the shelf optics available for use here included a range of Melles Griot large numerical aperture spherical triplet lenses specifically designed for use with laser diodes, and 10 and 40 mm focal length cylindrical lenses fabricated by Spindler and Hoyer. All of the lenses considered here were antireflection coated for the wavelength range 780 to 810 nm, and so had very low insertion losses.

Commercially available Beam4™ ray tracing software was used to assess potential optical arrangements. This proved a useful tool for highlighting experimental set ups likely to be most successful at yielding the required tight focussing of the diode output. However, because it used ray tracing techniques, little quantitative information on the size of the focussed pump spots was forthcoming.

Using a combination of ray tracing and subsequent experimentation with the available lenses, the optics train shown schematically in figure 4.4 was finalised upon, which allowed pump intensities well in excess of those required to reach lasing threshold to be achieved. The results of the ray tracing indicated that significant spherical aberration would be present due to the highly divergent diode output beam.

The highly divergent output of the laser diode was initially collected by a 6.5 mm focal length spherical lens, which produced an astigmatic magnified image of the diode

output facet approximately 170 mm from the front of the laser diode package. This spherical lens is in fact a triplet lens, with a short working distance (distance from back focal plane to first surface of lens) resulting in the window of the diode package almost being in contact with the lens. A numerical aperture of 0.65 allows essentially all of the diode output to be captured by this triplet lens. The 40 mm focal length cylindrical lens acted to reduce the divergence of the beam in the plane of the diode p-n junction corresponding to the wide dimension of the output facet, which is the many times diffraction limited (poor beam quality) orientation. Both the ray tracing and the subsequent experimentation showed that the separation of the 6.5 mm focal length spherical lens and this cylindrical lens was not critical to the overall performance of the optics train. A separation of 45 mm was chosen, being midway between the extremes of separation allowed. The 10 mm focal length cylindrical lens was then positioned so as to overlap its focus with the diffraction limited focus produced by the spherical lens acting in the plane perpendicular to the diode p-n junction. In this set-up, the second cylindrical lens was positioned such that its final plane surface was 110 mm from the plane surface of the first cylindrical lens. The inclusion of the 40 mm focal length cylindrical lens allowed a greater depth of focus to be achieved with the 10 mm lens, without compromising the ability of the optics to focus the diode output to a sufficiently small size. Using these components, transmission through the optics train of greater than 95% was achieved.

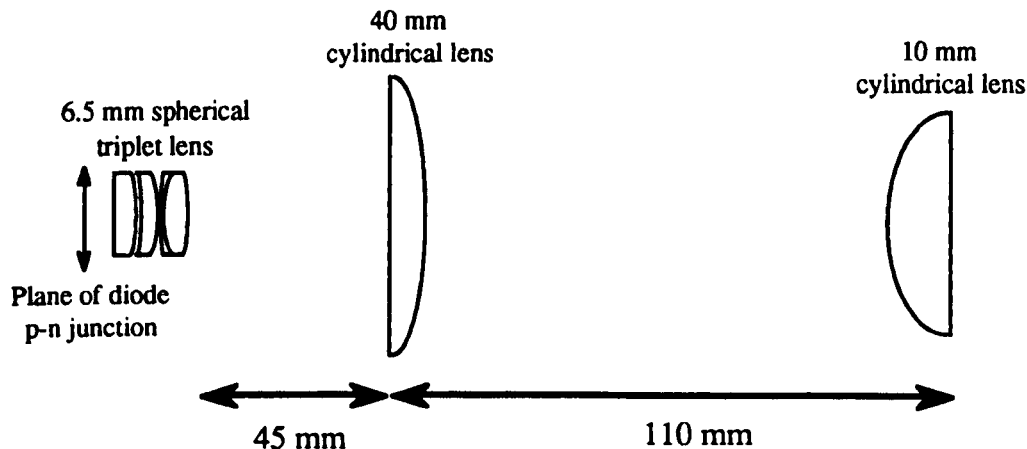


Figure 4.4 Schematic diagram of optics train employed

The size of the focussed diode beam was measured using a silicon photodiode located behind a pinhole with aperture less than 10 μm . By mounting this assembly on an XYZ translation stage, vertical and horizontal beam profiles at a range of separations from the final cylindrical lens were measured. Shown in figure 4.5 are typical

horizontal and vertical beam profiles close to their respective focal planes. The curve fit shown is an interpolation between the recorded data points, thus it appears jagged. More data points would result in a smoother curve fit being possible, but this was found not to significantly alter the spot sizes determined by these beam profiling measurements.

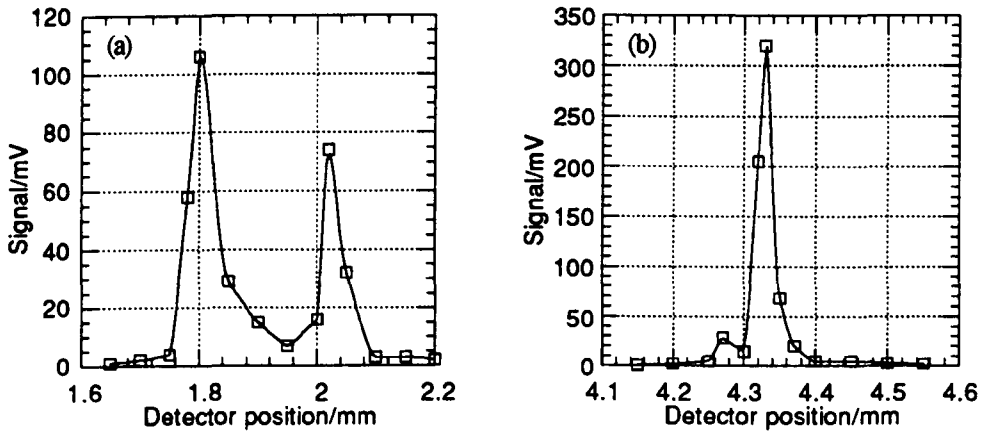


Figure 4.5 Focussed diode beam profiles in the (a) horizontal and (b) vertical orientations

The beam profiles of figure 4.5 illustrate the characteristic dual-lobed output of the laser diode in the horizontal plane, with a spot size of full width at half maximum (FWHM) of approximately $250\ \mu\text{m}$. In the vertical plane, the spot size was measured to be of order $25\ \mu\text{m}$. The vertical beam profile was measured by scanning across the peak of one of the two lobes highlighted by the horizontal beam profile. In practice there was found to be a difference of less than 10% between vertical spot sizes obtained by scanning across both lobes of the diode output. In figure 4.5(b), the small side-lobe is attributed to either aberrations in the optics train (this portion of the diode output has a large numerical aperture) or nonuniformities in the multimode output of the laser diode. Figure 4.6 depicts the horizontal beam profile measured three millimetres from the focal plane.

The dual-lobed nature of the beam profile is still evident, but with significant additional structure. The laser diode is a multilongitudinal and multitransverse mode source in the plane of the p-n junction (horizontal plane), which could give rise to the structure in the beam profile. In addition, imperfections in the curved surface of each cylindrical lens could lead to degradation of the beam profile in the horizontal plane.

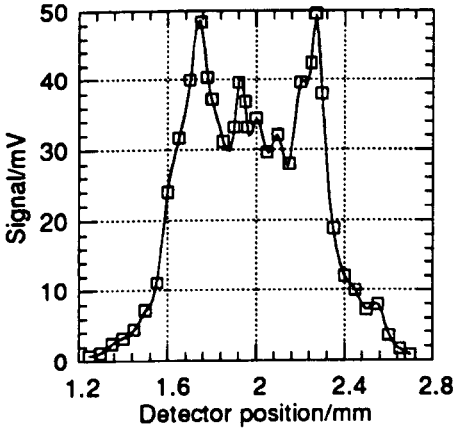


Figure 4.6 Horizontal beam profile 3 mm from focal plane of pump optics

Figure 4.7 was obtained by measuring the FWHM spot sizes at a range of separations from the final cylindrical lens, in both the horizontal and vertical planes.

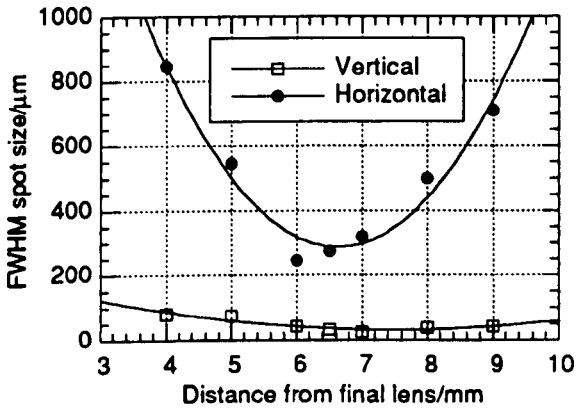


Figure 4.7 Diode spot sizes as a function of distance from final lens

A parabolic fit to the data was made in order to obtain a best estimate of the variation in spot size of the diode beam profile. We can see from the above figure that in the horizontal plane the diode output was focussed to a FWHM spot size of approximately $290\ \mu\text{m}$ 6.5 mm from the back surface of the 10 mm focal length cylindrical lens. In the vertical plane, the focal plane was found to be 7.5 mm from the back surface of the 10 mm focal length cylindrical lens, with a corresponding FWHM spot size of $35\ \mu\text{m}$. A more judicious choice of position for the final cylindrical lens would produce a better overlap of the two focal planes, but with no significant change to the actual spot sizes.

The disparity of beam qualities in the two planes is immediately apparent. The diffraction-limited vertical component of the output is brought to a soft focus by the spherical lens but still produces a spot eight times smaller than in the many times diffraction-limited horizontal component of the output, where much tighter focussing is generated by the 10 mm focal length cylindrical lens. Although the focussed diode output is still obviously elliptical in cross-section, the aspect ratio has been reduced by a factor of order sixty from the dimensions of the diode output facet. This marked reduction has produced a pump beam suitable for end-pumping a two micron solid-state laser.

With the optics scheme employed here, the most sensitive parameter relating to the resultant focussing of the diode output was the alignment of the spherical lens relative to the diode, in particular the separation of the diode output facet from the first surface of the spherical lens. The spherical lens was mounted on a translation stage to allow variation of this separation. After initial laser experiments had been carried out, and the alignment optimised to produce maximum output power at two microns, the laser crystal was removed and the diode spot sizes remeasured. They were found to be very similar to the initial set of measurements shown in figure 4.7.

4.3 Laser experiments

A schematic (not to scale) of the layout of the cw laser experiments is shown in figure 4.8.

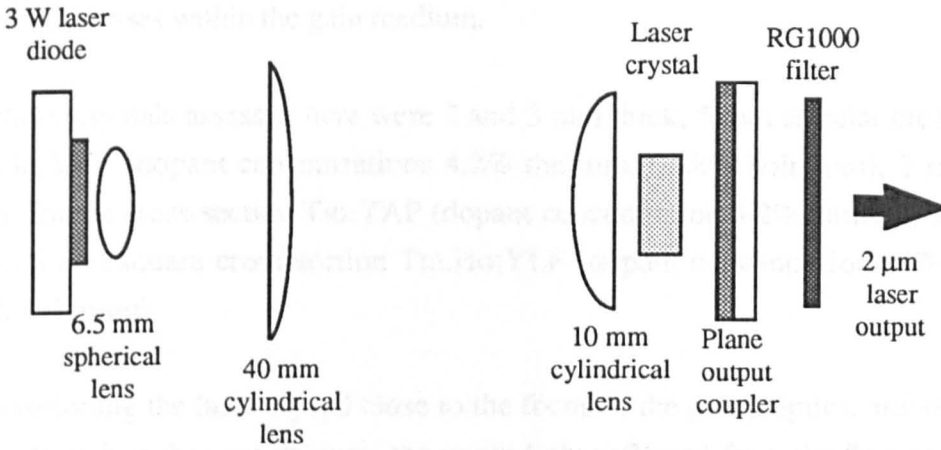


Figure 4.8 Schematic of laser

The laser diode and the pump optics are as described in the previous sections of this chapter. The laser crystals used were all polished plane/parallel with the pumped face coated to be highly reflecting at the two micron laser wavelength, with high transmission of the pump beam; the opposing end of the crystal was antireflection coated at the two micron laser wavelength. The resonator was then completed with a plane output coupler mirror, relying on thermal lensing in the gain medium caused by heat deposition on absorption of the diode pump beam to form a stable resonator mode. The thermal modelling results of chapter three indicate the possibility of very short length focal length thermal lenses being formed in the YAP crystals. This simple resonator design, with one of the mirrors coated onto the pumped face of the laser crystal, allowed resonators of length as short as 6 mm to be constructed. The laser crystal was mounted on a brass heatsink finger with indium foil sandwiched between the sides of the laser crystal and the walls of the heatsink to ensure good thermal contact. The heatsink temperature was held at a constant 15°C by a thermoelectric cooler. At temperatures below 15°C, condensation on the heatsink started to become a problem. A 6 mm thick slice of RG1000 glass in front of the output mirror completely attenuated any residual pump beam, and allowed 80% transmission of the solid-state laser output in the two micron waveband. In order to align the optical components in

figure 4.8, the output of a HeNe laser was propagated in the opposite direction to the two micron laser output.

The laser crystal heatsink was adjusted relative to the diode pump beam such that the laser crystal was being pumped close to its cooled edge, in order to reduce the temperature rises within the gain medium.

The laser crystals assessed here were 2 and 3 mm thick, 5 mm circular cross-section Tm,Ho:YAP (dopant concentrations 4.2% thulium, 0.28% holmium), 2 mm thick, 5 mm square cross-section Tm:YAP (dopant concentration 4.2% thulium) and 4 mm thick, 5 mm square cross-section Tm,Ho:YLF (dopant concentrations 6% thulium, 0.4% holmium).

By positioning the laser crystal close to the focus of the pump optics, and tilting it at an angle of less than ten degrees, the pump light reflected from the first surface was measured using a Gentec TPM-330 power meter, in order to determine the fraction of the pump light transmitted by the dichroic coating. Using this method, transmission figures of 81.0%, 93.5% and 96.5% were obtained for Tm,Ho:YAP, Tm:YAP and Tm,Ho:YLF respectively. Immediately it is apparent that the dichroic coating on the double-doped YAP sample is far from ideal in terms of allowing maximum transmission of the pump light. This is an important measurement in determining the conversion of the pump light to two micron laser output in the laser crystals under investigation.

In all cases, the laser crystals were orientated to align their crystallographic c-axis with the laser diode output polarisation, in order to maximise the pump absorption.

4.3.1 Laser output power behaviour

The two micron laser output power transmitted through the RG1000 filter was measured by a Scientech 362 power meter. Once lasing had been achieved, the laser diode was temperature tuned at maximum output power in order to maximise the two micron laser output. Further optimisation of the two micron laser output was achieved by altering the alignment of the output mirror, and by altering the separation of the laser crystal from the final cylindrical lens of the pump optics. This latter adjustment was a relatively sensitive one, as it determined the position of the pumped face of the laser crystal relative to the focussed spot of the diode pump beam. After optimising

the laser to give maximum output power, the pump power was attenuated by reducing the diode forward current until the threshold pump power was reached. Threshold was determined by viewing the laser output with a thermal imager camera (Insight Vision Series 80) connected to a PC with a framegrabber card controlled by Beamcode™ software. This proved to be an invaluable tool both in determining laser thresholds and more importantly in detecting laser action when the two micron laser was aligned for the first time.

Each laser crystal was measured in turn, producing the set of figures 4.9 to 4.11, which show the output power behaviour as a function of diode pump power for a range of output coupler mirrors. Three plane output coupler mirrors were available for these laser experiments, nominally of reflectivities 99%, 97% and 95%. The actual reflectivity, hence transmission, depends on the particular laser wavelength being investigated. Note here that the abscissa scale is incident pump power, which takes account of the transmission of the pump beam through the optics and the first face of the laser crystal.

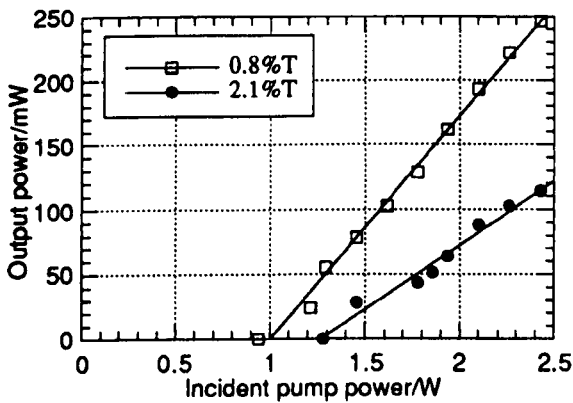


Figure 4.9 Output power performance of 2 mm thick Tm,Ho:YAP laser crystal

Using the 2 mm thick Tm,Ho:YAP crystal, the highest output coupling mirror was not used, as it can be seen clearly that it is the lowest output coupling mirror which is the optimum, in terms of producing the maximum laser output power. The transmissions of the two mirrors used were 0.8% and 2.1% at the holmium laser wavelength of 2.12 μm . The respective threshold powers and slope efficiencies were 1.00 W and 17.3% for the 0.8%T mirror, 1.27 W and 9.9% for the 2.1%T mirror. The maximum output power recorded was 245 mW, operating at 2.5 times threshold.

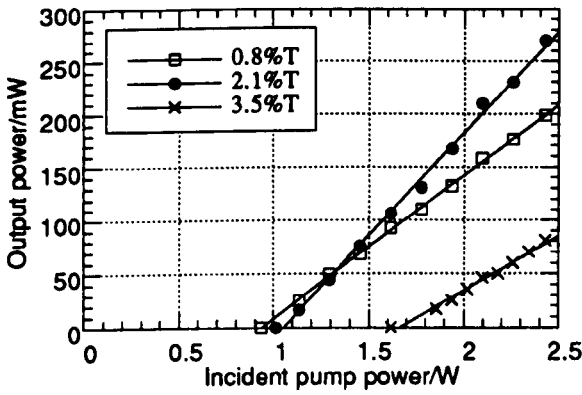


Figure 4.10 Output power performance of 3 mm thick Tm,Ho:YAP laser crystal

Using the 3 mm thick Tm,Ho:YAP crystal, maximum laser power was generated using the 2.1%T output mirror. In order of increasing output coupling, the three sets of threshold and slope efficiency measurements were 0.94 W and 13.3%, 1.06 W and 19.3% and 1.66 W and 10.2%. The maximum recorded output power was 270 mW, operating at 2.3 times threshold.

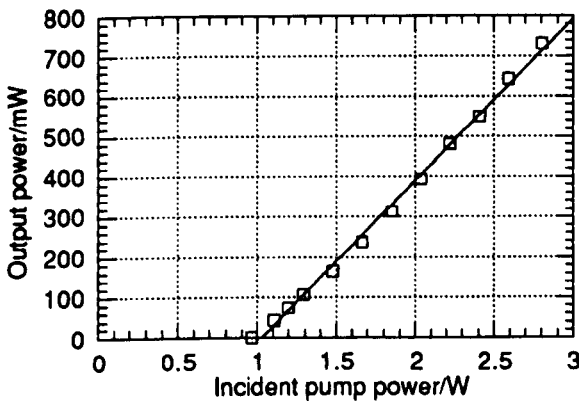


Figure 4.11 Output power performance of 2 mm Tm:YAP laser crystal

The broad gain bandwidth of Tm:YAP allowed it to lase on several lines in the waveband 1.965 to 2.020 μm . Over this spectral region the three mirrors available all had similar transmission profiles which were a strong function of wavelength, as this was outside the waveband the mirror coatings had been specified for. Here changing the output mirror resulted in a change in the output wavelength, with the effective output coupling remaining in the range 1.4 to 1.8%T. A threshold pump power of 1.03 W was measured, with a slope efficiency of 40.3%, from data with a maximum recorded output power of 730 mW. This corresponded to operation at 2.8 times threshold.

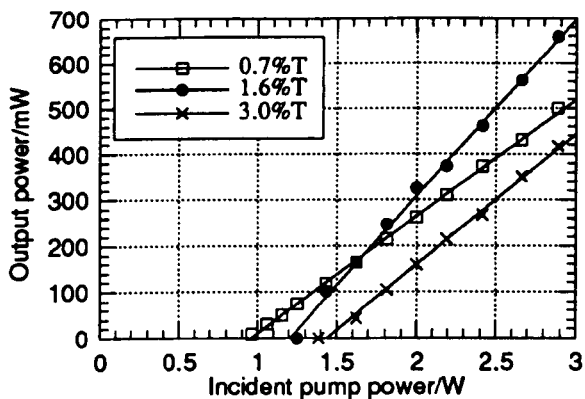


Figure 4.12 Output power performance of 4 mm thick Tm,Ho:YLF laser crystal

Because of the different laser wavelength of holmium in YLF, the same three output mirrors had slightly different transmissions than for holmium in YAP, as noted in the legend of figure 4.12. Maximum output power was achieved with an output mirror transmission of 1.6%. In order of increasing output coupling, the three sets of threshold and slope efficiency measurements were 0.96 W and 25.5%, 1.21 W and 38.9%, and 1.44 W and 28.4%. The maximum recorded output power was 660 mW, operating at 2.4 times threshold.

These results highlight that for the fixed wavelength operation in double-doped YAP and YLF, output power performance is a relatively strong function of output coupling. This is typically the case with four-level lasers where the output coupling is the single biggest contribution to the laser threshold. At the other extreme, in a three-level laser the major contribution to the laser threshold is the need to excite half the ground-state population into the upper laser level to reach inversion threshold. In this case, laser threshold and slope efficiency are both weak functions of the output coupling. For quasi-three level holmium lasers (co-doped with thulium), the threshold and the slope efficiency are both functions of the relative contribution of the lower laser level population and the output coupling to the laser threshold, as well as the magnitude of the depletion of the holmium ground state, and the magnitude of the upconversion rate from the holmium first excited state. As the output coupling increases, higher population densities in the holmium 5I_7 first excited state are required to achieve threshold. These higher population densities lead to increased upconversion and therefore decreased slope efficiency (the topic of upconversion is dealt with in more detail in chapter six). This contrasts with the behaviour of an ideal four-level laser,

where the slope efficiency increases asymptotically to a maximum value as the output coupling increases.

It is instructive to take the best output power data set for each laser crystal and plot them together. The significantly poorer performance of Tm,Ho:YAP, both 2 and 3 mm thick crystals, is immediately apparent (data for the 3 mm crystal is plotted in figure 4.13). Threshold incident pump intensities were measured to be 8.9 kW cm^{-2} for Tm:YAP, 9.2 kW cm^{-2} for Tm,Ho:YAP and 10.5 kW cm^{-2} for Tm,Ho:YLF.

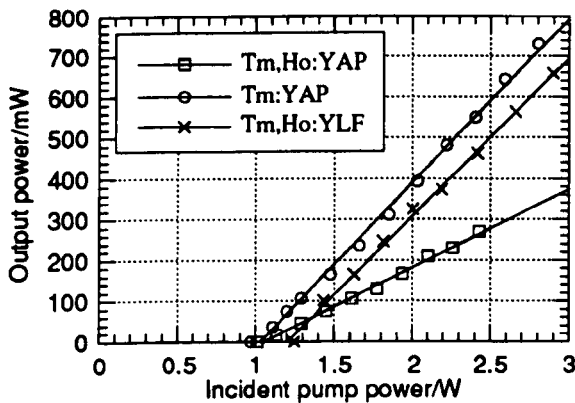


Figure 4.13 Best output power curves for the three laser crystals

In terms of the maximum output powers measured, the optical-to-optical conversion efficiency from diode pump light to two micron laser light is 24% for Tm:YAP, 22% for Tm,Ho:YLF and 9% for Tm,Ho:YAP. These conversion efficiencies are partly determined by the transmission of the pump light through the dichroic coating on the laser crystal, the value for which is different for the three crystal types. Extrapolating the linear curve fits to an incident power of 3 W, the experimental results predict that Tm,Ho:YAP will be of order a factor of two down in output power compared to the other two laser crystals (380 mW predicted versus 795 mW for Tm:YAP and 700 mW for Tm,Ho:YLF).

A further refinement to the calculation of the efficiency of the lasing process would be to measure not only the pump power incident on the laser crystal, but how much is actually absorbed by the laser crystal. The simplest way to measure this is to remove the output mirror and use the large area Gentec TPM-330 power meter to capture any transmitted pump light. However this apparently simple measurement is complicated by various pump absorption effects in the laser crystals. This topic is discussed in more detail in chapter five.

The output power results presented previously were for a laser crystal heatsink temperature of 15°C. By keeping the diode output constant at maximum power, and then varying the laser crystal heatsink temperature, a measure of the temperature sensitivity of the lasing transition can be obtained.

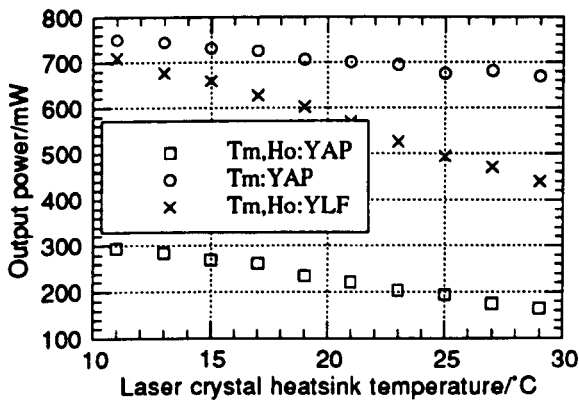


Figure 4.14 Comparison of temperature dependence of output power

Over this limited temperature range, a linear fit to the experimental data reveals the output power to change at $-4.5 \text{ mW/}^\circ\text{C}$ for Tm:YAP, $-7.5 \text{ mW/}^\circ\text{C}$ for Tm,Ho:YAP and $-15.0 \text{ mW/}^\circ\text{C}$ for Tm,Ho:YLF. Assuming that this linear dependence can be extended to lower temperatures, it is clear that once the heatsink temperature is reduced to below 4°C , the output power of the Tm,Ho:YLF laser starts to exceed that of Tm:YAP, with Tm,Ho:YAP always lagging behind.

Referring back to section 3.6 of the previous chapter we see that at room temperature both the lower laser level of thulium and holmium in YAP contain between 1 and 1.5% of the total ground state population (the holmium lower laser level being fractionally more populated than the thulium lower laser level), and that holmium in YLF contains approximately 7% of the total ground state population in the lower laser level. The variation of maximum laser output power with heatsink temperature partly depends on the corresponding change in laser threshold. However the disparity in measured output power variations does not correlate particularly well with the calculated disparity in lower laser level populations. The effects of various upconversion processes, particularly in the double-doped materials, are also temperature-dependent due to the thermal distribution of population within energy level manifolds, and make a contribution to the experimentally measured temperature-dependent output power. Upconversion rates are greater in double-doped than single-doped laser crystals, producing higher losses to the two micron laser transition as more excitation is removed from the energy level manifold containing the upper laser

level. The inherently larger phonon energies of oxide hosts compared to fluoride hosts results in a greater fraction of any upconverted excitation decaying nonradiatively with the former. This leads in turn to further losses as the additional heat load produces a greater temperature rise hence higher laser threshold.

Therefore of the three laser hosts investigated, Tm,Ho:YAP suffers the most from deleterious upconversion processes, negating the favourable spectroscopic and mechanical properties predicted in previous chapters which highlighted it as the best gain medium of the three.

4.3.2 Laser spectral and spatial behaviour

It is of some value to measure the wavelength of the laser crystals under investigation, in order to assign the transition or transitions providing stimulated emission. During the course of the output power characterisation described in the previous section, both a monochromator and a Fabry-Perot interferometer were used to determine the spectral content of the laser output.

For both the 2 and 3 mm thick Tm,Ho:YAP laser crystals, independent of the output mirror used, the laser output was centred around 2.12 μm , and was linearly polarised parallel to the YAP c-axis. This wavelength corresponds to the transition from the lowest two levels of the holmium 5I_7 first excited state to the second from highest level of the 5I_8 ground state (see Appendix A). The wavelength spectrum was measured using a Bentham M300HRA monochromator with a large area InAs photodiode behind the output slit, which was set at a width of 50 μm providing a resolution of 0.3 nm. The results shown in the following figures are for laser operation with the 2 mm thick sample.

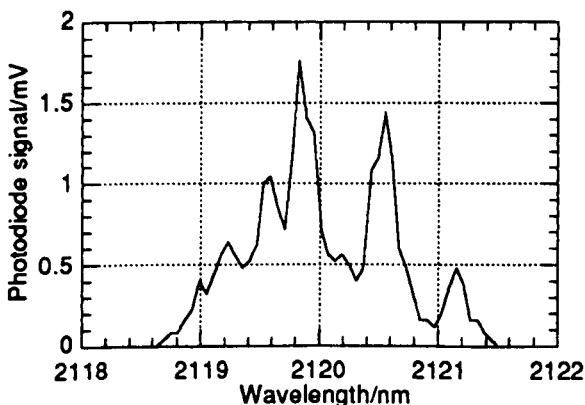


Figure 4.15 Spectrum of Tm,Ho:YAP laser output

The spectrum shown in figure 4.15 was obtained by stepping the monochromator in intervals of 0.1 nm, and recording the photodiode signal at each increment. The longitudinal mode structure of the laser output is starting to be resolved by this technique, revealing a FWHM of just over 1 nm. In order to see the longitudinal structure more clearly, the laser output was interrogated with a plane-plane scanning Fabry-Perot interferometer (Burleigh RC140), again using a large area InAs photodiode to detect the instrument throughput. Typical spectra, as recorded on a digital oscilloscope, are shown in figure 4.16. Here the abscissa scale is time, representing the duration of the ramp voltage applied to a piezoelectric stack scanning one of the interferometer mirrors.

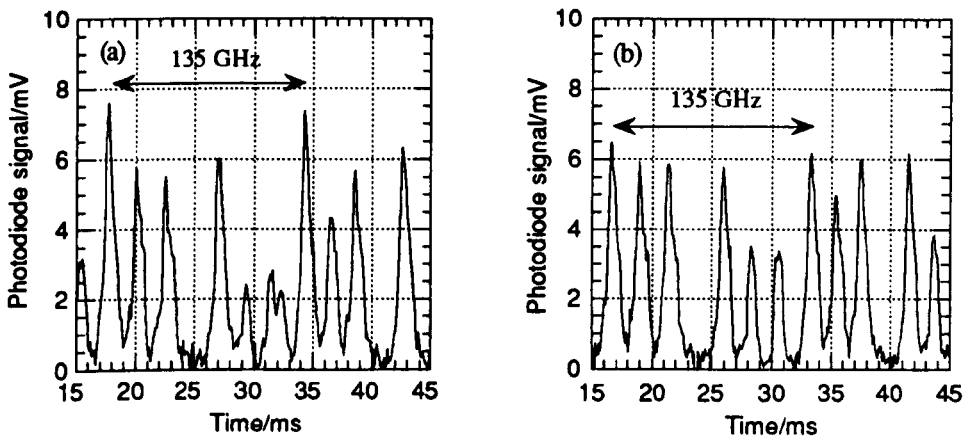


Figure 4.16 Typical Fabry-Perot traces of Tm,Ho:YAP laser output

The mirrors of the Fabry-Perot interferometer were 1.1 mm apart, corresponding to a free spectral range (FSR) of 135 GHz. From data supplied by the manufacturer, the reflectivity of the mirrors at 2.12 μm is approximately 92%, producing a finesse of 38. The finesse can be estimated by the ratio of the fringe width to the FSR. Using the recorded traces, the finesse is found to be approximately 20, one half of the theoretical value¹¹. Misalignment between the interferometer mirrors can account for much of this reduced finesse.

Both the recorded traces indicate the laser to be running on typically six longitudinal modes. Mode separations of between 18 and 19 GHz correspond well to the 19.2 GHz longitudinal mode spacing of a 6 mm resonator with a 2 mm thick Tm,Ho:YAP laser crystal. Perturbations to the laser resonator, for example by tapping the output mirror or laser crystal heatsink mount, induced amplitude fluctuations in the lasing modes, and indeed could cause new modes to appear.

Amplitude variations of order $\pm 20\%$ in the mode pattern were present when the laser was left unperturbed. This mode behaviour means that the wavelength spectrum of figure 4.15 is in fact some average of the actual time-varying spectrum. Leaving the monochromator at a fixed wavelength for a period of many seconds, the photodiode signal could be seen to vary as the particular longitudinal mode being viewed changed in amplitude. Therefore the recorded wavelength spectrum serves to indicate the peak of the laser transition as well as its linewidth, without yielding a great deal of information on the mode structure of the transition.

In solid-state laser media, the laser transition is predominantly homogeneously broadened due to the interaction of the lasing ion with the lattice vibrations of the crystalline host, which would imply that the laser would operate on a single longitudinal mode, as the first mode to reach laser threshold would extract all the available gain. However, in the two-mirror standing wave resonator employed here, strong spatial holeburning effects occur which allow other modes to reach threshold even in this homogeneously broadened gain medium¹². In addition, any defects or strains in the crystalline host will result in the lasing ion residing in more than one type of site in the lattice, leading to an inhomogeneous contribution to the total broadening which allows multilongitudinal mode operation via spectral holeburning. Evidence of multiple crystalline sites can be obtained from absorption and emission spectra at cryogenic temperatures, but was not performed during the course of this work.

The wavelength spectrum of Tm,Ho:YLF was measured in similar fashion. Independent of the output mirror used, the laser output was centred around $2.065 \mu\text{m}$, and was linearly polarised parallel to the YLF a-axis. This wavelength corresponds to the transition from the lowest three levels of the holmium 5I_7 first excited state to the two highest lying levels of the 5I_8 ground state (see Appendix A).

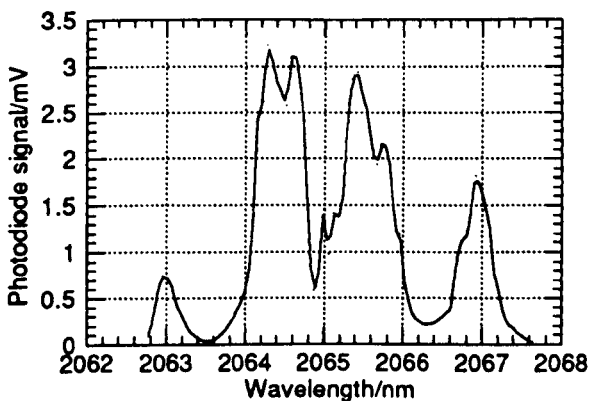


Figure 4.17 Spectrum of Tm,Ho:YLF laser output

A FWHM of 3 nm is inferred from the spectrum in figure 4.17, significantly broader than the Tm,Ho:YAP laser linewidth. Using the same Fabry-Perot interferometer, the following mode patterns were recorded.

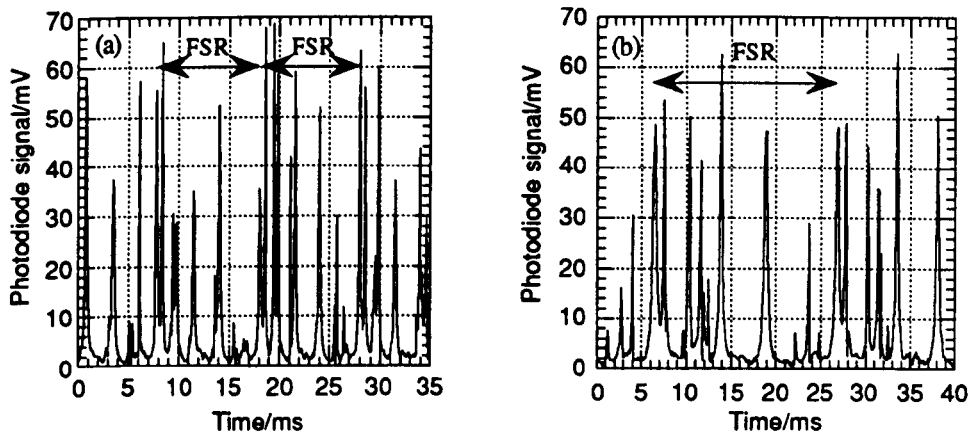
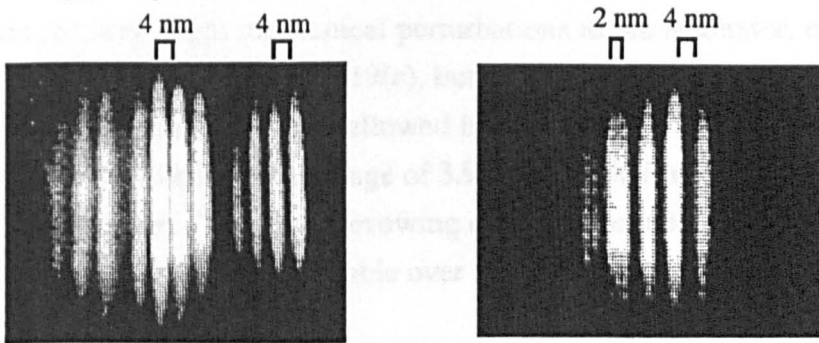


Figure 4.18 Typical Fabry-Perot traces of Tm,Ho:YLF laser output

A lower ramp voltage (slower scan rate) has been employed in figure 4.18(b). At the Ho:YLF laser wavelength, the interferometer mirrors have reflectivity 97.5%, producing a finesse of 125. The value of finesse from the recorded mode patterns is approximately 60, again reduced from the ideal principally by misalignment between the interferometer mirrors. It is difficult in this case to determine exactly the number of modes oscillating at any one time, because the measured spectral linewidth of 3 nm, which corresponds to a 210 GHz bandwidth at 2.065 μm , is greater than the FSR of the Fabry-Perot interferometer. Based on the Tm,Ho:YAP results at least six longitudinal modes are expected to be lasing. Similar amplitude stability to the Tm,Ho:YAP laser was demonstrated, with the longitudinal mode pattern sensitive to mechanical perturbations of the resonator. In both cases, the short resonator length employed leads to a longitudinal mode separation of order 19 GHz. This separation is sufficiently large that spatial holeburning allows adjacent longitudinal modes to lase.

The wavelength of the Tm:YAP laser was found not to have a fixed value, but instead varied over the range 1.965 to 2.02 μm , polarised parallel to the YAP a-axis. This wavelength range corresponds to transitions from the lowest two levels of the $^3\text{F}_4$ first excited state to one of the three highest lying levels of the $^3\text{H}_6$ ground state (see Appendix A). Using a larger dispersion Jarrell Ash Monospec 27 monochromator, the output slit could be opened up to 3 mm, allowing the instrument to function as a

spectrograph with a bandwidth of approximately 40 nm. The transmitted signal was imaged with a lens onto an Insight Series 80 thermal imager attached to a monitor screen. The output spectrum was found to consist of a comb of wavelengths, the separation of which was in the range 2 to 8 nm, far in excess of the longitudinal mode spacing of the resonator employed. The number of lines lasing at any one time varied from two to ten, depending critically on the resonator length, alterations in alignment, and whether or not the output coupler was plane or curved (a 50 cm radius of curvature (RoC) mirror with an identical coating to the plane mirror was also used as an output coupler). Viewing the lines simultaneously, it was evident that the lines were in competition with each other, one line or several lines dying away as others grew in strength. Figure 4.19 depicts scanned images of photographs of typical thermal imager outputs as viewed on the monitor screen.



(a) Wavelength interval 1.980 to 2.020 μm (b) Wavelength interval 1.980 to 2.004 μm

(c) Wavelength interval 1.991 to 1.999 μm

Figure 4.19 Representative wavelength spectra of Tm:YAP with a curved output mirror (a) and a plane output mirror (b and c)

This behaviour is attributed to the broad gain bandwidth of thulium allowing a series of lines to lase simultaneously. In general, the curved output mirror allowed more lines to lase than the plane mirror, with the total number of lines lasing at any one time very sensitive to alignment changes or other perturbations to the resonator. Such behaviour is indicative of multiple etalon effects occurring due to the output mirror (the back surface of both mirrors used was antireflection coated, but not wedged), or

between the output mirror and the antireflection coated end of the laser crystal, or even between the two ends of the laser crystal, but the mode pattern was so unstable as to make quantitative analysis very difficult. Multiple etalon effects combined with a broad gain bandwidth will lead to very unstable behaviour.

Figure 4.19(a) depicts the broadband output using the 50 cm RoC output mirror. The maximum number of lines seen was thirteen, spanning the wavelength interval 1.965 to 2.020 μm , but because of the monochromator maximum slit width of 3 mm (spectral width approximately 40 nm) not all the lines can be viewed simultaneously. Using the plane output mirror, typically a maximum of six or seven lines lased. Figure 4.19(b) depicts two pairs of closely spaced lines (one pair barely resolved here), and three wider spaced lines. Fractional adjustments to the output mirror alignment, or very slight mechanical perturbations to the resonator, could reduce the output to two lines, as in figure 4.19(c), but never down to a single line. Opening up the resonator to a length of 2 cm allowed inclusion of a 27 μm thick uncoated fused silica etalon with a free spectral range of 3.9 THz, equivalent to 50 nm at wavelengths around two microns. This line narrowing element produced single line output from the Tm:YAP laser, which was tunable over a limited wavelength range by altering the angular tilt of the etalon.

This unstable spectral behaviour, both for the single and double-doped laser crystals, did not manifest itself in laser output power measurements, where the power meter absorbed the optical radiation converting it to heat which then allowed the optical power to be inferred. These thermal measurements integrated the incident signal over a period of seconds, "washing out" any rapid intensity fluctuations which were occurring.

This instability was thought to be due to having the laser crystal and output mirror on separate adjustable mechanical mounts. Subsequent experimentation using a more mechanically robust set-up significantly reduced the sensitivity of the longitudinal mode spectrum of the double-doped lasers to mechanical perturbations (but did not alter the number of modes lasing), but produced no noticeable change to the Tm:YAP behaviour.

Two other potential sources of instability in the laser output were feedback of the solid-state laser output back into the resonator, or by feedback of pump light back into the laser diode, producing intensity fluctuations in the pump beam. The former was

eliminated as a source of instability by placing an optical isolator adjacent to the output mirror. For all three lasers, there was no detectable change in the spectral behaviour on inclusion of this isolator. The latter source of instability, namely feedback of pump light back into the laser diode, was also investigated. Positioning of the front surface of the laser crystal at or close to the focal plane of the pump optics meant that any reflected pump light was efficiently coupled back into the laser diode. The laser diode package contained a built-in monitor photodiode. By observing the photocurrent generated, it was obvious that feedback was occurring, because when a laser crystal was placed at the focus of the optics train, the photocurrent increased and was unstable in time. A silicon photodiode monitoring the pump light transmitted through the optics train showed the same behaviour, with inclusion of one of the laser crystals introducing intensity fluctuations onto the pump beam, which were largest for the Tm,Ho:YAP crystal with its higher reflectivity at the diode wavelength. A crude optical isolator was made using a polariser and a quarter-wave plate, which, when placed between the two cylindrical lenses in the optics train, was demonstrated to completely suppress the feedback (35 dB of isolation quoted by the manufacturers). For all three laser crystals, inclusion of this isolator produced no detectable change in the laser spectral output.

The results of these tests confirm that the spectral output of the double-doped lasers is dominated by spatial holeburning effects, while the broadband output of the Tm:YAP laser in the absence of any linewidth control appears to be fundamental to its operation. In the homogeneously broadened Ti:sapphire laser, the output is broadband around the peak of the gain profile if no linewidth narrowing elements such as intracavity etalons or birefringent tuners are employed¹³⁻¹⁵.

The polarisation of the laser output is determined by which transition has the lowest threshold i.e. which transition will lase first. This is a trade-off between the magnitude of the stimulated emission cross-section and the inversion threshold of the possible transitions. Inspection of the ground to first excited state absorption spectra in figures 2.7 to 2.9 reveals that the laser transitions occur in the long wavelength tail of peaks in the absorption profile, where smaller lower laser level populations reduce the inversion threshold.

The transverse beam profiles of these lasers were investigated using the thermal imager camera connected to a PC with a framegrabber card controlled with Beamcode™ software. Accurate measurement of beam diameters using this apparatus

required careful setting of the ADC in the framegrabber card, in order that there was a sensible background noise level captured by the camera. Only then could the software perform a meaningful Gaussian fit to the captured beam profiles. This was checked initially by transforming the output beam of the Tm,Ho:YAP laser through a weak lens, and then at a common plane comparing the beam profiles measured by scanning a photodiode across the beam with the profile captured by the camera. An InGaAs photodiode with a 50 μm pinhole aperture was used, with the resulting profiles shown here.

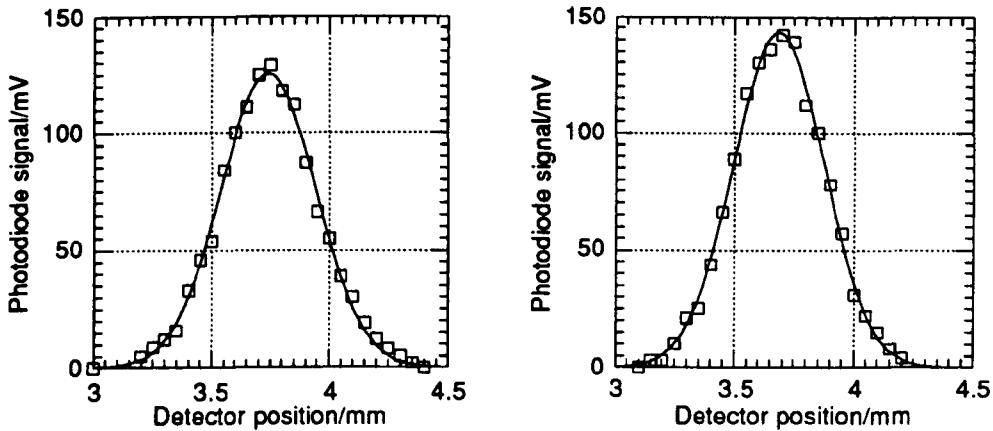


Figure 4.20 Tm,Ho:YAP beam profiles in (a) horizontal and (b) vertical planes

The $1/e^2$ diameters were 830 μm by 750 μm in the horizontal and vertical planes. The Gaussian fit to the captured profile on the camera was of corresponding dimension 780 μm by 680 μm . There is better than 10% agreement between the two measurement methods, but the camera image has increased ellipticity. However the agreement is sufficient that the far less time consuming technique of beam profiling using the Beamcode™ system was considered valid.

The far-field beam divergence was measured using the standard technique of forming a focus with a lens, and then characterising the beam propagating from this new beam waist position. For a Gaussian TEM₀₀ beam, the beam waist divergence product (BWDP) is given by λ/π , using the half-angle divergence. The respective values for Tm,Ho:YAP, Tm:YAP and Tm,Ho:YLF are 0.68, 0.64 and 0.66 mm.mrad. Comparing this BWDP with that measured experimentally as described above, a measure of the beam quality of the laser output can be obtained in terms of how far removed it is from being diffraction-limited. Both Tm,Ho:YAP and Tm:YAP were investigated in this manner, and in both cases, within the accuracy of the profile

measurements being made, the laser output was determined to be very close to diffraction-limited, that is the lasers ran on the fundamental transverse mode. In both cases the elliptical pump beam shape produced astigmatic thermal lensing as a direct consequence of the resulting non-circularly symmetric temperature gradients, which in turn resulted in different foci in the horizontal and vertical planes when the output beam was transformed through a lens to investigate the far-field divergence. Treating these orthogonal planes separately, the diffraction-limited operation reported above was determined.

Misaligning the resonator by tilting the output mirror eventually extinguished lasing altogether, without operation on higher order transverse modes being allowed. This provided confirmation that the diode pump beam was focussed tightly enough to provide good mode-matching with the fundamental mode of the two micron laser resonator. Operation on higher order transverse modes was also made difficult by the unpumped region of the gain medium, which acted as a very lossy element to the two micron stimulated emission, behaving in effect as a "soft" aperture.

With the use of a plane output coupler, it was the thermal lensing in the gain medium that allowed a stable resonator mode to be formed. The magnitude of the thermal lens determined the size and shape of the resonator mode, which formed a beam waist at the output mirror. A stronger thermal lens acted as a mirror with shorter radius of curvature, producing a smaller beam waist at the output mirror. This manifested itself in the laser output as a more highly divergent beam. The thermal imager camera was placed approximately 30 cm from the output mirror for the three types of laser crystal. Tm,Ho:YLF possessed the output beam with the least divergence, markedly less than both Tm:YAP and Tm,Ho:YAP, principally because of the weaker thermal lensing predicted in chapter three (see data in table 3.2). For the particular experimental arrangement here, the thermal lensing in the YLF was also weaker because the integrated pump spot size was larger than in the YAP crystals due to the longer crystal length (chosen because of the lower absorption coefficient of thulium in YLF). The single and double-doped YAP laser crystals contained the same thulium doping level, and therefore had the same absorption coefficient at the diode pump wavelength. However pump saturation and upconversion effects mentioned in the previous section and dealt with in the following chapters resulted in the heat deposition, hence thermal lensing, being greater in the double-doped YAP crystals. This was highlighted by the Tm,Ho:YAP crystals (both the 2 and 3 mm thick samples) exhibiting the largest beam divergence.

Some quantification of the relative magnitude of the thermal lensing can be provided. For Tm:YAP and Tm,Ho:YLF, the laser output was linearly polarised parallel to the crystallographic a-axis, while for Tm,Ho:YAP the output polarisation was parallel to the c-axis. The laser mode "sees" the thermally induced lens in the birefringent gain medium which corresponds to the polarisation of the laser radiation. Rather than simply using the data in table 3.2, results presented in the following chapter concerning the heat load deposited in the laser crystals under lasing conditions were used. At maximum diode pump power, the heat loads deposited in the 2 mm Tm:YAP, 2 mm Tm,Ho:YAP and 4 mm Tm,Ho:YLF laser crystals were respectively 500 mW, 850 mW and 780 mW. The corresponding thermally induced focal lengths are calculated to be of order 5 cm, 3 cm and 10 cm. The 3 mm thick Tm,Ho:YAP, with its longer absorption path length, is estimated to have a thermal lens of focal length 20% shorter than in the 2 mm thick crystal. Therefore the Tm,Ho:YAP laser will exhibit the highest divergence, with the 3 mm crystal more so than the 2 mm crystal, in agreement with the measurements made.

It is worth noting that the short resonator lengths employed here allowed the Tm,Ho:YLF to operate on an a-axis polarised transition, with thermal lensing almost an order of magnitude stronger than if the laser radiation was polarised parallel to the c-axis. The holmium a-axis transition at 2.066 μm has the lowest threshold of the possible lasing transitions, and so if the resonator will support the accompanying thermal lens then this mode will preferentially lase. A Tm,Ho:YLF laser with a long resonator length (greater than 10 cm using the same pump spot size as in this work) would not support this transition, and a higher threshold, but thermally stable, c-axis transition would lase instead.

This technique of analysing the output beam behaviour can be used to confirm the expected relative magnitude of the thermal lensing, without providing quantitative figures on the thermally induced focal lengths. Further verification of the short focal length of the thermal lens in Tm:YAP was obtained by simply lengthening the resonator until lasing action ceased. This occurred for resonator lengths in excess of 20 mm. A similar measurement with Tm,Ho:YLF revealed that at these longer resonator lengths the laser still operated, confirming the weaker thermal lensing in YLF as compared to YAP.

In practice it was very difficult to measure experimentally the actual thermal lenses induced in the laser crystals. A standard technique for performing such a

measurement involves probing the laser crystal with a HeNe beam and observing any focussing of this beam produced by the thermal lens. However the compact pump optics arrangement employed here, with tight focussing of the diode pump beam in an end-pumped geometry, renders it nontrivial to probe the small pumped volume in the laser crystal with a HeNe laser. Calculation of the focal length of the thermal lens in the gain medium by measurement of the divergence of the two micron laser output requires very accurate measurement of the beam size otherwise large errors are introduced into the focal length calculation. This technique also assumes an ideal spherical lens is formed in the gain medium, whereas in reality the small pumped volume can lead to short focal length lenses which will have significant aberrations.

4.4 Conclusions

This chapter has detailed the comparison of three laser hosts, 4.2% Tm:YAP, 4.2% Tm,0.28% Ho:YAP and 6% Tm,0.4% Ho:YLF, under identical experimental conditions. The pump source for these experiments was a 3 W cw laser diode, the wavelength of which could be temperature-tuned to match the absorption peak of the particular laser crystal being investigated. Using a spherical and two cylindrical lenses, which transmitted greater than 95% of the laser diode output, the pump beam was focussed to an elliptical spot of diameter 290 by 35 μm , a beam size considered appropriate for end-pumping a two micron solid-state laser.

The laser crystals were tested in a simple standing wave plane/plane resonator, one mirror deposited as a dichroic coating on the pumped face of the laser crystal, relying on thermal lensing in the gain medium to form a stable resonator mode. Maximum recorded output powers, at a laser crystal heatsink temperature of 15°C, were 730 mW for a 2 mm thick Tm:YAP crystal, 660 mW for a 4 mm thick Tm,Ho:YLF crystal and 270 mW for a 3 mm thick Tm,Ho:YAP crystal. In terms of the 3 W optical output of the laser diode, the optical-to-optical conversion efficiency of each laser crystal was 24%, 22% and 9% respectively, with corresponding threshold pump intensities of 8.9, 10.5 and 9.2 kW cm⁻². Tm,Ho:YAP demonstrated the poorest conversion efficiency partially because of significantly poorer pump light transmission through the dichroic coating, but principally because of increased upconversion losses compared to the other two laser crystals. Upconversion losses in the double-doped crystals manifested itself as decreasing slope efficiency with increasing output coupling. Investigation of the temperature sensitivity of the laser output power revealed the output power to tune at -4.5 mW/°C for Tm:YAP, -7.5 mW/°C for Tm,Ho:YAP and -15.0 mW/°C for Tm,Ho:YLF. This temperature sensitivity is not only a measure of the change in laser threshold with temperature, but is also a measure of the temperature sensitivity of any upconversion processes occurring.

The performance of Tm,Ho:YLF, demonstrating a slope efficiency of 38.9% and an optical-to-optical conversion efficiency of 22%, is superior to the room temperature operation reported by McGuckin *et al.*², where the slope efficiency was 17% with a corresponding conversion efficiency 11.5%. It also compares well with the reported work of Budni *et al.*⁴, where Tm,Ho:YLF cooled to 77 K demonstrated a slope efficiency of 49.4% and an optical-to-optical conversion efficiency of 45.6%. Here

the reduced temperature of the gain medium acted principally to decrease the laser threshold.

These comparisons were made more difficult to quantify by pump beam saturation effects which occurred to different degrees in the three laser hosts. The following chapter provides an analysis of these phenomena. The thicknesses of the laser crystals used here were initially selected based upon the known absorption strengths of thulium in YLF and YAP at the diode pump wavelengths (figures 2.3 and 2.4), in order to allow identical fractions of the pump power to be absorbed in the crystals assessed.

Tm,Ho:YAP was found to lase at 2.120 μm with a linewidth of 1 nm, the laser output linearly polarised to the YAP c-axis. Tm,Ho:YLF was found to lase at 2.065 μm with a linewidth of 3 nm, the laser output linearly polarised to the YLF a-axis. In both cases, in the cw free-running mode, typically six longitudinal modes lased under the measured transitions. Spatial holeburning was the dominant mechanism producing this multilongitudinal mode output.

Tm:YAP displayed markedly different spectral behaviour, attributed to its very broad gain bandwidth. The laser ran on a comb of distinct wavelengths over the interval 1.965 to 2.020 μm , the exact number and wavelength of which was very sensitive to perturbations to the resonator. With no intracavity line-narrowing elements, the laser operated on a minimum of two distinct wavelengths, and on a maximum of thirteen. All the lines were linearly polarised parallel to the YAP a-axis. The wavelength and polarisation of the laser output was determined by which of the many possible transitions reached threshold first, a balance between the emission cross-section of a particular transition and its inversion threshold.

The three laser hosts investigated were found to lase on the fundamental transverse mode, aided by the tight focussing of the pump beam and the large losses to higher order transverse modes offered by the "soft" aperture of the surrounding unpumped region of the gain medium. Knowledge of the maximum heat load deposited in the laser crystals under lasing conditions, combined with the experimentally measured output polarisation states, allowed the focal lengths of the thermal lenses to be calculated as 3 cm, 5 cm and 10 cm for Tm,Ho:YAP, Tm:YAP and Tm,Ho:YLF respectively.

This work has highlighted some of the difficulties in making a comparison between the laser performance of a range of host crystals under nominally identical experimental conditions. Practical problems encountered include the different transmission profiles of the dielectric coatings deposited on the laser crystals, and the varying transmission of the output mirror over the range of laser wavelengths generated. These are unwanted variables which can be eliminated by more rigorous coating specifications. A more fundamental problem concerns the degree of saturation or bleaching of the absorption of pump light that occurs in the particular hosts being investigated.

Despite these difficulties we can say that for room temperature cw operation of both Tm:YAP and Tm,Ho:YLF optically excited by a 3 W laser diode, the highly divergent output of the pump diode was efficiently converted into a diffraction-limited laser beam in the two micron waveband. The favourable spectroscopic properties of holmium in YAP highlighted in chapter two, combined with the robustness of the host crystal, failed to produce an efficient room-temperature Tm,Ho:YAP laser.

4.5 References

- [1] H. Hemmati, '2.07 μm cw diode-laser pumped Tm,Ho:YLiF_4 room temperature laser', *Opt. Lett.*, vol. 14, no. 9, 435 (1989)
- [2] B. T. McGuckin, R. T. Menzies & H. Hemmati, 'Efficient energy extraction from a diode-pumped Q-switched Tm,Ho:YLiF_4 laser', *Appl. Phys. Lett.*, vol. 59, no. 23, 2926 (1991)
- [3] B. T. McGuckin & R. T. Menzies, 'Efficient cw diode-pumped Tm,Ho:YLF laser with tunability near 2.067 μm ', *IEEE J. Quantum Electron.*, vol. 28, no. 4, 1025 (1992)
- [4] P. A. Budni, M. G. Knights, E. P. Chicklis & H. P. Jenssen, 'Performance of a diode-pumped high PRF Tm,Ho:YLF laser', *IEEE J. Quantum Electron.*, vol. 28, no. 4, 1029 (1992)
- [5] G. J. Koch, J. P. Deyst & M. E. Storm, 'Single-frequency lasing of monolithic Ho, Tm:YLF ', *Opt. Lett.*, vol. 18, no. 15, 1235 (1993)
- [6] M. G. Jani, N. P. Barnes, K. E. Murray & G. E. Lockard, 'Long-pulse-length 2 μm diode-pumped YLiF_4 laser', *Opt. Lett.*, vol. 18, no. 19, 1636 (1993)
- [7] R. C. Stoneman & L. Esterowitz, 'Efficient 1.94 μm Tm:YAlO laser', *IEEE J. of Selected Topics in Quantum Electron.*, vol. 1, no. 1, 78 (1995)
- [8] M. J. Weber, M. Bass, T. E. Varitimos & D. P. Bua, 'Laser action from Ho^{3+} , Er^{3+} and Tm^{3+} in YAlO_3 ', *IEEE J. Quantum Electron.*, vol. 9, no. 11, 1079 (1973)
- [9] A. O. Ivanov, I. V. Mochalov, A. M. Tkachuk, V. A. Fedeov & P. P. Feofilov, 'Spectral characteristics of the thulium ion and cascade generation of stimulated radiation in a $\text{YAlO}_3:\text{Tm}^{3+}:\text{Cr}^{3+}$ crystal', *Sov. J. Quantum Electron.*, vol. 5, no. 1, 117 (1975)
- [10] SDL, Inc. 1995 Product Catalogue
- [11] E. Hecht & A. Zajac, 'Optics', Massachusetts: Addison-Wesley Publishing Company (1974)
- [12] A. E. Siegman, 'Lasers', California: University Science Books (1986)
- [13] A. J. W. Brown, C. H. Fisher & D. D. Lowenthal, 'Injection-seeded, narrow-band, flashlamp-pumped $\text{Ti:Al}_2\text{O}_3$ oscillator', in *Proceedings on Advanced Solid-State Lasers*, (OSA, Washington, DC), 94 (1992)
- [14] N. J. Vasa, M. Tanaka, T. Okada, M. Maeda & O. Uchino, 'Comparative study of spectral narrowing of a pulsed Ti:sapphire laser using pulsed and CW injection seeding', *Appl. Phys. B*, vol. 62, no. 1, 51 (1996)
- [15] V. I. Donin, V. A. Ivanov, V. I. Kovalevskii & D. V. Yakovin, 'CW generation from Ti:sapphire pumped with a high power Ar^+ laser', *Opt. Comm.*, vol. 122, no. 1,2,3, 40 (1995)

Pump absorption effects

5.1 Introduction

During the course of the laser experiments detailed in the preceding chapter, it was of interest to determine the amount of pump light absorbed by the laser crystals, in order that the conversion efficiency from diode light to two micron laser output could be ascertained. A simple measurement was made by placing a power meter behind the laser crystal to capture any pump light not absorbed. In general, the transmitted power was found to be higher than expected given the previously measured absorption coefficients of the laser crystals investigated. These results are attributed principally to pump bleaching of the thulium ground state, and to temperature-dependent broadening of the absorption lines due to the heat load deposited in the gain medium on absorption of the pump light. An understanding of these pump absorption effects is required, if the conversion efficiency of the laser crystals under investigation is to be determined.

A search through the published literature revealed several papers dealing with this topic. The work of Krupke and Chase¹ covers some of the basic principles of pump saturation effects in quasi-three level lasers, but is principally concerned with the so-called "ground state depleted" laser transitions, where intense excitation of a weakly-doped host crystal removes a large fraction of the ground state population. The calculations performed here consider ytterbium (Yb) as the lasing ion, a simple system with only one excited state. This is somewhat different from the case with thulium or holmium as the lasing ion. In another publication by the same group² they consider the operation of the quasi-three level transition at 912 nm in Nd:Y₂SiO₅, both theoretically and experimentally, where pump saturation effects are very evident.

Laser operation of Tm:YVO₄, with particular interest in saturation of the pump transition, is considered in reference 3. Rate equation analysis is used to try and explain the experimentally derived data, with moderate success. The modelling work of Peterson *et al.*⁴ considers diode-pumping of Tm:YAG, but is restricted to considering only relatively low pump intensities (of order 1 kW cm⁻²), and is a plane

wave analysis. A full analysis of saturation effects requires the spatial profile of the pump beam to be considered, if meaningful results are to be obtained.

The quasi-three level nature of the two micron laser transitions of thulium and holmium means that the presence of stimulated emission alters the ground state population, hence the strength of any pump bleaching effects, from the case where lasing does not occur. Intimately connected with this difference is the heat load deposited in the laser crystal on absorption of the pump light, which determines the magnitude of the induced temperature rises and associated thermal lensing. The heat load also determines any temperature-dependent broadening of the absorption lines, an effect most noticeable in the double-doped laser crystals, where the presence of upconversion processes leads to additional nonradiative decay into the host lattice.

The aim of this chapter is to present results on the various effects of pump beam absorption in the three laser crystals of interest, including any changes induced by the presence of stimulated emission, with the ultimate aim of determining the conversion efficiency of absorbed pump light to laser output of these crystals. Rate equation analysis, treating the pump beam as having a Gaussian intensity profile, is carried out for the case of Tm:YAP under nonlasing conditions in order to investigate theoretically the effects of pump bleaching of the thulium ground state.

As in chapter three, computer modelling was carried out using THINKPascal™ software installed on a Macintosh Powerbook 180 laptop.

5.2 Investigation of pump absorption effects

5.2.1 Behaviour under nonlasing conditions

In order to investigate these pump absorption phenomena, the thinnest laser crystals available were used, as this maximised the effect any bleaching of the thulium ground state had on the transmitted pump beam strength. For both Tm:YAP and Tm,Ho:YAP, the 2 mm thick crystals were used, while for Tm,Ho:YLF a 3 mm thick laser crystal was used which was not available at the time of the initial laser experiments.

As part of the laser experiments detailed in the previous chapter, the transmission of the dichroic coating on the pumped face of each laser crystal at the diode wavelength was measured. In order to quantify the amount of pump light not absorbed by the laser crystal, the fraction of the pump reflected by the AR coating on the unpumped face of the laser crystal had to be measured. This measurement was performed in a similar manner to that in section 4.3, but now with the laser crystal reversed. The percentage transmission of these AR coatings was found to be 94.5% for Tm:YAP, 96.0% for Tm,Ho:YAP and 93.5% for Tm,Ho:YLF. These values indicate that reflection of unabsorbed diode light from the unpumped face made only a small contribution to the transmitted pump signal.

The absorption of diode light in the absence of pump bleaching, that is at low pump intensities, can be calculated by taking an absorption spectrum measured at relatively high resolution, and convoluting it with the measured diode spectral linewidth. Using known values for crystal thickness and coating reflectivities, the transmission through the laser crystal as a function of wavelength can be calculated.

The absorption spectra in figures 2.3 and 2.4, measured on a Perkin Elmer Lambda 9 spectrophotometer, were used to provide the absorption coefficient data for thulium in YAP and YLF. These were then convoluted with the normalised Gaussian spectral lineshape ($1/e^2$ width measured to be 1.1 nm) of the laser diode, using crystal thicknesses of 2 and 3 mm for YAP and YLF respectively. Figures 5.1 and 5.2 are the resulting transmission plots taking into account the coating reflectivities. The lineshapes shown are the inverse of the corresponding absorption profiles.

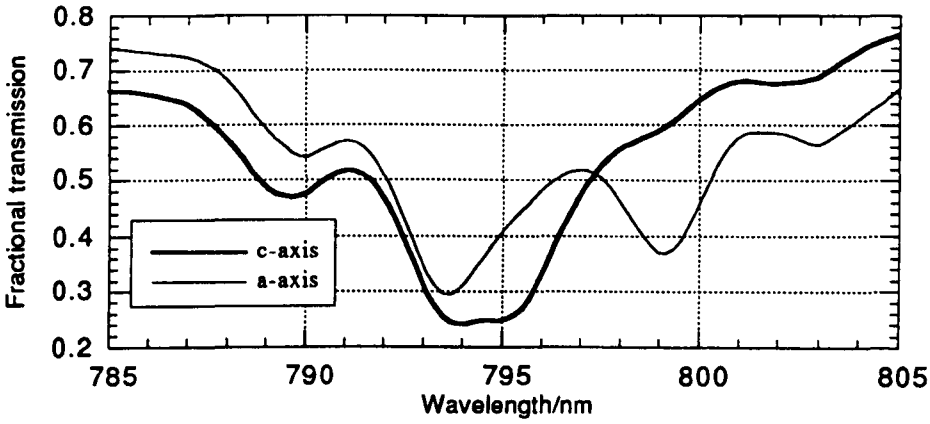


Figure 5.1 Calculated transmission function of 2 mm thick Tm:YAP laser crystal

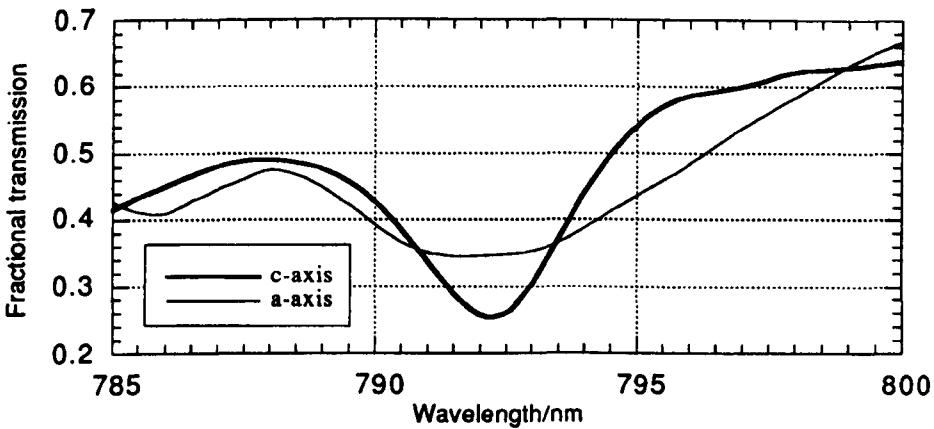


Figure 5.2 Calculated transmission function of 3 mm thick Tm,Ho:YLF laser crystal

The effect of the 1.1 nm $1/e^2$ linewidth of the laser diode is to smooth out the absorption spectra measured at higher resolution. For Tm:YAP, the two closely spaced absorption peaks at 794 and 795.5 nm evident in figure 2.3 are barely resolved by the laser diode. In order to take account of the different coatings on the Tm,Ho:YAP crystal, the transmission values shown in figure 5.2 need to be reduced by 12% for the double-doped crystal.

Diode output centred on 795.3 nm was used to excite Tm:YAP, with the pump light polarised parallel to the crystallographic c-axis. This yields an effective absorption coefficient of 6.78 cm^{-1} according to the transmission data plotted in figure 5.1. Therefore, for an incident power of 3 W, the expected transmitted pump power is 765 mW, with the corresponding value 675 mW for the 2 mm Tm,Ho:YAP crystal. A peak wavelength of 792 nm was used to excite Tm,Ho:YLF, again with the pump

light polarised parallel to the crystallographic c-axis, with a corresponding effective absorption coefficient of 4.53 cm^{-1} . 770 mW transmitted pump power is expected for 3 W incident power.

Using the measured absorption spectra, combined with the energy levels listed in Appendix A for the thulium $^3\text{H}_6$ and $^3\text{H}_4$ energy level manifolds, the pump absorption cross-section for thulium in YAP is calculated to be $8.28 \cdot 10^{-21} \text{ cm}^2$, and for thulium in YLF is $8.91 \cdot 10^{-21} \text{ cm}^2$. Saturation of the thulium absorption transition depends on the product of the absorption cross-section and the lifetime of the $^3\text{F}_4$ energy level manifold. From section 2.3.3.3 the measured fluorescence lifetime of thulium is 4.4 ms in YAP and 8.0 ms in YLF. Therefore we would expect the pump transition in YLF to show signs of ground state bleaching at lower intensities than in YAP (the cross-relaxation process also needs to be considered when considering pump bleaching in thulium - its relative magnitude in YAP compared to YLF is not known).

Figure 5.3 is a schematic diagram of the initial pump bleaching experiments. Varying the separation d of the laser crystal and the 10 mm focal length cylindrical lens in effect alters the intensity of the diode light incident on the crystal as it traverses through the focus of the pump optics. Referring back to figure 4.7, the diode pump beam is focussed approximately 6.5 mm from the plane face of the 10 mm focal length cylindrical lens.

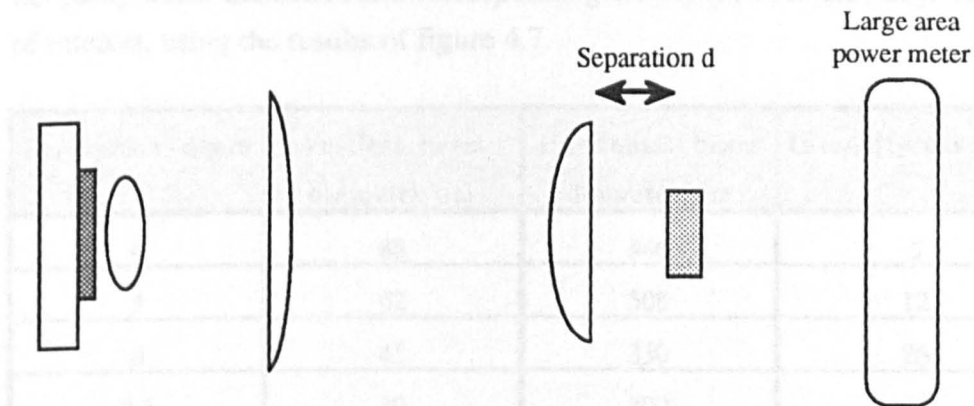


Figure 5.3 Schematic of pump saturation experiment

During the laser experiments, the crystals were pumped close to their cooled face, in order to minimise the induced temperature rises. The experiment described here, where the laser crystal was moved relative to the pump beam focus, required the crystal to be pumped down its centre, in order to minimise any aperturing effects due to the finite width of the laser crystal.

The first crystal tested was the 2 mm Tm:YAP crystal, producing the results plotted in figure 5.4. Here the diode was operated at its 3 W maximum output power. It is immediately apparent that the measured transmitted power is significantly higher than the previously calculated value of 765 mW. Furthermore, there is a 20% variation in the transmitted signals recorded, with maximum transmission around the focal plane of the pump optics where the pump beam is at its most intense.

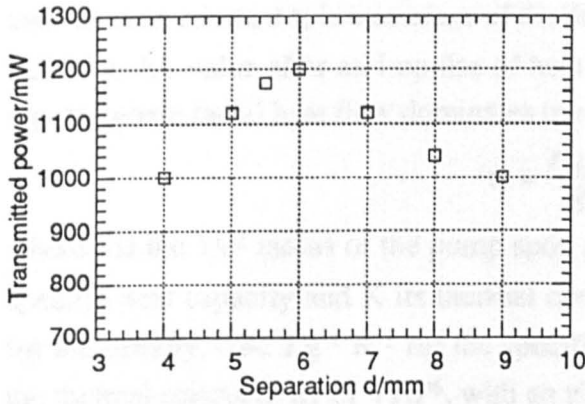


Figure 5.4 Transmitted pump power through 2 mm Tm:YAP laser crystal

Decreasing the separation d below 4 mm or increasing it above 9 mm caused aperturing problems as the diode spot size in the horizontal plane becomes of comparable dimension to the 5 mm width of the Tm:YAP laser crystal. Table 5.1 lists the pump beam diameters and corresponding intensities over the range of separations of interest, using the results of figure 4.7.

Separation d /mm	Vertical beam diameter/ μm	Horizontal beam diameter/ μm	Intensity/ $\text{kW}\cdot\text{cm}^{-2}$
4	88	846	5
5	62	508	12
6	45	330	26
6.5	39	300	33
7	36	310	35
8	35	446	25
9	43	740	12

Table 5.1 Pump spot sizes and intensity as a function of separation d

One possible explanation for this behaviour concerns the increase in temperature as a smaller region of the laser crystal is pumped. This leads to the absorption transition lowering in peak strength (and increasing in width), in turn increasing the transmitted signal. In order to test this hypothesis, the diode beam was periodically blocked using a chopper in order to produce pulsed excitation of the laser crystal (driving the diode with current pulses rather than cw produced chirping in the optical output spectrum which altered the transmission throughout the duration of the output pulse). The thermal time constant τ_r is a measure of the decay time of the initial peak temperature to fall to its $1/e$ value after an impulse of heat is deposited in the gain medium. In the regime where radial heat flow dominates over axial flow, τ_r is given by the expression

$$\tau_r = \frac{r^2 \rho c}{K} \quad 5-1$$

where r is the $1/e^2$ radius of the pump spot, ρ is the density of the gain medium, c its specific heat capacity and K its thermal conductivity⁵. Using values of 5.35 g cm^{-3} for the density, $0.42 \text{ J g}^{-1} \text{ K}^{-1}$ for the specific heat capacity and $0.11 \text{ W cm}^{-1} \text{ K}^{-1}$ for the thermal conductivity of YAP⁶, with an elliptical focussed pump spot of dimension 35 by $300 \text{ }\mu\text{m}$, the thermal time constant is in the range 0.25 to 18 ms. The chopped output of the diode was observed using a silicon photodiode. The raw output of the diode was then compared to the signal transmitted through the laser crystal. Unfortunately this technique was not wholly accurate, as the pump pulse durations required to see any of the long time constant thermal decays necessitated slow chopper speeds with long switch-on times (a measure of the time taken for the edge of the chopper blade to traverse the pump beam). This tended to mask any time-dependent transmission due to temperature decay in the gain medium, but did serve to show that any such effects were small, and could not account fully for the results in figure 5.4.

An alternative method of determining whether temperature-dependent lowering of the absorption coefficient was causing the observed pump beam transmission was also considered. After fixing the position of the laser crystal relative to the focus of the pump optics, any variation in the transmitted pump power could be observed by simply altering the laser crystal heatsink temperature, hence the temperature in the pumped region of the crystal. Repeatable results were obtained indicating that as the heatsink temperature was increased over a 20°C range around room temperature, there was a less than 5% increase in the transmitted pump power. This behaviour was independent of the position of the laser crystal relative to the focus of the pump optics. These results indicate that temperature-dependent transmission does occur, but that it is not a strong effect, corroborating the chopper results.

The thermal modelling of chapter three, combined with the measured diode spot sizes, shows that altering the position of the laser crystal relative to the focus of the pump optics produces a change in peak temperature of order 10°C. This is an upper bound on the temperature variation, as the effects of pump bleaching are not included here. These calculations further illustrate that the measured variation in pump beam transmission cannot be solely attributed to temperature broadening of the absorption spectrum. Therefore we can conclude that intensity-dependent bleaching of the pump transition is the principal mechanism producing the experimental results.

Similar measurements were made with Tm,Ho:YAP and Tm,Ho:YLF. The variation in transmission through the former is shown in figure 5.5.

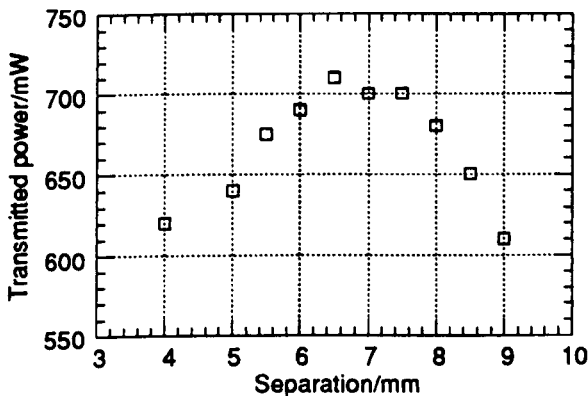


Figure 5.5 Transmitted pump power through 2 mm Tm,Ho:YAP laser crystal

It is immediately apparent that the transmitted pump power is significantly lower through the double-doped than through the single-doped crystal, both of the same thickness. In fact, over the range of incident pump intensities, the transmission through the Tm,Ho:YAP crystal was centred around the 675 mW expected, with a 16% increase in transmission as the laser crystal was moved from a position of low to high pump intensity.

Absorption measurements in a Perkin Elmer Lambda 9 spectrophotometer were used to confirm that the two crystals had nominally identical thulium concentrations (there was at most a 2% difference between the concentration levels in the two samples), thus discounting this as a source of the different pump transmission behaviour. Rather it is the double-doping that causes the difference in behaviour. Absorption of diode light occurs in thulium, followed by cross-relaxation which efficiently populates the thulium first excited state. In materials co-doped with holmium, excitation sharing between the first excited states of thulium and holmium occurs. Transfer of excitation

onto the holmium de-excites the thulium to the ground state, increasing the population available for absorbing the pump radiation, and so acting to negate any bleaching effects.

As detailed in the following chapter, significant amounts of upconversion occur in double-doped materials, more so in YAP than in YLF (see figures 6.13 and 6.14 for reference). One upconversion mechanism involves absorption of pump light from the holmium first excited state. It is this additional absorption which reduces the pump beam transmission below its expected value. However it is evident from figure 5.5 that there is still significant variation in the transmitted signal depending on the incident pump intensity. The principal upconversion mechanism does not involve further absorption of the pump beam, but nevertheless depends critically on the pump intensity. In the oxide YAP host, most of the population excited to higher levels via this upconversion route decays nonradiatively, producing additional heating of the crystal. The upconversion rates scale with the intensity of the excitation source. Therefore at higher pump intensities, increased nonradiative decay occurs, producing greater temperature rises in the laser crystal which in turn lower the peak absorption coefficient, increasing the transmitted pump power.

Figure 5.6 shows the corresponding results for the 3 mm Tm,Ho:YLF crystal. This sample was of square cross-section of dimension 2.5 mm, a smaller aperture than the YAP samples, which limited the range of spot sizes used to pump it.

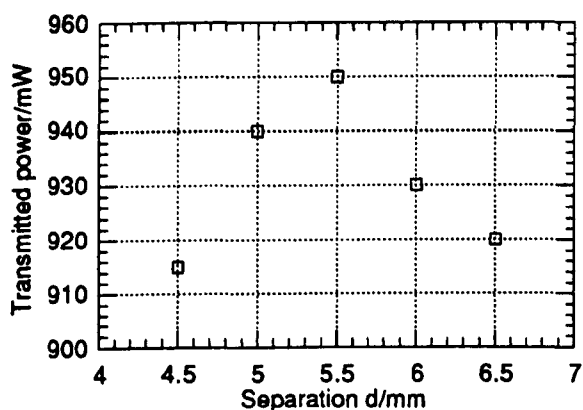


Figure 5.6 Transmitted pump power through 3 mm Tm,Ho:YLF laser crystal

It is worth noting here that the position of peak transmission occurs closer to the 10 mm focal length cylindrical lens than in the case of both YAP crystals. This can be explained simply by the thicker YLF sample intercepting the focus of the pump beam

at smaller separations d , an effect further accentuated by the lower refractive index of YLF than YAP.

Unlike the Tm,Ho:YAP results, but similar to the Tm:YAP results, the transmitted power is higher than the expected 775 mW over the range of pump intensities employed. The transmitted signal varies by 4% over this range of pump intensities. The corresponding variations in the Tm:YAP and Tm,Ho:YAP results are 9% and 12%. YLF has a thermal conductivity approximately one half that of YAP, and so for a given heat deposition the temperature rise is greater in YLF. Therefore temperature-broadening of the absorption profile is more pronounced in YLF than YAP. This was confirmed by repeating the measurement performed with Tm:YAP of varying the laser crystal heatsink temperature and observing any changes in the transmitted power level. Over the same 20°C range, the transmitted power level changed by approximately 10%, twice the corresponding change with Tm:YAP (the change in Tm,Ho:YAP was found to be the same as in Tm:YAP). Therefore we would expect the transmission in general to be high relative to the calculated value, with more intense pumping producing higher temperatures and transmission. Upconversion is not as great in Tm,Ho:YLF as in Tm,Ho:YAP, and so the change in transmission with pump intensity is not as marked. Finally, as calculated previously, the product of absorption cross-section and fluorescence lifetime is higher for thulium in YLF than for thulium in YAP. For a given pump intensity, the fluoride host will show a greater degree of ground state bleaching.

Further investigation was carried out concentrating on the two YAP samples, as they showed the extremes of behaviour. Referring back to figure 5.3, each crystal in turn was positioned at a separation d of 6 mm, where the transmitted pump power was at a maximum. The laser diode was run at maximum output power, with a range of pump intensities obtained by attenuating the diode output using neutral density filters. Simply reducing the diode output by decreasing the drive current also changes the output wavelength which alters pump transmission independent of any bleaching effects. The neutral density filters used were placed between the two cylindrical lenses, and angled to ensure no reflected light was fed back into the laser diode. At this point in the optics train the diode beam was of dimension 3 by 5 mm, large enough that thermal lensing in the neutral density filters was considered insufficient to significantly alter the focussing of the diode output. Using this technique, the data displayed in figure 5.7 were obtained.

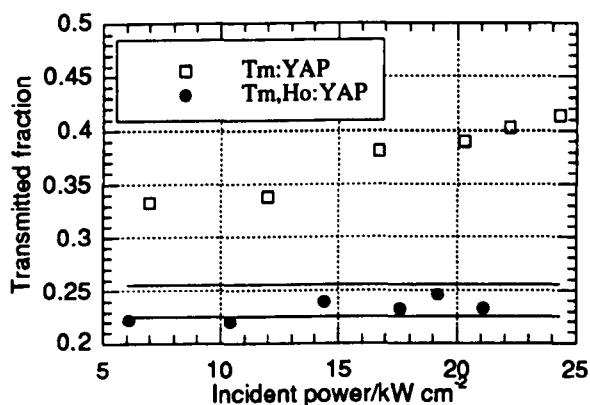


Figure 5.7 Intensity-dependent pump beam transmission in Tm:YAP and Tm,Ho:YAP

The horizontal lines at transmission values of 0.255 and 0.225 represent the expected transmission derived from figure 5.1 through Tm:YAP and Tm,Ho:YAP respectively, where no temperature-dependent or pump bleaching effects occur. These results corroborate the behaviour shown in figures 5.4 and 5.5. Tm:YAP displays higher transmission than expected, principally due to bleaching of the thulium ground state. Tm,Ho:YAP has a pump transmission centred around the calculated value over the range of pump intensities generated, the exact value determined by the magnitude of temperature-dependent lowering of the absorption coefficient due to the upconversion mechanisms occurring in the double-doped crystal.

5.2.2 Effects of stimulated emission

In the quasi-three level thulium and holmium laser systems being investigated here, the presence of stimulated emission on the two micron transition in these ions efficiently repopulates the ground state energy level manifold as compared to the situation where lasing does not occur. Therefore, when stimulated emission is present, the absorption of the pump beam is expected to be greater due to the larger ground state population. This will alter the fraction of the incident pump beam absorbed, hence the conversion efficiency.

Furthermore, stimulated emission removes excitation from the gain medium which otherwise would de-excite via a combination of radiative and non-radiative decay routes. This rapid removal of excitation under lasing conditions is expected to reduce the heat load in the gain medium.

A simple experimental arrangement was devised in order to measure these effects in Tm:YAP and Tm,Ho:YAP. With the laser set-up of figure 4.8, the RG1000 filter used to block the unabsorbed diode light was removed and replaced with a glass prism. This served to spatially separate the diode light from the two micron laser output, allowing both to be individually monitored. Laser action was inhibited by misaligning the output mirror sufficiently, then the appropriate realignment performed to reinstate lasing. The glass prism used had faces of dimension 25 by 15 mm, large enough to capture most of the highly divergent diode beam.

The laser crystal was mounted on a brass heatsink, the temperature of which was controlled using a thermoelectric cooler. Monitoring the electrical power input to the thermoelectric cooler required to keep the heatsink at a fixed temperature gives a direct measure of the heat load in the laser crystal.

Each laser in turn was operated over a range of output powers, with the changes in pump beam transmission and heat load recorded over this range. It is not the absolute values that are of most interest, but the ratio of values with and without the presence of stimulated emission. For the heat load measurements, care had to be taken to ensure that environmental conditions were constant over the course of each experimental run. The thermoelectric cooler was sandwiched between the laser crystal heatsink mount and a water-cooled copper block, with the tap water left running for several hours to allow its temperature and flow rate to stabilise. The laser crystal heatsink temperature was kept fixed at 15°C which was below the typical ambient room temperature of $20\pm 2^\circ\text{C}$. This meant that the electrical power to the thermoelectric cooler to hold the heatsink at 15°C with no heat load in the laser crystal had to be subtracted from all measurements. Typical results are shown in figures 5.8 and 5.9, the former for the 2 mm Tm:YAP crystal, the latter for the 2 mm Tm,Ho:YAP crystal (with the 0.8%T output mirror).

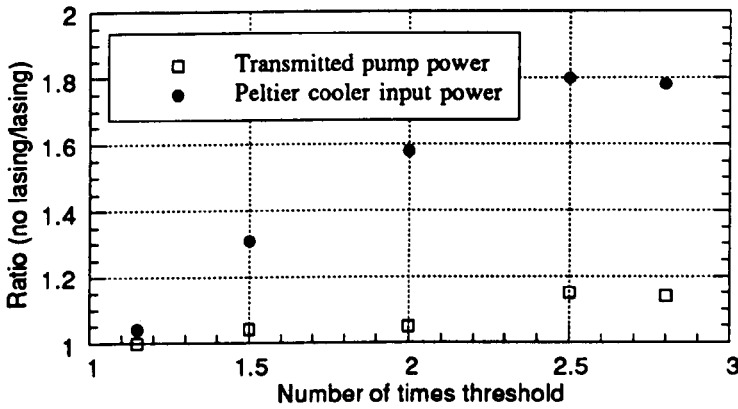


Figure 5.8 Behaviour of Tm:YAP with and without the presence of lasing

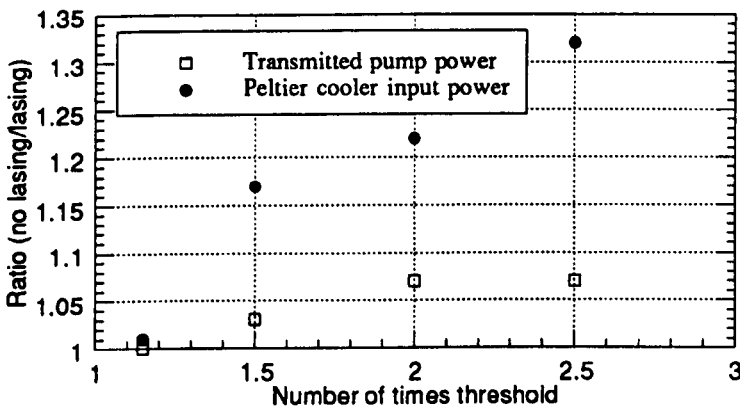


Figure 5.9 Behaviour of Tm,Ho:YAP with and without the presence of lasing

Operation further from threshold leads to a larger heat load in the gain medium simply because the pump power is higher. It also leads to a greater disparity in terms of heat load and transmitted pump beam between conditions of lasing and no lasing, as more excitation is removed by stimulated emission further from threshold. This more than compensates for the greater ground state population during lasing, which increases pump beam absorption hence heat deposition. This effect was more pronounced in Tm:YAP than Tm,Ho:YAP because the former was a much more efficient laser; at maximum output Tm:YAP produced 730 mW of laser output operating at 2.8 times threshold, while Tm,Ho:YAP produced 245 mW, approximately one third the power, operating at 2.5 times threshold. Therefore in Tm:YAP when lasing was terminated there was a much greater increase in the excitation level able to contribute to heating of the gain medium via nonradiative decay. As threshold is approached, the disparity between lasing and nonlasing conditions will decrease, as verified by the experimental

measurements. The dip in the Tm:YAP plots at the highest pump power is attributed to ground state bleaching effects.

The dependence of the amount of pump beam transmission on the pumping ratio is similar to that of the heat load dependence. Experimental measurement of this dependence allows the amount of pump light absorbed under lasing conditions to be found, from which a figure for the conversion of pump power to laser output power within the gain medium can be calculated. This figure allows a more accurate comparison of the efficiencies of the different laser crystals tested than simply from the total diode power available because, as has already been discussed, pump bleaching and associated effects vary significantly between different laser crystals, as do the transmission of dielectric coatings at the pump wavelengths.

From figure 5.8, at maximum output power the ratio of transmitted pump powers for Tm:YAP was measured to be 1.14. Referring back to figure 5.4, the maximum transmitted pump power under nonlasing conditions was measured to be 1.2 W. Therefore when lasing occurred, the transmitted pump power fell to 1.05 W, implying that 1.76 W was absorbed in the 2 mm thick crystal. Given the maximum recorded laser output power of 730 mW, the conversion efficiency within the gain medium was 42%.

Using figures 5.5 and 5.9, the corresponding calculation for Tm,Ho:YAP can be carried out. A maximum transmitted pump power of 710 mW under nonlasing conditions translated to 665 mW during lasing, resulting in 1.76 W being absorbed in the 2 mm thick crystal. Given the maximum recorded laser output power of 245 mW, the conversion efficiency within the gain medium was 14%, a factor of three down on the conversion efficiency of Tm:YAP. The best laser performance in terms of output power was obtained with the 3 mm Tm,Ho:YAP crystal, generating 270 mW at 2.3 times threshold. Under nonlasing conditions the transmitted pump power through this crystal was measured to be 475 mW, implying that 1.96 W of pump was absorbed. With stimulated emission present this value will increase. Therefore an upper bound on the conversion efficiency in the 3 mm crystal of 14% was calculated.

A comparison of Tm,Ho:YLF behaviour under lasing and nonlasing conditions was not carried out. However, as with the 3 mm Tm,Ho:YAP, an upper bound on the conversion efficiency in the gain medium can be found. Under nonlasing conditions, the transmitted pump power through the 4 mm crystal used in the lasing experiments

was measured to be 675 mW, 2.2 W having been absorbed. The laser produced a maximum output power of 660 mW, yielding a conversion efficiency of 30%, twice that of Tm,Ho:YAP, but down by 30% on Tm:YAP. The results of the conversion efficiency calculations are summarised in table 5.2.

Laser crystal	Maximum output power/mW	Pump power absorbed/W	Conversion efficiency/%
2 mm Tm:YAP	730	1.76	42
2 mm Tm,Ho:YAP	245	1.76	14
4 mm Tm,Ho:YLF	660	2.20	30

Table 5.2 Summary of conversion efficiency calculations

We can use the values for absorbed pump power and laser output power to estimate the magnitude of the thermal lensing, by subtracting the measured laser output power from the calculated pump power absorbed, then assuming that 50% of the remaining absorbed pump power is converted to heat.

For the 2 mm thick Tm:YAP, the heat load when lasing was estimated to be 500 mW at maximum pump power. Armed with knowledge that the laser output was polarised parallel to the YAP a-axis, the induced thermal lens was estimated to be of focal length 5 cm, using the results of the calculations in section 3.4 of the thermal modelling chapter.

Considering now the 3 mm thick Tm,Ho:YAP laser crystal, the lower bound on the absorbed pump power was 1.96 W, therefore the heat load when lasing was estimated to be 850 mW. The holmium lasing transition was polarised parallel to the YAP c-axis, yielding a thermal lens of focal length of approximately 3 cm.

Finally, for the 4 mm Tm,Ho:YLF laser crystal, the lower bound on the absorbed pump power was 2.2 W, producing a heat load of order 780 mW under lasing conditions. With the laser output polarised parallel to the YLF a-axis, the resulting thermal lens was estimated to have a focal length of 10 cm.

Not unexpectedly, the Tm,Ho:YAP crystal suffers the severest thermal lensing problems, given its poor conversion efficiency of absorbed pump light to laser output. These results are summarised in table 5.3.

Laser crystal	Deposited heat load/mW	Laser output polarisation	Thermal lens focal length/cm
2 mm Tm:YAP	500	a-axis	5
3 mm Tm,Ho:YAP	850	c-axis	3
4 mm Tm,Ho:YLF	780	a-axis	10

Table 5.3 Summary of thermal lens focal length calculations

The resonator containing the shortest focal length thermal lens will have the smallest mode size at the output mirror. This in turn produces the output beam with the highest divergence, as was measured for Tm,Ho:YAP in section 4.3.2 of the previous chapter.

5.3 Rate equation analysis of pump beam transmission

Rate equation analysis of the distribution of population amongst the relevant energy levels allows the experimentally obtained results to be compared with theory. The most straightforward scenario to investigate using rate equation analysis involves a thulium doped crystal optically pumped but not lasing. The presence of stimulated emission adds significant complexity to the resulting rate equations, making analytical solutions difficult, even in steady-state operation. Double-doped systems require numerical techniques in order to analyse the relevant rate equations, both for the absence and presence of stimulated emission. Here it is the excitation sharing and various upconversion mechanisms that make analytical solutions very difficult to derive.

The particular crystal investigated here is Tm:YAP, in order to compare the calculations with the experimental results of the previous section. The relevant energy levels and excitation/de-excitation processes are shown in figure 5.10.

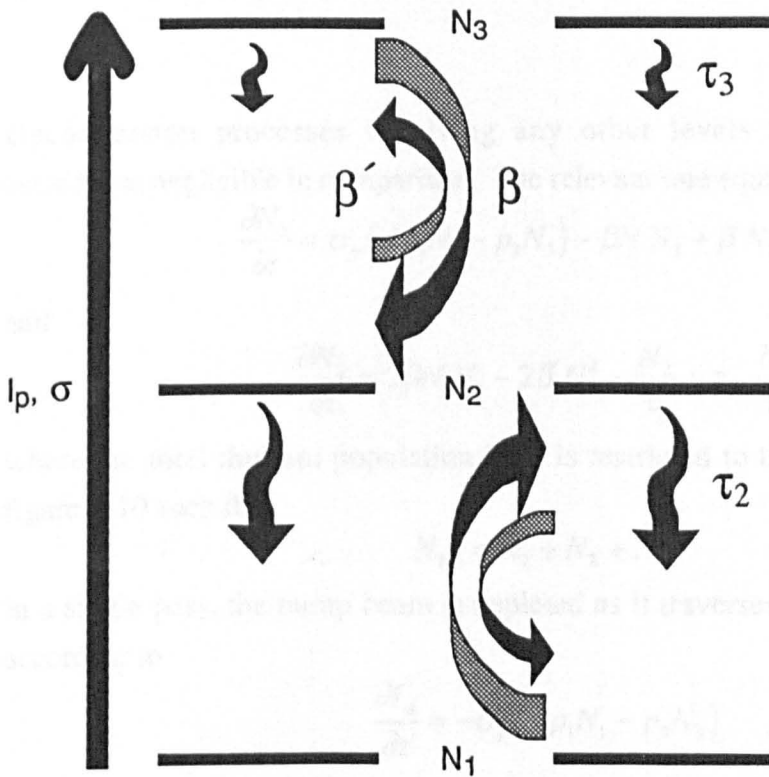


Figure 5.10 Energy level diagram showing parameters used in rate equation analysis

The following is the symbol list for this section:

N_{Tm}	-	total thulium concentration (cm^{-3})
N_1	-	$^3\text{H}_6$ ground state manifold population density (cm^{-3})
N_2	-	first excited state ($^3\text{F}_4$ lasing band) population density (cm^{-3})
N_3	-	second excited state ($^3\text{H}_4$ pump band) population density (cm^{-3})
ν_p, λ_p	-	pump frequency, wavelength (Hz, cm)
$p_1(p_3)$	-	fractional occupation of pump lower (upper) level(s)
σ_p	-	pump absorption cross-section (cm^2)
I_p	-	pump intensity ($\text{W cm}^{-2} \text{ s}^{-1}$)
I_p'	-	pump photon rate (photons $\text{cm}^{-2} \text{ s}^{-1}$)
β	-	cross-relaxation rate ($\text{cm}^3 \text{ s}^{-1}$)
β'	-	reverse upconversion rate ($\text{cm}^3 \cdot \text{s}^{-1}$)
τ_2, τ_3	-	level decay lifetime (s)
γ_{32}	-	branching ratio level 3 to level 2
P_p	-	pump power (W)
w	-	$1/e^2$ pump beam radius (cm)

Upconversion processes involving any other levels have been ignored here, considered negligible in comparison. The relevant rate equations in full are

$$\frac{\partial N_3}{\partial t} = \sigma_p I_p' (p_1 N_1 - p_3 N_3) - \beta N_1 N_3 + \beta' N_2^2 - \frac{N_3}{\tau_3} \quad 5-2$$

and

$$\frac{\partial N_2}{\partial t} = 2\beta N_1 N_3 - 2\beta' N_2^2 - \frac{N_2}{\tau_2} + \gamma_{32} \frac{N_3}{\tau_3} \quad 5-3$$

where the total thulium population N_{Tm} is restricted to the three levels depicted in figure 5-10 such that

$$N_{Tm} = N_1 + N_2 + N_3. \quad 5-4$$

In a single pass, the pump beam is depleted as it traverses through the gain medium according to

$$\frac{\partial I_p'}{\partial z} = -\sigma_p I_p' (p_1 N_1 - p_3 N_3) \quad 5-5$$

where the pump intensity has been converted to a pump rate by the following normalisation

$$I_p' = \frac{I_p}{h\nu_p}. \quad 5-6$$

Steady-state solutions are obtained by setting the derivatives in equations 5-2 and 5-3 to zero, leading to the following pair of expressions

$$N_3 = \frac{\sigma_p I_p p_1 N_1 + \beta' N_2^2}{\sigma_p I_p p_3 + \beta N_1 + \frac{1}{\tau_3}} \tag{5-7}$$

$$N_2 = \frac{N_3 \left(2\beta N_1 + \frac{\gamma_{32}}{\tau_3} \right)}{2\beta' N_2 + \frac{1}{\tau_2}}$$

Some simplification of these equations can take place, by considering the relative magnitudes of the various rates. It is well understood that at thulium concentrations equivalent to 4% thulium in YAG or greater, the rapid cross-relaxation process dominates the removal of excitation from level 3, resulting in the population N_3 being much less than the populations in the other two levels^{7,8}. Therefore the $p_3 N_3$ term in the pump rate can be neglected. No value for the cross-relaxation parameter β of thulium in YAP could be found in the literature. However the corresponding value for 6% thulium in YAG^{9,10} has been quoted as $10^{-16} \text{ cm}^3 \text{ s}^{-1}$. A similar value was assumed for the 4.2% Tm:YAP laser crystal being assessed here. Using this value, the rate βN_1 is the range 8250 to 82,500 s^{-1} , with the ground state population varying between 10% and 100% of the total thulium population. For a pump wavelength of 795 nm with absorption cross-section of order 10^{-20} cm^2 , and a peak incident intensity of order 25 kW cm^{-2} (see table 5-1), the pump rate is less than 1000 s^{-1} . The spontaneous emission rate from level 3 is given as 1164 s^{-1} for thulium in YAP¹¹, comparable with the pump rate. Both can be neglected in determining the population of level 3, as they are very much smaller than the cross-relaxation rate.

An important issue to address is the size of the reverse upconversion process β' relative to the cross-relaxation β . The two are related by the expression

$$\beta' = \beta \exp\left(-\frac{\Delta E}{kT}\right) \tag{5-8}$$

where ΔE is the thermal equilibrium energy deficit between the initial state of a ground state thulium ion and a thulium ion excited by absorption of a pump photon, and the final state of two thulium ions in level 2, populated by cross-relaxation. The expression for this energy deficit is

$$\Delta E = \bar{E}_1 + \bar{E}_3 - 2\bar{E}_2 \tag{5-9}$$

where the thermal average as derived from the Boltzmann distribution is used for each level⁴. Over the range around room temperature, the value of β' is calculated (using

the energy levels listed in Appendix A) to be 0.2% that of β . Therefore the upconversion rate is always significantly less than the cross-relaxation rate, even when a large fraction of the ground state population has been removed.

The relative magnitudes of the relevant rates can be summarised thus

$$\begin{aligned}\beta N_1 &> \sigma_p I_p p_1, \frac{1}{\tau_3} \\ 2\beta N_2 &< \frac{1}{\tau_2} \\ \beta N_2^2 &< \sigma_p I_p p_1 N_1\end{aligned}\tag{5-10}$$

which allows the pair of expressions in equation 5-7 to be reduced to

$$\begin{aligned}N_3 &= \frac{\sigma_p I_p p_1}{\beta} \\ N_2 &= 2\beta N_1 N_3 \tau_2 \\ N_1 &= \frac{N_{Tm} - \frac{\sigma_p I_p p_1}{\beta}}{1 + 2\sigma_p p_1 I_p \tau_2}.\end{aligned}\tag{5-11}$$

Here the final expression is obtained using the first two in conjunction with equation 5-4. The pump beam depletion can now be written as

$$\begin{aligned}\frac{\partial I_p'}{\partial z} &= -\sigma_p I_p' p_1 N_1 \\ &= -\frac{\sigma_p I_p' p_1 \left(N_{Tm} - \frac{\sigma_p I_p' p_1}{\beta} \right)}{1 + 2\tau_2 \sigma_p I_p' p_1}.\end{aligned}\tag{5-12}$$

Integrating this expression leads to the following

$$\ln I_p' - (1 + 2\tau_2 N_{Tm} \beta) \ln \left(1 - \frac{\sigma_p p_1}{\beta N_{Tm}} I_p' \right) + C = -\sigma_p p_1 N_{Tm} z.\tag{5-13}$$

In order to determine the constant C, we use the boundary condition that $I_p = I_{p0}$ at $z = 0$. This results in the final expression for the change in pump intensity along the length of the gain medium given by

$$\ln \frac{I_p'}{I_{p0}} - (1 + 2\tau_2 N_{Tm} \beta) \ln \left(\frac{\beta N_{Tm} - \sigma_p p_1 I_p'}{\beta N_{Tm} - \sigma_p p_1 I_{p0}} \right) = -\sigma_p p_1 N_{Tm} z.\tag{5-14}$$

The bracketed term in front of the second part of the left hand side of equation 5-14 is dominated by the $2\tau_2 N_{Tm} \beta$ term.

The rate equation analysis outlined here takes no account of the spatial profile of the pump beam, an important factor in determining the degree of pump bleaching occurring. Assuming a Gaussian intensity profile for the pump beam, the following expressions apply to the beam incident on the laser crystal

$$I_p(r) = I_{p_0} \exp\left(-\frac{2r^2}{w^2}\right) \quad 5-15$$

$$P_{p_0} = \frac{1}{2} \pi w^2 I_{p_0}.$$

For the purpose of this analysis, the pump beam is assumed to have zero divergence. In similar fashion to the thermal modelling in chapter three, the gain medium is divided into a series of slices of thickness Δz . The incident beam on the pumped face of the laser crystal is treated as a series of annular discs, radius r , thickness dr , the incident intensity in each disc being calculated from equation 5-15. Substituting Δz for z in equation 5-14, the transmitted intensity at radius r can be calculated. Using the fact that the area of each annular disc can be approximated as $2\pi r dr$, the transmitted power through each disc can be found, with the total transmitted power through a slice obtained by summing over all the discs. From equation 5-15, at a beam radius of three times the $1/e^2$ radius, the intensity in a Gaussian beam has fallen to 10^{-8} of the peak intensity, with essentially all the power contained within this radius. Therefore it is necessary only to consider a beam of maximum radius three times the waist radius when performing these bleaching calculations.

The algorithm outlined above was encoded in Pascal, employing a simple loop structure in order to propagate through the laser crystal, at each slice iterating across the width of the incident beam, calculating the transmitted intensity in each annulus. These transmitted intensities were stored in an array, with the transmitted intensities through one slice serving as the incident intensities for the next slice. After the final slice of the gain medium had been traversed, the transmitted power was obtained by summing over the transmitted powers in each annulus. The fractional transmission was then obtained by comparing the transmitted to the incident power.

The assumption that the incident pump beam has a Gaussian intensity profile is a reasonable assumption at or close to the focus of the pump optics. However the actual pump beam used in the experimental work, even if considered as having a Gaussian intensity profile, was elliptical in cross-section. With the front face of the 2 mm thick Tm:YAP crystal 6 mm from the final cylindrical lens of the optics train (the position of maximum pump beam transmission, and also the laser crystal position yielding

maximum laser output power) the incident pump beam had FWHM dimensions of 45 by 330 μm . This is equivalent in area to a circular Gaussian beam of $1/e^2$ radius 100 μm . In order to greatly simplify the computer code, the pump beam was assumed to have a circular rather than an elliptical cross-section.

The computer code was validated by inputting extremes of incident intensities, and noting the calculated transmission. For incident intensities below 0.1 kW cm^{-2} , the transmission approaches the expected small-signal value of 0.255 asymptotically. As the incident intensity is increased to high values of order 1 MW cm^{-2} and above, the transmission asymptotes to the expected value of 0.935 (the transmission of the pump beam through the dichroic coating on the laser crystal). Testing of the computer code revealed that the calculated transmission was highly insensitive to the value of the cross-relaxation parameter. Changing it by an order of magnitude either side of the quoted value of $10^{-16} \text{ cm}^3 \text{ s}^{-1}$ for thulium in YAG altered the calculated transmission by less than 1%. Cross-relaxation occurs far more rapidly than any other process, therefore altering its value even by an order of magnitude still leaves it the dominant parameter determining the distribution of population amongst the thulium energy levels.

In order to compare theory and experiment, the incident pump intensities used to generate the data in figure 5.7 were fed into the computer code, and the resulting pump beam transmissions calculated. The resulting comparison is shown in figure 5.11.

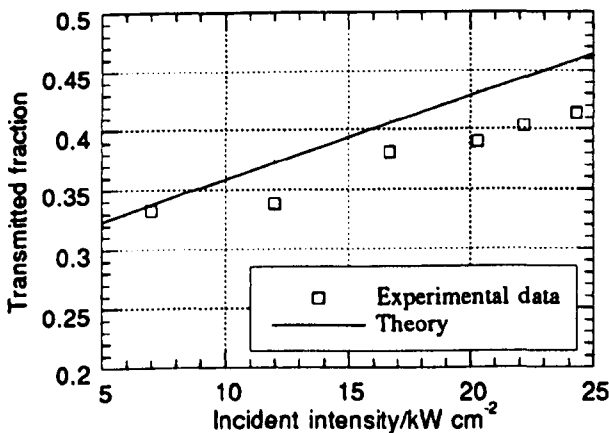


Figure 5.11 Comparison between theory and experiment

Over the limited range of incident pump intensities that could be generated experimentally, the theoretical transmission increased linearly with incident intensity. The experimental points follow a similar trend at the higher intensities, with a 14%

offset at the highest intensity, falling to 10% for the lower intensities, with the exception of the lowest intensity point, where theory and experiment were in close agreement. Unfortunately, it was not possible to generate lower pump intensities experimentally. The technique used involved attenuating the diode beam with neutral density filters, but higher density filters suffered from increased heating on absorption of the diode light, so much so that eventually these filters would fracture. In addition, transmitted pump beam signals smaller than the lowest value of 300 mW plotted in figure 5.7 were difficult to measure accurately with the large area power meter employed, as it was sensitive to air currents at signals of order 100 mW and below.

The results plotted in figure 5.7 were repeatable to within $\pm 3\%$, insufficient to account for the observed deviation from theory at the higher pump intensities. The rate equation analysis made several assumptions, the principal one being that the pump beam had zero divergence and was circular in cross-section with a Gaussian intensity profile, whereas in reality the diode beam employed experimentally was highly divergent and elliptical in cross-section, with an intensity profile that could only be approximated as Gaussian. Moreover, the fact that the discrepancy between theory and experiment is largest at the highest incident pump intensity suggests that an additional mechanism occurs in the Tm:YAP which causes increased pump absorption at higher intensities.

Although the neutral density filters employed only produced relatively weak attenuation, and were positioned in the optics train to intercept the pump beam when it was of large dimension, there is the possibility that sufficient thermal lensing occurred to alter the pump spot size at the Tm:YAP crystal, altering the incident intensity and therefore the transmitted pump signal.

With the experimental set-up employed it is very difficult to determine whether the discrepancy between theory and experiment is due principally to errors in one or the other, or if both are equally deficient. Ideally what is required is a pump beam with a TEM₀₀ transverse mode, most readily achieved by using a Ti:sapphire laser tuned to give the correct output wavelength. Utilising such a pump source, conditions analysed theoretically can be better approximated experimentally. Despite these uncertainties, the modelling results show a reasonable match to the experimental data, thus confirming that intensity-dependent pump bleaching is the principal mechanism causing increased transmission of the pump light in single-doped thulium crystals.

5.4 Conclusions

In this chapter results have been presented concerning an investigation of pump beam absorption effects in quasi-three level thulium and holmium lasers. For single-doped thulium laser crystals, the principal effect was an intensity-dependent bleaching of the ground state population. Measurements on a 2 mm thick Tm:YAP crystal confirmed this, backed up by computer modelling using rate equation analysis.

The behaviour of double-doped thulium,holmium lasers was more complicated. Excitation sharing between the thulium and holmium acted to reduce the depletion of the thulium ground state population, counteracted by an upconversion process causing additional absorption of the pump light. With these measurements of pump beam transmission through laser crystals, consideration had to be taken of temperature-dependent broadening of the absorption band producing increased transmission. In Tm,Ho:YAP intensity-dependent upconversion processes contributed significant additional heating of the crystal via nonradiative decay. In Tm,Ho:YLF the lower thermal conductivity of the host crystal produced stronger temperature-dependent transmission behaviour at all incident pump intensities. Additionally, the thulium pump absorption transition in YLF centred at 792 nm had a cross-section nearly 10% larger than the corresponding transition at 795 nm of thulium in YAP, making the former easier to saturate.

For both single and double-doped laser crystals, the presence of stimulated emission acted to efficiently repopulate the ground state population, reducing any pump depletion present under nonlasing conditions. Removal of excitation through lasing reduced the heat load in the gain medium, with the magnitude of the reduction dependent on both the efficiency of the lasing process and how far the laser operated above threshold. This resulted in a greater disparity between lasing and nonlasing conditions for Tm:YAP as compared to Tm,Ho:YAP when considering both the heat load deposited in the gain medium and pump beam transmission.

These measurements allowed the conversion of pump light to laser output within the laser crystals to be calculated. At the maximum diode output of 3 W, 1.76 W of pump light was absorbed in the Tm:YAP crystal, producing 730 mW of laser output, a conversion efficiency of 42%. The corresponding efficiency of Tm,Ho:YAP, where 1.76 W was also absorbed in the gain medium, producing 245 mW laser output, was a factor of three down at 14%. An upper bound of 30% for the conversion efficiency

of the Tm,Ho:YLF laser crystal was obtained. Therefore, for room temperature cw operation, thulium in YAP, free of the losses introduced by excitation sharing and upconversion in the double-doped crystals, had the highest conversion efficiency, despite having a much lower stimulated emission cross-section than either holmium in YAP or YLF.

At maximum laser output power, the values of heat load in the laser crystals derived from the measured absorbed pump power were used to estimate the focal lengths of the induced thermal lenses. For the particular laser crystals studied in this work, heat loads of 850, 500 and 780 mW were calculated to produce thermal lenses of focal lengths 3, 5 and 10 cm for Tm,Ho:YAP, Tm:YAP and Tm,Ho:YLF respectively.

Bleaching of the ground state absorption by an intense pump beam leads to a reduction in the temperature gradient along the length of the gain medium, producing a more uniform distribution of thermally induced stresses and strains, which results in the gain medium being less liable to thermal fracture. If the gain medium is sufficiently long such that it is still optically thick even in the presence of strong bleaching effects at or near its pumped face, efficient absorption of the pump beam will still take place.

The reduction in heat load due to the presence of stimulated emission means that for cw operation it is preferable, in terms of decreased stress and strain, to have the gain medium lasing if it is to be optically excited with a laser diode. This heat load reduction also weakens the thermal lensing during lasing, allowing the resonator to remain stable at higher pump powers than anticipated. However for Q-switched operation, where the laser crystal is pumped cw with a laser diode or laser diodes then repetitively Q-switched at some specified frequency, stimulated emission is present in the form of a giant pulse for a very short period of time (in the tens to hundreds of nanoseconds regime), making the duty cycle very low indeed. Therefore the heat load deposited in the gain medium remains essentially as it would with no lasing present at all.

For high power solid-state laser operation, considerations of thermal management within the gain medium are of paramount importance, particularly for quasi-three level thulium and holmium lasers, even more so if Q-switching is the desired mode of operation.

5.5 References

- [1] W. F. Krupke & L. L. Chase, 'Ground-state depleted solid-state lasers: principles, characteristics and scaling', *Optical and Quantum Electronics*, vol. 22, S1 (1990)
- [2] R. Beach, G. Albrecht, R. Solarz, W. Krupke, B. Comaskey, S. Mitchell, C. Brandle & G. Berkstresser, 'A ground state depleted laser in neodymium doped yttrium orthosilicate', *SPIE*, vol. 1223, 160 (1990)
- [3] C. Hauglie-Hanssen & N. Djeu, 'Further investigations of a 2 μm Tm:YVO₄ laser', *IEEE J. Quantum Electron.*, vol. 30, no. 2, 275 (1994)
- [4] P. Peterson, A. Gavrielides & M. P. Sharma, 'Diode-pumped Tm:YAG solid-state lasers with indirect and direct manifold pumping', *Appl. Phys. B*, vol. 61, 195 (1995)
- [5] U. O. Farrukh, A. M. Buoncristiani & C. E. Byvik, 'An analysis of the temperature in finite solid-state laser rods', *IEEE J. Quantum Electron.*, vol. 24, no. 11, 2253 (1988)
- [6] M. J. Weber, 'CRC Handbook of Laser Science and Technology', Volume IV Part 2 (1986) & Volume V Part 3 (1987), Florida: CRC Press, Inc.
- [7] R. C. Stoneman & L. Esterowitz, 'Intracavity-pumped 2.09 μm Ho:YAG laser', *Opt. Lett.*, vol. 17, no. 10, 736 (1992)
- [8] M. A. Noginov, A. M. Prokhorov, G. K. Sarkisyan, V. A. Smirnov & I. A. Shcherbakov, 'Cross-relaxation deactivation of the ground state of ions of rare-earth elements in crystals', *Sov. J. Quantum Electron.*, vol. 21, no. 9, 945 (1991)
- [9] R. R. Petrin, M. G. Jani, R. C. Powell & M. Kokta, 'Spectral dynamics of laser-pumped Y₃Al₅O₁₂:Tm,Ho lasers', *Optical Materials*, vol. 1, no. 2, 111 (1992)
- [10] G. Armagan, B. M. Walsh, N. P. Barnes, E. A. Modlin & A. M. Buoncristiani, 'Determination of Tm-Ho rate coefficients from spectroscopic measurements', in *OSA Proceedings on Advanced Solid-State Lasers*, (OSA, Washington, DC), vol. 20, 144 (1994)
- [11] J. A. Caird, L. G. DeShazer & J. Nella, 'Characteristics of room-temperature 2.3 μm laser emission from Tm³⁺ in YAG and YAlO₃', *IEEE J. Quantum Electron.*, vol. 11, no. 11, 874 (1975)

Upconversion processes

6.1 Introduction

From consideration of conservation of energy we would not expect absorption of a photon of light to cause emission of a shorter wavelength photon. However, stepwise absorption of pump radiation can lead to promotion of excitation to a high-lying level producing fluorescence at a shorter wavelength than the excitation wavelength; this is the upconversion effect.

There are at least three distinct multiphoton mechanisms which are capable of producing upconversion in doped crystalline or glass hosts:

- (1) Excitation in which the summing of energy occurs in the excited state(s) of a single ion through sequential step-by-step absorption - excited state absorption (ESA).
- (2) Excitation in which the summing occurs in the virtual state(s) of a single ion.
- (3) Excitation in which absorption occurs in different ions with subsequent migration of energy by means of a cooperative mechanism resulting in the accumulation of excitation in one ion.

The relative magnitude of these multiphoton mechanisms depends very much on the particular system under investigation, both the dopant ion(s) and the host lattice.

The excellent article by Auzel¹ details the various upconversion mechanisms that can occur, as well as reviewing experimental progress and discussing potential applications for materials exhibiting upconversion. Initial research in this field stemmed from a proposal by Bloembergen² for an infrared quantum counter (IRQC) detector using ESA of infrared radiation to generate visible fluorescence. In more recent times, compact sources of visible laser radiation have been sought to satisfy demands for displays and optical disc storage.

Initial laser work required two distinct pump wavelengths to provide the necessary excitation³, but with the advent of higher brightness AlGaAs laser diodes, a single pump wavelength became sufficient⁴. The most efficient upconversion source of

green radiation is the erbium ion, particularly when doped in low phonon energy hosts. Lasing action is obtained by operating the laser crystal at cryogenic temperatures, as in reference 4, where 100 mW of green output at 551 nm was generated from Er:YLF cooled to 48 K and pumped with a 3 W cw laser diode. The higher brightness of a Ti:sapphire laser allows higher power upconversion lasers to be demonstrated e.g. 500 mW at 551 nm from cryogenically cooled Er:YLF with 5 W pump power⁵, and also operation at room temperature e.g. 45 mW from Er:YLF with 250 mW pump power⁶. Upconversion lasing in holmium doped fibres offers an alternative green source to erbium doped hosts^{7,8}. The confinement of the pump beam in a waveguide structure enhances the upconversion efficiency, making possible room temperature lasing at modest pump powers.

Praesodymium (Pr^{3+}) doped crystalline or glass hosts, both in bulk or fibre form, have been investigated as potential sources of laser radiation in the blue, green and red parts of the visible spectrum⁹⁻¹¹. Upconversion lasing in thulium offers the possibility of a coherent source of blue radiation^{12,13}. The published work on upconversion lasers has been accompanied by considerable efforts regarding the spectroscopic investigation of the wide range of materials exhibiting upconversion, with particular regard to understanding the excitation mechanisms involved. A selection of such papers is referenced here¹⁴⁻¹⁸.

It has been observed that double-doping laser crystals with thulium and holmium increases the total amount of upconversion occurring when compared with single-doped thulium crystals^{19,20}. During the course of the cw laser experiments described in chapter four it was observed that Tm,Ho:YAP emitted yellow-green fluorescence, Tm,Ho:YLF a much darker green fluorescence, and Tm:YAP a barely visible pale blue fluorescence on excitation with infrared radiation from a laser diode. The presence of upconversion degrades laser performance through the removal of excitation from the upper laser level. As a loss mechanism upconversion requires investigation in order to properly assess two micron laser operation of thulium and holmium doped crystals.

This chapter details the experiments performed to characterise the observed visible upconversion fluorescence and the subsequent determination of the excitation mechanisms producing this upconversion fluorescence. Measurement of the infrared fluorescence decay from the coupled first excited states of the double-doped laser crystals provides evidence of additional upconversion mechanisms.

6.2 Visible emission spectra of thulium and holmium

Given that visible upconversion fluorescence was observed upon diode-pumping of the laser crystals under investigation, it was important to determine the nature of these visible emission bands, in order to assign the upconversion fluorescence to particular transitions in the thulium and holmium ions.

A computer-controlled SPEX fluorimeter was used to excite a range of YAP and YLF crystals at short wavelengths, generally in the UV, in order to produce downconverted visible room temperature emission spectra. This instrument had as its light source a xenon lamp which was spectrally filtered with a monochromator in order to produce the appropriate excitation wavelength. The output slit of this first monochromator was imaged onto the sample, and the resulting fluorescence analysed by a second monochromator. A photomultiplier tube (PMT) was the detector used - its S20 tube operated over the range 350 to 800 nm, with peak sensitivity at 430 nm²¹. The combination of light source and focussing power onto the sample provided insufficient excitation to be able to excite the samples in the infrared and then observe any upconversion fluorescence, hence the downconverted emission was instead measured.

Both the monochromators contained a 1200 l/mm grating, with blaze angles 250 nm and 500 nm for the excitation and analyser monochromators respectively. The dispersion of these gratings was 3.3 nm/mm. Typically the excitation monochromator was used with 2 mm wide slits, yielding a spectral bandwidth of 6.6 nm for the pump radiation, with a 1 mm slit width employed in the analyser monochromator, yielding a resolution of 3.3 nm for the spectra obtained. In the absence of suitable polarisers, the pump light was unpolarised, with no polarisation selection carried out on the resulting fluorescence. The wavelength scales of both monochromators were calibrated using a mercury spectral lamp as well as a HeNe laser.

The YAP spectroscopic samples measured were single-doped 1.5% holmium, single-doped 4.2% thulium and double-doped 4.2% thulium, 0.28% holmium; the corresponding YLF samples were 1.5% holmium, 4% thulium and double-doped 4% thulium, 0.4% holmium. In all cases the samples were of order 5 mm thick, with end faces polished clear but not to laser standards.

From the energy levels published in the literature²²⁻²⁴, figure 6.1 was generated. Potential transitions to the ground state producing visible fluorescence are labelled accordingly. This diagram will be referred to throughout the course of this chapter.

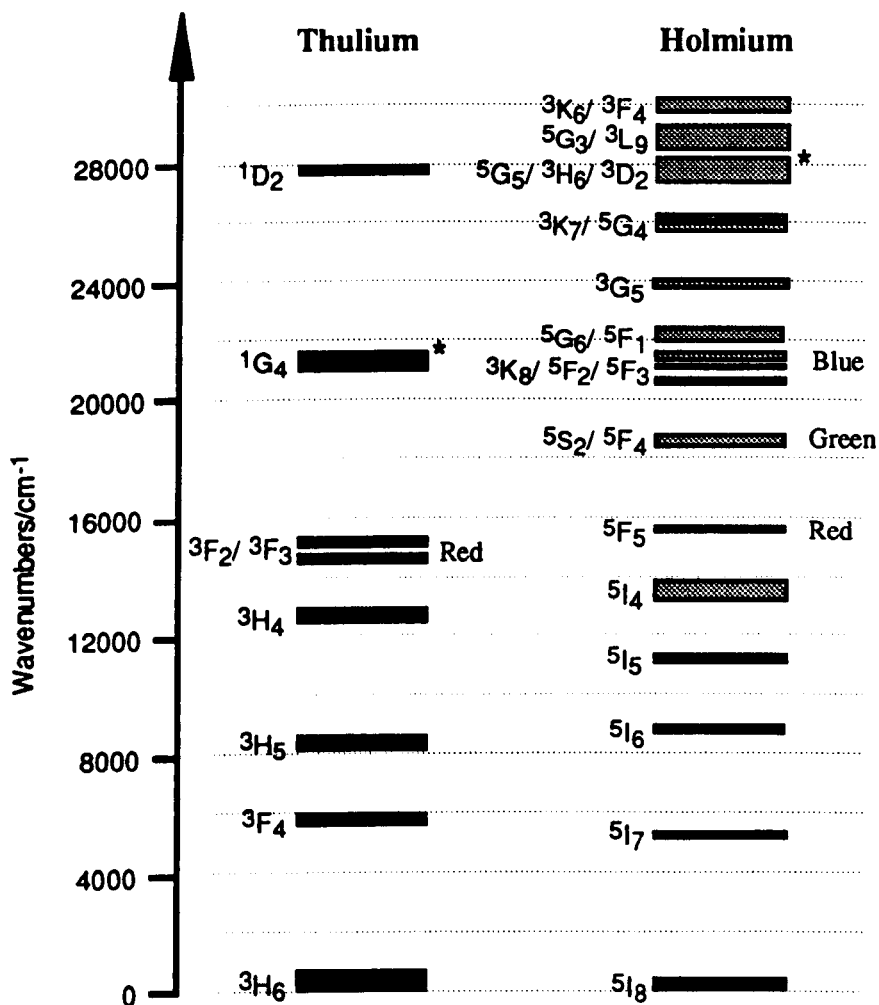


Figure 6.1 Energy level diagram of thulium and holmium in YAP

The levels depicted are for the trivalent thulium and holmium ions in YAP, with the width of the energy level manifolds a measure of the broadening induced by the crystal field. The lighter shaded holmium levels are in fact for the crystalline host YAG, in the absence of published data for the corresponding levels in YAP (comparison of levels listed for both hosts revealed them to be similar, with the YAP energy level manifolds slightly broader in general, the lowest levels being closer to the ground state by at most 150 cm⁻¹). In YLF, the positions of the energy level manifolds are similar to both YAP and YAG, with the manifold widths smaller in general^{25,26}. This

similarity in the gross spectral features of the different hosts is indicative of the weak crystal field interaction with the rare earth ions.

Examination of figure 6.1 reveals that holmium has possible transitions in the green and the red which terminate in the ground state, while thulium possesses no transition to the ground state in the green, but has two closely spaced levels offering the possibility of red emission. Armed with this knowledge excitation spectra can be obtained, by setting the analyser monochromator in the waveband of interest, then scanning the first monochromator to alter the pump wavelength. Correcting for any variations of the strength of the pump signal, the optimum pump wavelength is obtained. For single-doped holmium in YAP and YLF, the optimum excitation wavelength for the green spectral band was found to be 361 nm (this was the excitation wavelength used for the double-doped crystals as well). An excitation wavelength of 467 nm was used to produce red emission from the single-doped thulium in YAP and YLF samples. The energy level manifolds containing the excitation levels are marked by an asterisk in figure 6.1 (note that the short excitation wavelength employed in the holmium samples also allows blue emission to occur).

For each crystal in turn, the first monochromator was set at the fixed excitation wavelength, while the second monochromator was then scanned across the visible waveband and the spectra recorded. The fluorescence data obtained in this manner was then corrected for the effects of absorption of the pump light in the sample and additionally, in the case of ground state transitions, for reabsorption of the fluorescence produced taking into account the front surface emission geometry employed in the fluorimeter.

The spectra in figure 6.2 were generated on UV excitation of the 1.5% Ho:YAP sample. Examination of the energy levels in figure 6.1 allows transitions to be assigned to the observed spectra. In the blue, the weak spectral features centred on 420, 450 and 485 nm are assigned to transitions from 3G_5 , $^5G_6/{}^5F_1$ and 5F_3 to the ground state respectively. In the green, the band from 535 to 555 nm is produced by fluorescence from the closely spaced 5S_2 and 5F_4 multiplets to the ground state. Finally, in the red, the band from 640 to 690 nm is attributed to emission from the 5F_5 multiplet, with the band starting to appear at 740 nm due to a transition from 5I_4 , both to the ground state. The spectral feature centred on 710 nm is not due to a transition to the ground state, but instead to fluorescence from the 5G_5 multiplet (one of the three closely spaced multiplets containing the 361 nm excitation transition) to the 5I_4 state.

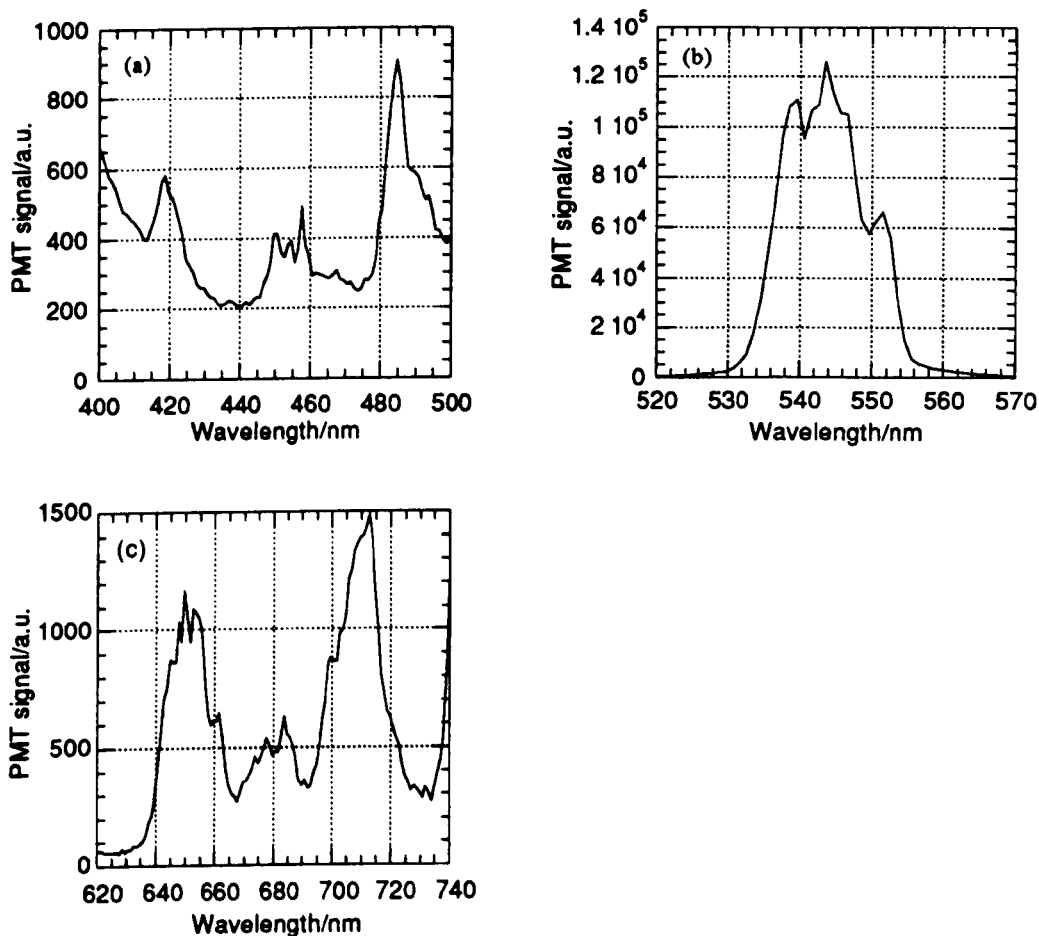


Figure 6.2 (a) Blue, (b) green and (c) red fluorescence bands of holmium in YAP

Figure 6.3 illustrates the red fluorescence band of the 4.2% Tm:YAP sample.

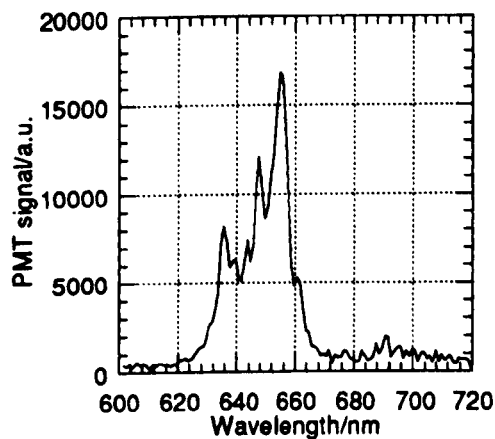


Figure 6.3 Red fluorescence band of thulium in YAP

Here the sample was excited at 467 nm into the 1G_4 multiplet. The resulting red spectrum is dominated by emission from this multiplet to the 3F_4 state (630 to 665 nm), with the weak emission in the range 680 to 720 nm produced by emission from 3F_3 to the ground state.

The double-doped Tm,Ho:YAP was excited at 361 nm, and the visible spectrum recorded. This spectrum is dominated by a band from 440 to 460 nm, corresponding to a mixture of transitions from holmium 5G_5 to 5I_7 and thulium 1D_2 to 3F_4 . None of the blue holmium transitions of figure 6.2(a) are evident. There was also a strong green band, corresponding to the holmium transition of figure 6.2(b). The red spectrum of the double-doped sample shown in figure 6.4 is much weaker than the other two bands.

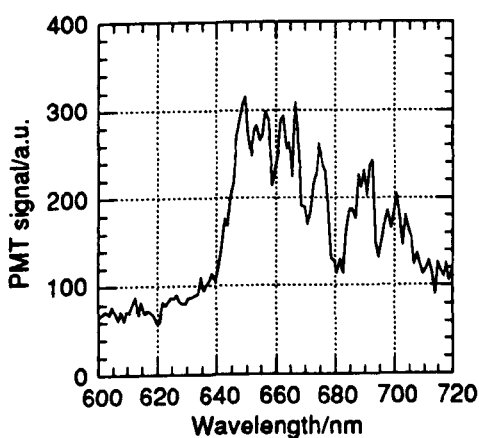


Figure 6.4 Red fluorescence band of double-doped Tm,Ho:YAP

In this case, the thulium 1G_4 to 3F_4 red transition has been suppressed. The resulting weak red spectrum can be attributed to the holmium 5F_5 to 5I_8 transition (640 to 680 nm), with contribution from the thulium 3F_3 to 3H_6 transition (680 to 720 nm). The holmium 3D_2 to 5I_4 transition is not present.

The corresponding fluorescence bands of the 1.5% Ho:YLF sample are shown in figure 6.5.

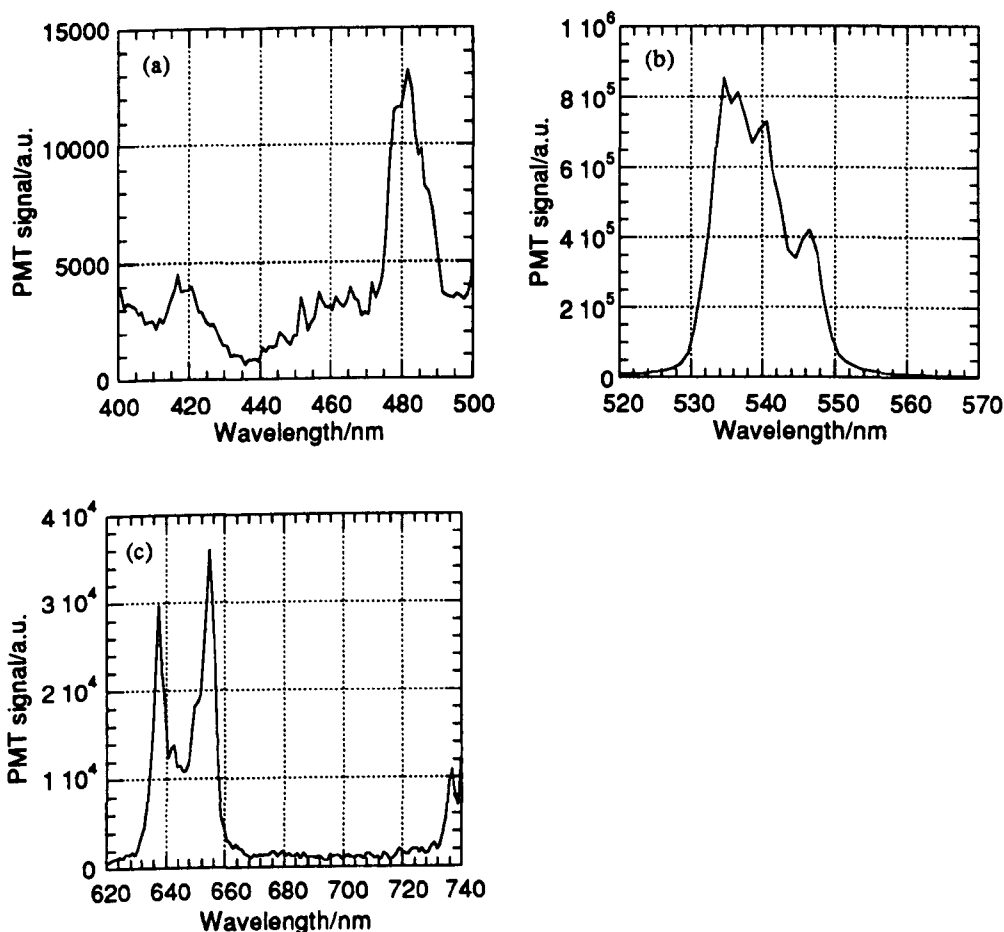


Figure 6.5 (a) Blue, (b) green and (c) red fluorescence bands of holmium in YLF

The blue and green bands can be assigned to the same transitions as in Ho:YAP, noting that in YLF the strength of the 5F_3 emission centred on 485 nm is much greater than the other two bands, whereas in YAP this difference in strength is not as apparent (see figure 6.2(a)). In the red portion of the visible spectrum, the emission between 630 and 660 nm arises from the 5F_5 multiplet, with the emission at 740 nm from the 5I_4 multiplet, both transitions to the ground state. There is no sign of the 5G_5 to 5I_4 emission which was present in the Ho:YAP spectrum (see figure 6.2(c)).

Figure 6.6 illustrates the red fluorescence band of the 5% Tm:YLF sample. As with the Tm:YAP crystal, an excitation wavelength of 467 nm (pumping into the 1G_4 multiplet) was employed. In this case, there is no evidence of the 1G_4 to 3F_4 emission which dominated the YAP spectrum. The three peaks are produced by emission from the 3F_3 level to the ground state.

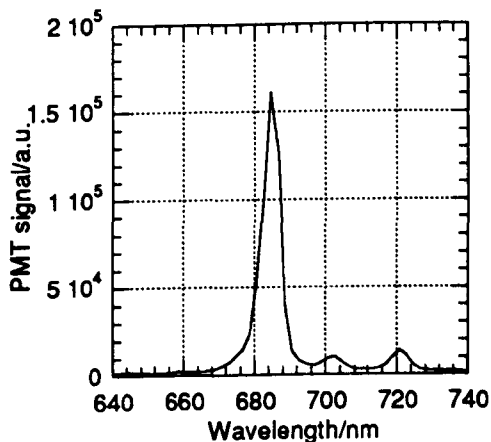


Figure 6.6 Red fluorescence band of thulium in YLF

The double-doped Tm,Ho:YLF sample was excited at 361 nm, and the visible spectrum recorded.

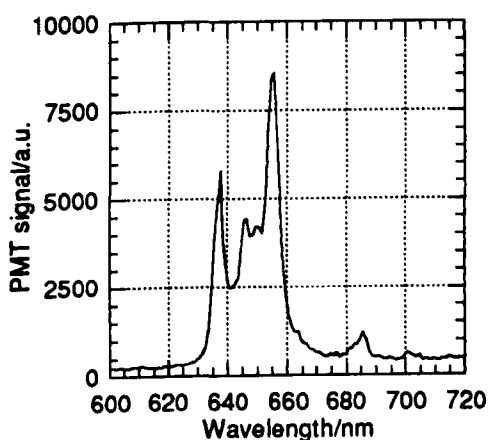


Figure 6.7 Red fluorescence band of double-doped Tm,Ho:YLF

In the red the spectrum is dominated by the emission from holmium 5F_5 , with a much weaker signal due to the transition from thulium 3F_3 .

One general result of these measurements is the consistently larger signal strengths in all spectral bands of YLF over YAP, whether the dopant be thulium or holmium (or co-doping with both). The lower phonon energy host YLF suffers less from nonradiative decay than YAP, thus increasing the fluorescence efficiency of the transitions.

In both single-doped thulium in YAP and YLF, the 3F_2 and 3F_3 multiplets are very closely spaced (the difference in mean energy levels between these multiplets is of

order 600 cm^{-1} in both crystalline hosts). Nonradiative decay efficiently de-excites the $^3\text{F}_2$ multiplet, with radiative emission occurring from the lower energy $^3\text{F}_3$ multiplet. Red emission was observed from both thulium and holmium in the double-doped crystals. In YAP the splitting between the lowest levels of the holmium $^5\text{F}_5$ and thulium $^3\text{F}_2$ multiplets is 278 cm^{-1} ; the corresponding splitting in YLF is 381 cm^{-1} . These multiplets are in effect coupled, with excitation sharing occurring between the two, in a similar fashion to the thulium $^3\text{F}_4$ and holmium $^5\text{I}_7$ first excited states. Excitation sharing between these "red bands" heavily favours population of the thulium, because of the higher concentration and lower energy levels. Examination of the red fluorescence emission of double-doped YAP and YLF (figures 6.4 and 6.7 respectively) reveals that in the former the holmium and thulium contributions to the combined spectrum are comparable in strength, while in the latter the holmium fluorescence is orders of magnitude stronger than the thulium fluorescence. This suggests that the oscillator strength of the holmium red transition in YLF is far greater than the thulium transition, while in YAP the two ions have similar oscillator strengths in the red.

Armed with this information concerning the spectral content and lineshape of the visible emission of the laser crystals of interest, the upconversion spectra generated by these crystals upon excitation with a laser diode can be analysed and compared with the fluorimeter results.

6.3 Measurement of visible upconversion spectra

The experimental arrangement used to measure the visible upconversion fluorescence is shown in figure 6.8.

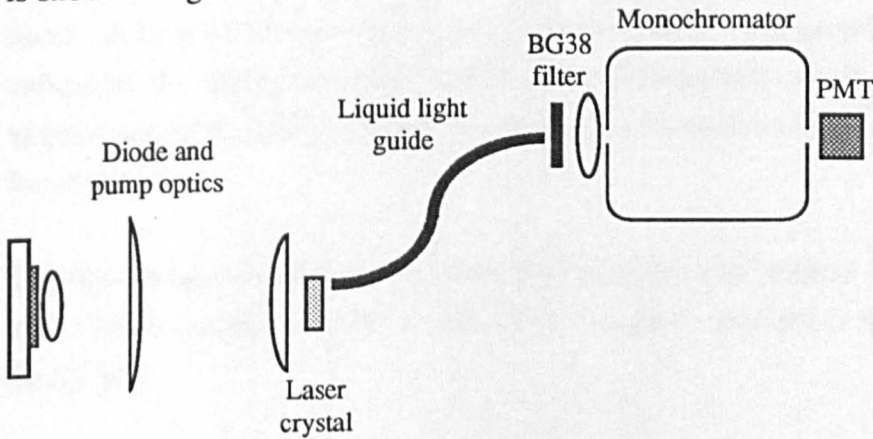


Figure 6.8 Schematic of experiment to measure visible upconversion spectra

The mechanical mounts used meant that it was only possible to measure the upconversion spectra with the output mirror of the two micron laser removed i.e. without the presence of stimulated emission. A liquid light guide was used to capture the visible fluorescence emitted through the unpumped face of the laser crystal, with the pumped region being close to the crystal side to minimise reabsorption effects. The light transmitted through the light guide was then spectrally filtered using a monochromator, the resulting signal falling onto a photomultiplier tube (PMT), the output of which was displayed as a voltage on an oscilloscope. A BG38 glass filter was employed to block any diode light scattered into the light guide. The monochromator was a Spectral Energy Corp. GM252-50 model, with a 590 l/mm grating producing a dispersion of 6.6 nm/mm at the output slit. This grating was blazed for a wavelength of 1 μm , not ideal for operation in the visible part of the spectrum. The transmission function of the liquid light guide over the range 250 to 750 nm was known²⁸, and the BG38 filter was measured in a spectrophotometer to have transmission over the range 400 to 700 nm, peaking at 500 nm. The PMT had a Hamamatsu R928 tube, quoted by the manufacturers²⁹ as having sensitivity from 185 to 900 nm, with a peak response at 400 nm.

The measured visible spectra, figures 6.9 and 6.10, were recorded with a diode pump power of 3 W, at a laser crystal heatsink temperature of 15°C, with the laser crystal positioned relative to the pump optics at the location which yielded maximum laser output power during the experiments of chapter four. For both YAP and YLF crystals

the pump beam was aligned parallel to the crystallographic *c*-axis. No polarisation selection was employed when capturing the upconversion fluorescence. The recorded signals from the PMT were corrected for transmission through the light guide and BG38 glass filter, as well as for the wavelength-dependent sensitivity of the PMT itself. A first order correction has also been made for reabsorption using measured values of the absorption coefficients at the fluorescence wavelengths, taking into account the back surface emission geometry employed to capture the upconversion fluorescence.

The first sample tested was the 2 mm thick Tm,Ho:YAP crystal, which was found to emit visible radiation in two bands, one in the green and one in the red, as shown in figure 6.9.

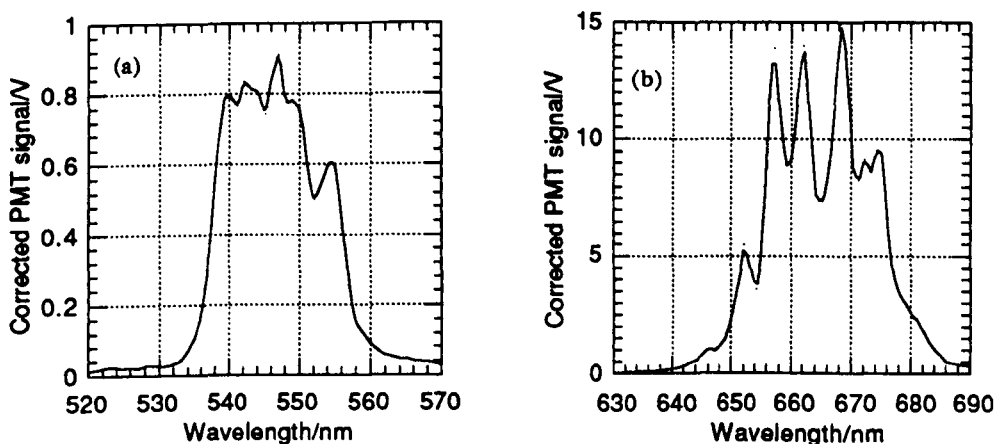


Figure 6.9 (a) Green and (b) red upconversion fluorescence bands in Tm,Ho:YAP

A slit width of 0.25 nm was employed yielding a resolution of approximately 1.6 nm. Comparison with figure 6.2(b) reveals that the green upconversion fluorescence matches well the 5S_2 and 5F_4 emission to the ground state.

The lineshape of the red upconversion fluorescence does not match particularly well the spectra recorded with the fluorimeter (figures 6.2(c), 6.3 and 6.4). The wavelength range of the upconversion suggests it to be dominated by emission from the holmium 5F_5 multiplet. Unfortunately the BG38 glass filter becomes opaque at wavelengths greater than 700 nm. Removal of this filter revealed that any emission in the range 700 to 720 nm (corresponding to emission from the thulium 3F_3 multiplet to the ground state) was very weak compared to the shorter wavelength signals. Unfortunately without the BG38 filter present, large amounts of scattered diode light

reached the photomultiplier tube which tended to swamp any weak fluorescence signals in the red portion of the spectrum. Therefore it was difficult to ascertain accurately the strength of the 700 to 720 nm fluorescence relative to the shorter wavelength emission in figure 6.9(b).

For Tm,Ho:YAP, no blue upconversion fluorescence could be detected with the apparatus used.

Replacing the double-doped YAP with the 3 mm thick Tm,Ho:YLF laser crystal, visible upconversion spectra in the blue, green and red were observed and recorded, and are shown in figure 6.10.

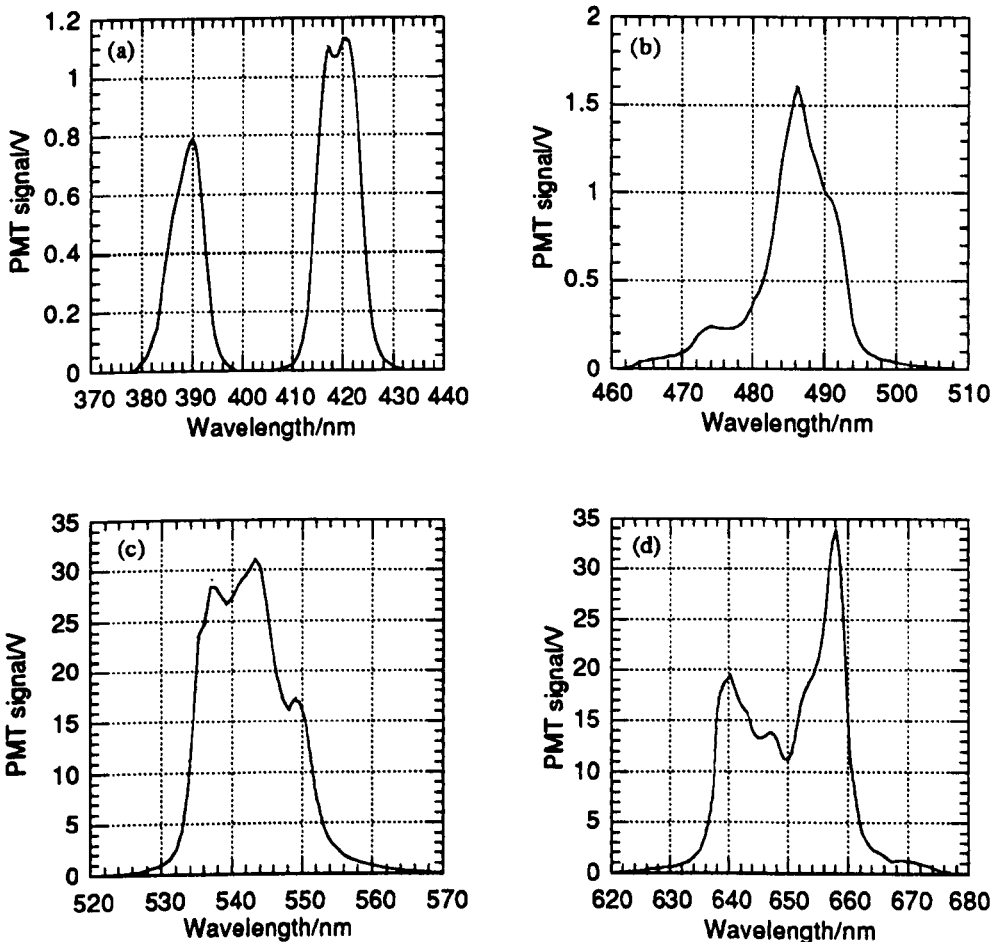


Figure 6.10 Visible upconversion in Tm,Ho:YLF

In order to obtain the data plotted in figure 6.10(a), a monochromator slit width of 0.5 mm was used, with a resulting resolution of 3.3 nm. For the other spectral

bands, there was sufficient signal reaching the PMT to increase the resolution to 1.6 nm by narrowing the slits to 0.25 mm.

The short wavelength transitions in figure 6.10(a) centred on 390 and 420 nm are attributed to transitions from the closely spaced holmium $^3K_7/{}^5G_4$ and the 3G_5 multiplets respectively, both to the ground state. The blue transition centred on 485 nm (figure 6.10(b)) is due to emission from holmium 5F_3 to the ground state. Referring back to figure 6.5(a) in the previous section, there is no evidence in the upconversion fluorescence of emission from the holmium ${}^5G_6/{}^5F_1$ multiplets to the ground state, nor of the 1D_2 to 3F_4 emission in thulium.

The green upconversion fluorescence in figure 6.10(c) matches well in wavelength the emission band in figure 6.5(b), although the lineshape is slightly different, with the latter having a stronger short wavelength portion of the emission from 530 to 535 nm.

The red upconversion fluorescence in figure 6.10(d) matches well in wavelength and lineshape the holmium fluorescence band from 5F_5 to the ground state illustrated in figure 6.5(c). There is no evidence of the longer wavelength emission from the thulium 3F_3 multiplet to the ground state.

It is difficult to make quantitative comparisons between the relative strengths of the upconversion fluorescence bands because of the diffraction grating employed to make these measurements. This grating was blazed for a wavelength of 1 μm , and so in the visible spectrum the diffraction efficiency is low, but more importantly varies significantly with wavelength, being lowest in the blue and greatest in the red. However, despite this handicap, figure 6.9 and 6.10 clearly illustrate the superior fluorescence efficiency of YLF over YAP, confirming the results of the fluorimeter work in the previous section. Furthermore, in YAP there is more than one order of magnitude between the peak signal in the red and green upconversion fluorescence, whereas in YLF the corresponding difference is at most 10%. We can conclude from this result that the holmium 5F_5 multiplet in YAP is more efficiently populated than in YLF. The greater content of red fluorescence in the YAP upconversion fluorescence was evident to the naked eye; with YAP the fluorescence had a yellow-green colour, whereas with YLF the fluorescence took on a much deeper green hue. This was due both to the reduced level of red emission, but also because blue upconversion fluorescence was also present, unlike in YAP. It is also worth noting here that the

upconversion fluorescence measurements produced no transitions terminating in excited states, unlike the fluorimeter work of the previous section.

The final observation to be made is that no emission was observed from thulium levels in these double-doped samples when excited with the laser diode. Examination of figure 6.1 reveals that there are many pairs of thulium and holmium multiplets that are closely spaced in energy, and could be amenable to excitation sharing. However, the fact that no emission was observed from thulium indicates that the upconversion occurs principally in holmium, and that any excitation sharing is negligible (apart from the coupling of the first excited states), suggesting that the total amount of excitation involved in the upconversion processes resulting in visible fluorescence is small.

For the purposes of comparison, the 2 mm Tm:YAP laser crystal was looked at in the apparatus of figure 6.8. Very faint blue/white fluorescence was visible to the naked eye, but no signal could be detected on the PMT. A slight alteration of the pump optics increased the incident pump intensity on the crystal (witnessed by the fact that there was a 25% increase in the pump beam transmitted through the crystal). With the monochromator slits set at 2 mm width, the increased upconversion fluorescence could now be resolved above the PMT dark current signal. Peaks at 480, 545 and 660 nm were detected. Since thulium possesses no transition in the green, the 545 nm peak is attributed to trace amounts of either erbium²³ or holmium in the YAP crystal. This crystal was prepared from an inhouse grown boule which was produced along with YAP boules containing erbium and holmium, and so there was the distinct possibility of trace amounts of these rare earths contaminating the crucible used in the growth of YAP. The low level of the green fluorescence signal indicates that the contaminant concentration is at least two orders of magnitude less than the 0.28% holmium concentration in the double-doped YAP crystal, and thus contributes negligible losses due to the resulting weak upconversion. The blue and red peaks could also be due to these contaminants, or to the thulium itself. In Tm:YAG, an upconversion process populating the 1G_4 level on absorption of two pump photons, with the 3F_4 level relaxing nonradiatively to 3H_5 after absorption of the first photon, leading to blue or red emission from this excited state, has been analysed^{13,20}. This is known to be very weak compared to the upconversion processes occurring in double-doped YAG and YLF, and so is assumed also to be so for YAP.

6.4 Determination of visible upconversion excitation mechanisms

In the previous section, transitions were assigned to the observed upconversion fluorescence bands upon infrared excitation of double-doped YAP and YLF crystals. The excitation mechanism(s) producing these fluorescence bands can be ascertained by measuring the variation of fluorescence signal strength with excitation power. This variation obeys a relationship of the form

$$F_p \propto P_p^n \quad 6-1$$

where F_p is the fluorescence power, P_p is the pump power and n is a fractional power¹. Experimentally, the pump power was varied by attenuating the diode output with neutral density filters, and the total fluorescence signal in each band measured by opening up the output slit of the GM252-50 monochromator to its maximum extent of 5 mm. This allowed the instrument to operate as a spectrograph with a bandwidth of 33 nm, wider than the measured upconversion fluorescence bands. Referring back to the results of chapter five, the absorbed pump power is used as the abscissa scale, taking into account the various pump absorption effects in these double-doped crystals.

The resulting data are plotted on a log-log scale in figure 6.11 for the green and red upconversion fluorescence emitted by Tm,Ho:YAP.

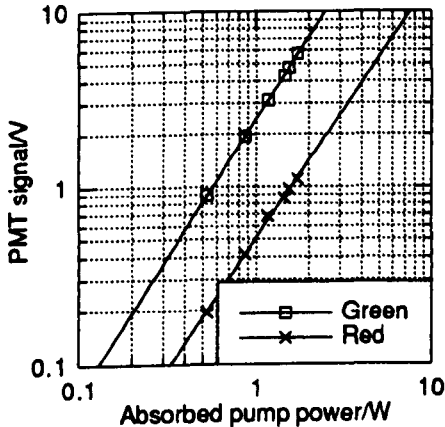


Figure 6.11 Variation of upconversion fluorescence with pump power in YAP

The slopes of the fits to the data are 1.57 and 1.47 for the green and red upconversion fluorescence bands respectively. Both these slopes are close in value to the fractional power 1.5, which implies that three pump photons have to be absorbed in order to generate two fluorescence photons in either the green or the red.

Figures 6.12(a) and (b) are the corresponding results for Tm,Ho:YLF.

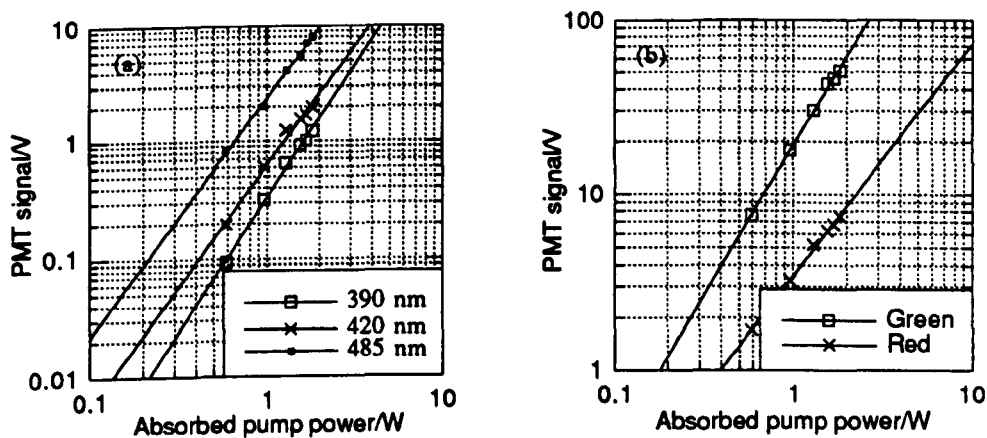


Figure 6.12 Variation of upconversion fluorescence with pump power in YLF

The slopes for the blue fluorescence bands centred on 390, 420 and 485 nm (figures 6.10(a) and (b)) are 2.27, 2.05 and 2.03, all close to the integer power of 2. This implies that two pump photons are required to generate one blue fluorescence photon. The slopes for the green and red fluorescence bands are 1.71 and 1.32, either side of the fractional value 1.5, the power dependence derived from the YAP results.

These values for the power dependence of the upconversion fluorescence on the excitation power, in combination with the transitions assigned to the measured spectra, allow the excitation mechanisms to be determined. The low holmium concentration in the crystals investigated allows holmium-holmium upconversion mechanisms to be considered as negligible. The work of chapters four and five highlighted the efficiency of the cross-relaxation process in thulium on absorption of diode pump light, and the excitation sharing between thulium and holmium in double-doped crystals. Therefore absorption of diode light in thulium leads to the bulk of the population residing in the first excited states of the ions. The results of the previous section, where all the upconversion fluorescence bands were assigned to transitions in holmium, select its 5I_7 first excited state multiplet as being the principal level governing upconversion. Direct evidence of this came during the laser experiments of chapter four. The onset of stimulated emission, which depopulated the holmium first excited state, was accompanied by a noticeable decrease in the brightness of the upconversion fluorescence as viewed by the naked eye.

Figure 6.13 illustrates the proposed excitation mechanism resulting in the green and red emission from double-doped YAP and YLF.

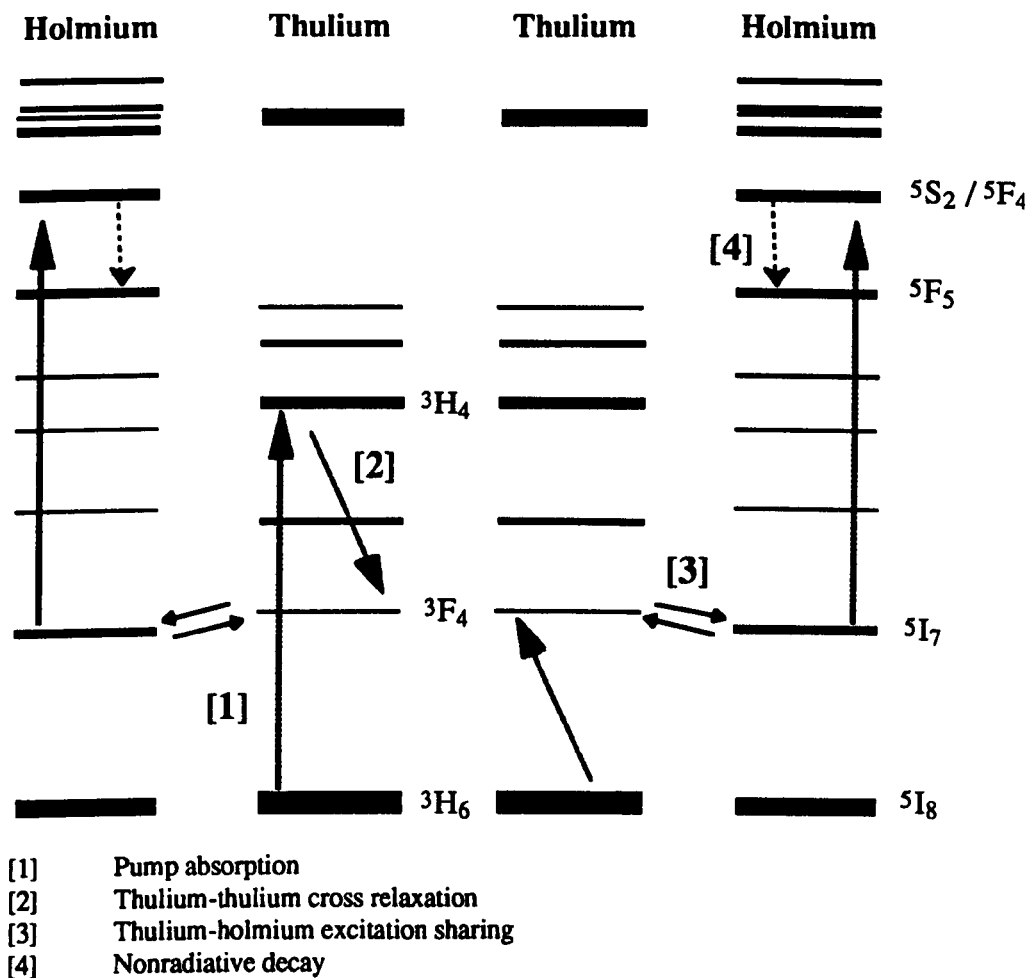


Figure 6.13 Excitation mechanism producing green and red upconversion

For the sake of simplicity only the relevant multiplets have been labelled. Absorption of pump light in thulium leads to population of the holmium first excited state via cross-relaxation and excitation sharing. In the steady-state regime, further absorption of the pump light can occur from this long-lived level, promoting holmium to the closely spaced $^5S_2/^5F_4$ multiplets. Green emission occurs from this pair of multiplets, accompanied by nonradiative decay to 5F_5 , from where red emission can occur. Figure 6.13 clearly shows that the absorption of three pump photons leads to the production of two upconversion fluorescence photons. Examination of the published energy levels shows that in YAP the diode pump wavelength of 795 nm matches well the separation of the 5I_7 and $^5S_2/^5F_4$ multiplets; in YLF the pump wavelength of 792 nm comes short of bridging this separation by approximately 640 cm^{-1} .

Therefore in YLF the upconversion transition is phonon-assisted, requiring one or two phonons to make up the shortfall (560 cm^{-1} is the maximum phonon wavenumber of YLF quoted in the literature³⁰). Red emission relies on nonradiative decay from the next highest multiplet to populate it. The oxide host YAP has a maximum phonon wavenumber of 740 cm^{-1} , producing significantly larger nonradiative decay rates than in YLF³¹. This partially accounts for the larger red to green emission strength ratio in YAP than YLF.

It is fairly well understood that in both Tm,Ho:YAG and Tm,Ho:YLF the upconversion mechanisms producing visible fluorescence are only a small fraction of the total upconversion taking place^{20,32,33}. In fact, the principal upconversion mechanism does not involve further absorption of pump light. Rather, a holmium ion in the 5I_7 first excited state is promoted to the 5I_5 multiplet, while a thulium ion in the 3F_4 first excited state is de-excited to the ground state, relying on the near-resonance of these transitions. For both YAP and YLF, there is a shortfall in the range 400 to 500 cm^{-1} between thulium 3F_4 to 3H_6 and holmium 5I_7 to 5I_5 . Therefore phonon assistance is required to complete the upconversion transition in both materials. Nonradiative decay rapidly quenches the 5I_5 multiplet in YAP, whereas in YLF this level is sufficiently long-lived to allow absorption of diode pump light, promoting the holmium to the 3G_5 multiplet. Blue fluorescence is emitted from this level and the adjacent lower-lying levels. Figure 6.14 overleaf shows this proposed excitation mechanism. The quadratic dependence of fluorescence signal on pump power is not immediately apparent. However we have to remember that the thulium ion de-excites in order to transfer excitation to the holmium, thus in order to promote the holmium ions to 5I_5 a second pair of excited state thulium ions has to be produced i.e. the absorption of two pump photons is required to generate two holmium ions in the 5I_5 multiplet. The quadratic dependence is now clear, with four pump photons generating two upconversion fluorescence photons.

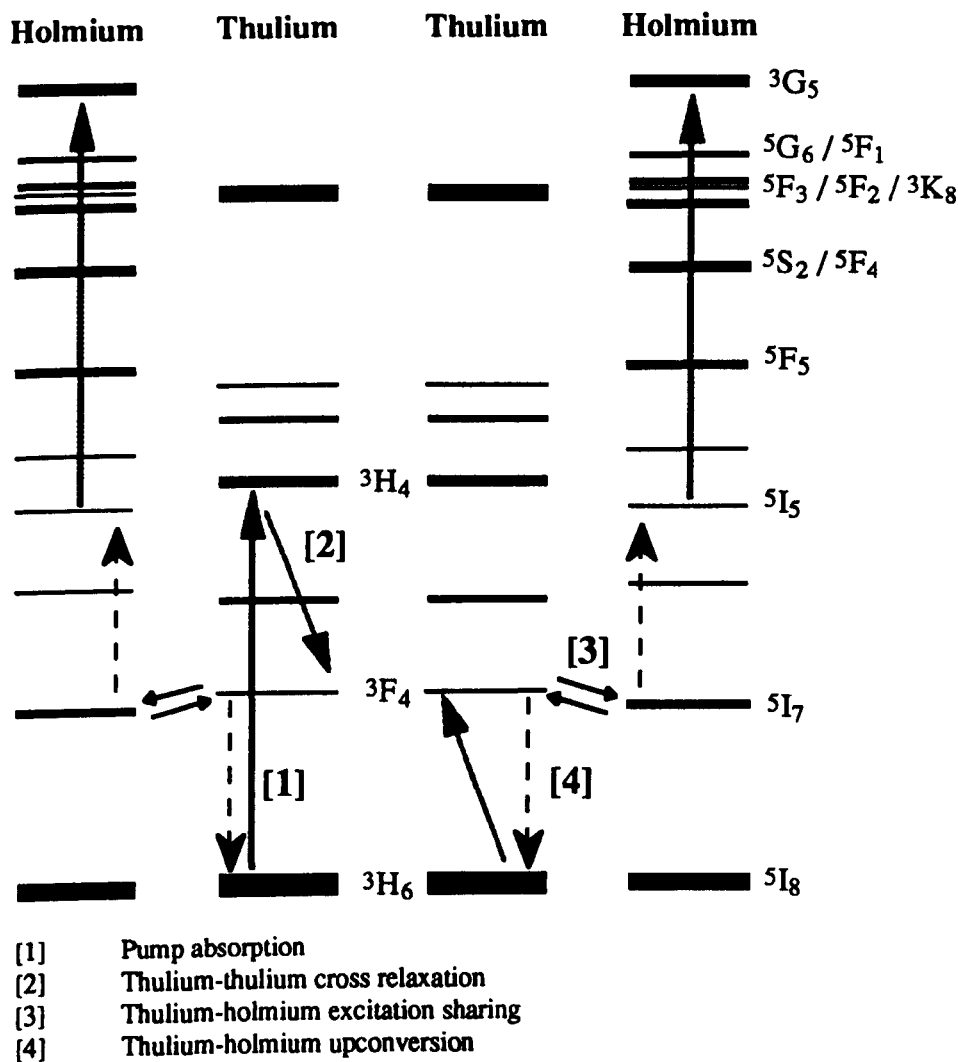


Figure 6.14 Excitation mechanism producing blue upconversion in YLF

The holmium 5I_7 multiplet contains the upper laser level for the two micron laser transition to the ground state. Therefore removal of excitation from this multiplet by upconversion represents a loss to the lasing transition. In YAP, the larger nonradiative decay rate compared to YLF results in a much larger fraction of the upconverted excitation decaying nonradiatively (principally from 5I_5 but also from $^5S_2/^5F_4$ to 5F_5), contributing additional heating to the YAP crystal lattice. The subsequent temperature rise alters the Boltzmann distribution of population in each multiplet so as to increase the laser threshold and reduce the achievable small-signal gain.

6.5 Near infrared upconversion processes

As mentioned in the previous section, the principal upconversion mechanism involves promotion of holmium 5I_7 to 5I_5 , at the expense of thulium (de-excited from 3F_4 to 3H_6). The excitation in 5I_5 can either decay nonradiatively back to the 5I_7 first excited state, decay nonradiatively back to the ground state or fluoresce back to the ground state. For both holmium in YAP and YLF this fluorescence is in the range 880 to 930 nm. Unfortunately, the R928 tube in the PMT had in effect no response beyond 800 nm, and so it was not possible to investigate this upconversion phenomenon using the apparatus of figure 6.8 (the liquid light guide was replaced by a multimode near IR fibre, and the BG38 filter with an RG850 filter).

However, examination of the fluorescence decay of the coupled thulium and holmium first excited states can be used as an indirect method of detecting the presence of upconversion mechanisms. If such processes are present, the fluorescence decay will not be the expected single exponential decay, but will instead have additional nonexponential components, usually faster than the spontaneous emission rate. Since the holmium 5I_7 to 5I_5 upconversion transition being investigated here does not depend on the presence of diode pump light (other than to provide initial population of thulium 3F_4), pulsed excitation of the laser crystals can be used, which then allows the fluorescence decay to be monitored.

The experimental arrangement employed is shown schematically in figure 6.15.

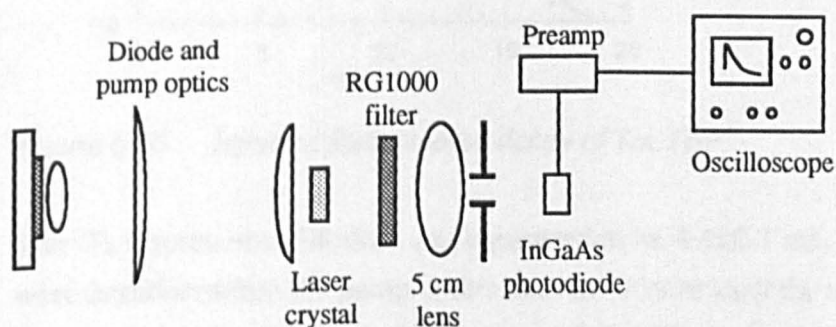


Figure 6.15 Fluorescence decay lifetime measurement apparatus

The laser diode was operated in pulsed mode, which allowed pulses from 10 μ s to 300 ms to be generated. In order to generate sufficient excitation to produce detectable fluorescence signals, the minimum pump pulse duration employed was 1 ms. Due to the nature of the brass finger holding the laser crystal, a longitudinal geometry was employed in order to collect the resulting fluorescence, using an $f/1$ lens

of focal length 5 cm. This was apertured down to a 5 mm diameter in order to produce a 1 mm depth of focus. An RG1000 glass filter attenuated any residual pump light transmitted through the laser crystal. The captured fluorescence was focussed onto an InAs photodiode, sensitive over the wavelength range 1.5 to 3 μm . The photocurrent was input to a preamplifier (bandwidth 35 MHz), and then displayed and stored on a digital oscilloscope. As with the visible upconversion fluorescence measurements, there was no polarisation discrimination in the detection of the resulting fluorescence.

The first sample measured in this manner was the 2 mm Tm:YAP laser crystal. Upconversion was known to be weak, and so the fluorescence decay was expected to be single exponential in nature, and independent of the incident pump intensity. Taking the natural log of a typical set of decay data results in figure 6.16. A straight line fit can be made, confirming the single exponential nature of the decay. Averaging over 128 pump pulses was performed in order to produce the decay profiles shown in this section.

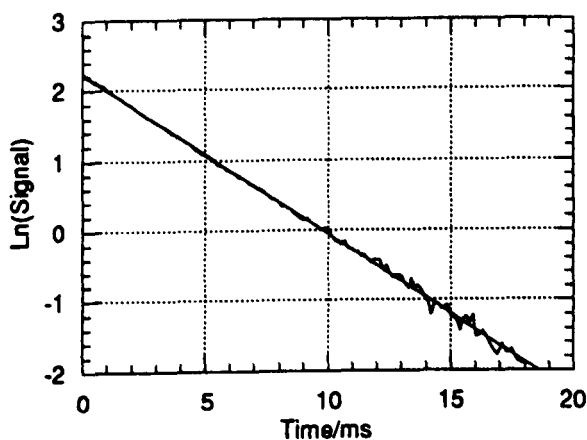


Figure 6.16 Infrared fluorescence decay of Tm:YAP

The 3F_4 fluorescence lifetime was measured to be 4.4 ± 0.1 ms. Neutral density filters were introduced into the pump optics train in order to vary the incident pump intensity on the laser crystal from 24 down to 2.6 kW cm^{-2} (taking into account the transmission of the HR coating on the laser crystal at the pump wavelength). This variation of nearly one order of magnitude was much greater than in the pump beam transmission experiments in chapter five because pulsed operation of the diode significantly reduced the thermal loading of the neutral density filters, allowing larger attenuation of the pump beam. The fluorescence lifetime was observed not to change from the quoted value over this range of pump intensities. In order to investigate

whether or not the lifetime was temperature-dependent, the heat load in the Tm:YAP crystal was altered by varying the pump pulse duration over the range 2 to 50 ms, and also by changing the duty cycle from 1 to 25% (both by altering the pump pulse duration and the pump pulse repetition rate). At pump pulse durations of 40 ms or greater, the infrared fluorescence signal was observed to reach a quasi-cw value. Over the range of pump pulse durations and duty cycles tested, the fluorescence lifetime was found to lie within the quoted value of 4.4 ± 0.1 ms. This is in reasonable agreement with the published value of 5 ms for the first excited state fluorescence decay lifetime of thulium in YAP³⁴.

The fluorescence decay time of the 2 mm Tm,Ho:YAP laser crystal was then measured, using the apparatus in figure 6.15. At the maximum incident pump intensity, the observed fluorescence decay profile was not a single exponential, but instead consisted of nonexponential initial decay, with a slow exponential tail. As the pump intensity was reduced, the initial decay became slower, with the exponential tail independent of the pump intensity. Figure 6.17 shows typical measured decay profiles at maximum and minimum incident pump intensities.

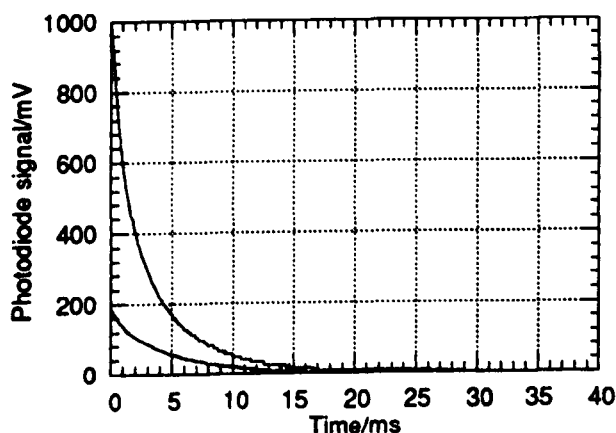


Figure 6.17 Intensity-dependent fluorescence decay profiles of Tm,Ho:YAP

The larger signal corresponds to the maximum incident pump intensity of 21 kW cm^{-2} , the lower signal to the minimum incident pump intensity of 2.3 kW cm^{-2} (again taking into account the transmission of the HR coating on the laser crystal). Independent of the pump intensity, the exponential tail of these decay profiles was measured to have a lifetime of 4.8 ± 0.3 ms. This exponential decay can then be subtracted from the recorded data to leave the portion due solely to the initial nonexponential decay. An effective lifetime can be defined as dividing the area under the curve by the peak fluorescence signal³⁵ (note that for a true exponential decay this definition yields the

1/e time). Performing this analysis, the initial decay was measured to vary from 2.1 to 4.0 ms as the incident pump intensity decreased from 21 to 2.3 kW cm⁻². This intensity-dependent portion of the total fluorescence decay is due to the holmium ⁵I₇ to ⁵I₅ upconversion becoming progressively weaker as the level of excitation decreases, while the exponential tail is the natural decay of the coupled thulium and holmium first excited state energy level manifolds. The effective lifetime of the total decay profile varied from 2.7 to 4.2 ms with decreasing pump intensity. This gives a measure of the energy storage lifetime of the upper laser level, an important parameter in Q-switched operation.

The final set of lifetime measurements were carried out on the 3 mm Tm,Ho:YLF laser crystal. Typical results are given in figure 6.18.

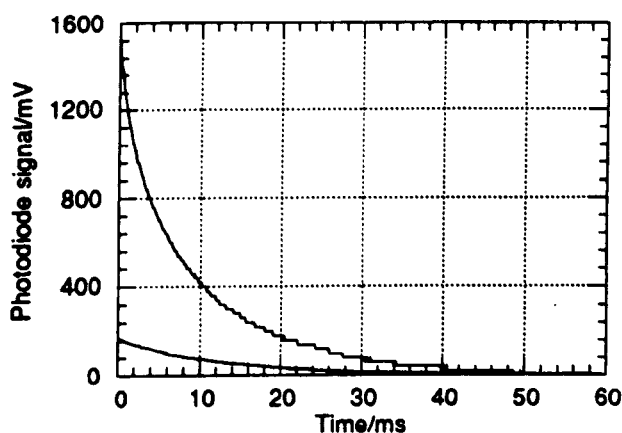


Figure 6.18 Intensity-dependent fluorescence decay of Tm,Ho:YLF

As with the Tm,Ho:YAP measurements in figure 6.17, the large signal decay curve was that recorded for the maximum incident pump intensity, the small signal curve the decay when the incident pump intensity was the minimum (taking into account the HR coating on the laser crystal, the incident pump intensity ranged from 25 to 2.7 kW cm⁻²). Once again, the double-doped crystal exhibits a nonexponential initial decay, with a slow exponential tail. This has a lifetime measured to be 12.4±1.0 ms, independent of the pump intensity. Subtracting this decay from the recorded fluorescence decay data, the initial nonexponential decay was measured to have an effective lifetime varying from 6.9 to 12.0 ms as the pump intensity was decreased. At incident pump intensities of 4 kW cm⁻² or less, the total decay curve was very close to being a single exponential, indicative of the holmium ⁵I₇ to ⁵I₅ upconversion becoming very weak. The effective lifetime of the total decay profile varied from 8.1 to 12.4 ms with decreasing pump intensity.

This decrease in the upconversion is more marked than in the YAP, and combined with the higher incident intensities experienced by the YLF crystal, is taken to indicate that the holmium 5I_7 to 5I_5 upconversion is weaker in YLF than in YAP. Armagan *et al.*³⁶ reported that a comparison of Tm,Ho:YAG and Tm,Ho:YLF with similar dopant concentrations showed upconversion losses to be greater in the former.

6.6 Conclusions

In this chapter results of the investigation of the visible and near infrared upconversion processes in double-doped YAP and YLF crystals have been presented. Excitation with a cw laser diode tuned to the thulium 3H_4 absorption band produced green fluorescence which appeared bright to the naked eye. Excitation of a single-doped Tm:YAP crystal under identical conditions produced barely visible pale blue fluorescence.

The visible upconversion fluorescence emitted by Tm,Ho:YAP was found to consist of a green band centred at 545 nm and a red band centred at 665 nm. With Tm,Ho:YLF green and red fluorescence bands were evident centred at 545 nm and 650 nm respectively, with additional blue emission in three bands centred on 390 nm, 420 nm and 485 nm. The very weak visible fluorescence from Tm:YAP could only just be resolved by the detection apparatus employed and was attributed to the presence of trace amounts of either holmium or erbium. Downconversion spectra recorded with a fluorimeter allowed the upconversion bands observed to be assigned to particular transitions. In all cases they were found to be due to transitions on the holmium which terminated in the ground state. The three blue fluorescence bands in double-doped YLF were assigned, in order of increasing wavelength, to transitions from the $^3K_7/{}^5G_4$, 3G_5 and 5F_3 multiplets. In both YAP and YLF the green and red fluorescence bands were assigned to transitions from the ${}^5S_2/{}^5F_4$ and 5F_5 multiplets respectively.

Measurements of the variation of fluorescence signal strength with pump power were then made in order to determine how many pump photons were required to generate an upconversion photon. For the transitions in the blue a slope of 2 was derived from the experimental data, implying that two pump photons were absorbed in order to generate a fluorescence photon, whereas for the green and red transitions the measured slope was close to 1.5, implying that three pump photons were absorbed in order to generate two fluorescence photons.

The combination of known visible transition and fluorescence signal dependency on pump power was used to determine the upconversion mechanisms producing the detected fluorescence. In all cases, rapid cross-relaxation in thulium followed by excitation sharing between thulium and holmium efficiently populated the holmium 5I_7 first excited state. This was the multiplet from which the upconversion occurred. The

multiplets producing green and red emission were populated by absorption of a pump photon from the holmium first excited state, nonradiative decay coupling the red to the green multiplet. In YAP the diode pump wavelength is resonant with the energy gap between holmium 5I_7 and $^5S_2/^5F_4$ whereas in YLF the pump absorption is phonon-assisted in order to bridge the energy gap. The multiplets producing the blue emission from YLF were populated by pump absorption from the holmium 5I_5 multiplet, this having been populated by an intermediary upconversion mechanism promoting holmium from 5I_7 , de-exciting thulium from 3F_4 to the 3H_6 ground state in the process.

In fact this intermediary thulium-holmium upconversion step is the principal upconversion mechanism taking place in double-doped materials. The reason that blue fluorescence was not detected from the Tm,Ho:YAP crystal is that in this large phonon energy oxide host the 5I_5 level is rapidly quenched by nonradiative decay. In addition the nonradiative decay between the $^5S_2/^5F_4$ and 5F_5 multiplets is much greater in YAP than in YLF, explaining the observed result that the ratio of the red to green fluorescence signal strengths in YAP was much greater than in YLF.

An indirect method of investigating this holmium 5I_7 to 5I_5 upconversion, in the absence of suitable apparatus to detect it directly, involved pulsed excitation of the laser crystals in order to measure the fluorescence decay profile of the coupled thulium and holmium first excited states. As a reference, single-doped Tm:YAP was investigated in a similar manner, and was found to have a fluorescence decay lifetime of 4.4 ± 0.1 ms, independent of the pump intensity used. This confirmed the expected result that upconversion is negligible in single-doped thulium materials. With both double-doped YAP and YLF the recorded profiles consisted of an initial intensity-dependent nonexponential decay, with a slow exponential decay in the tail of the profile independent of the pump intensity. This slow portion of the total fluorescence decay gives a measure of the natural fluorescence lifetime of the coupled multiplets. In the case of YAP this was measured to be 4.8 ± 0.3 ms, with the initial decay having an effective lifetime increasing from 2.1 to 4.0 ms as the pump intensity was reduced from 26 to 2.8 kW cm⁻². In the case of YLF the natural fluorescence lifetime was measured to be 12.4 ± 1.0 ms, with the initial decay having an effective lifetime increasing from 6.9 to 12.0 ms. These results clearly indicate the presence of the holmium 5I_7 to 5I_5 upconversion mechanism.

The upconversion present in double-doped YAP and YLF induces significantly more degradation in the laser operation of the former principally because a much larger fraction of the upconverted excitation undergoes nonradiative decay which contributes to additional heating of the host lattice, reducing the small-signal gain achievable and increasing the laser threshold. Additional heating also leads to increased thermal lensing in the laser crystal. In the low phonon energy fluoride host YLF any upconversion excitation efficiently fluoresces back to the ground state, contributing minimal additional heating. Furthermore, the phonon-assisted transition leading to the production of green and red upconversion fluorescence actually removes heat from the host lattice.

In conclusion, Tm,Ho:YAP as a potential two micron laser source suffers in comparison to Tm:YAP principally because of the presence of significantly higher upconversion rates which increase the laser threshold and reduce the slope efficiency through removal of excitation from the upper laser level; against Tm,Ho:YLF it suffers both because the upconversion rates are higher, and because a markedly greater fraction of the total upconversion contributes additional heating via nonradiative decay routes, imposing further penalties on efficient laser operation.

6.7 References

- [1] F. E. Auzel, 'Materials and devices using double-pumped phosphors with energy transfer', *Proc. IEEE*, vol. 61, no. 6, 758 (1973)
- [2] N. Bloembergen, 'Solid state infrared quantum counters', *Phys. Rev. Lett.*, vol. 2, 84 (1959)
- [3] D. C. Nguyen, G. E. Faulkner & M. Dulick, 'Blue-green (450 nm) upconversion $Tm^{3+}:YLF$ laser', *Appl. Opt.*, vol. 28, no. 17, 3553 (1989)
- [4] R. R. Stephens & R. A. McFarlane, 'Diode-pumped upconversion laser with 100 mW output power', *Opt. Lett.*, vol. 18, no. 1, 34 (1993)
- [5] R. A. McFarlane, 'High-power visible upconversion laser', *Opt. Lett.*, vol. 16, no. 18, 1397 (1991)
- [6] F. Heine, E. Heumann, P. Möbert & G. Huber, 'Room temperature cw green upconversion $Er^{3+}:YLiF_4$ laser pumped near 970 nm', in *OSA Proceedings on Advanced Solid-State Lasers*, (OSA, Washington, DC), vol. 24, 74 (1995)
- [7] J. Y. Allain, M. Monerie & H. Poignant, 'Room temperature cw tunable green upconversion holmium fibre laser', *Electron. Lett.*, vol. 26, no. 4, 261 (1990)
- [8] D. S. Funk, S. B. Stevens & J. G. Eden, 'Excitation spectra of the green $Ho:$ fluorozirconate glass fibre laser', *IEEE Photonics Technology Lett.*, vol. 5, no. 2, 154 (1993)
- [9] R. G. Smart, D. C. Hanna, A. C. Tropper, S. T. Davey, S. F. Carter & D. Szebesta, 'CW room temperature upconversion at blue, green and red wavelengths in infrared-pumped Pr^{3+} doped fluoride fibre', *Electron. Lett.*, vol. 27, no. 14, 1307 (1991)
- [10] P. Xie & T. R. Gosnell, 'Diode-pumped, cw blue, green, orange and red upconversion fibre lasers operating at room temperature', in *OSA Proceedings on Advanced Solid-State Lasers*, (OSA, Washington, DC), vol. 24, 101 (1995)
- [11] J. M. Sutherland, P. M. W. French, J. R. Taylor & B. H. T. Chai, 'New visible cw transitions in $Pr^{3+}:YLF$ and femtosecond pulse generation', in *OSA Trends in Optics & Photonics, "Advanced Solid-State Lasers"*, vol. 1, 277 (1996)
- [12] B. P. Scott, F. Zhao, R. S. F. Chang & N. Djeu, 'Upconversion-pumped blue laser in $Tm:YAG$ ', *Opt. Lett.*, vol. 18, no. 2, 113 (1993)
- [13] C. Borel, A. Rameix, P. Thony, B. Ferrand, D. P. Shepherd, A. C. Large, T. J. Warburton, A. C. Tropper, D. C. Hanna, S. Guy, M. F. Joubert & B. Jacquier, 'Growth by liquid phase epitaxy and laser performance at 2.012 μm of a $Tm:YAG$ planar waveguide', in *OSA Proceedings on Advanced Solid-State Lasers*, (OSA, Washington, DC), vol. 24, 37 (1995)
- [14] B. R. Reddy & P. Venkateswarlu, 'Infrared to visible energy upconversion in Er^{3+} -doped oxide glass', *Appl. Phys. Lett.*, vol. 64, no. 11, 1327 (1994)

- [15] L. B. Shaw, R. S. F. Chang & N. Djeu, 'Measurement of upconversion energy transfer probabilities in $Ho:Y_3Al_5O_{12}$ and $Tm:Y_3Al_5O_{12}$ ', Phys. Rev. B, vol. 50, no. 10, 6609 (1994)
- [16] X. X. Zhang, P. Hong, M. Bass & B. H. T. Chai, 'Blue upconversion with excitation into Tm ions at 780 nm in Yb and Tm codoped fluoride crystals', Phys. Rev. B, vol. 51, no. 14, 9298 (1995)
- [17] B. Dussardier, J. Wang, D. C. Hanna & D. N. Payne, 'Spectroscopy and cw 2-photon upconversion in Tm^{3+} -doped $ZnCl_2$ -based glass', Opt. Materials, vol. 4, no. 5, 565 (1995)
- [18] M. A. Noginov, P. Venkateswarlu & M. Mahdi, 'Two-step upconversion luminescence in Yb,Tb:YSGG crystal', J. Opt. Soc. Am. B, vol. 13, no. 4, 735 (1996)
- [19] T. Y. Fan, G. Huber, R. L. Byer & P. Mitzscherlich, 'Spectroscopy and diode laser-pumped operation of Tm,Ho:YAG', IEEE J. Quantum Electron., vol. 24, no. 6, 924 (1988)
- [20] M. Falconieri, A. Lanzi & G. Salvetti, 'Spectroscopic investigation of the visible and mid-infrared emission in Tm- and Ho-doped YAG and YLF crystals', Appl. Phys. B, vol. 62, no. 6, 537 (1996)
- [21] Thorn EMI photomultipliers catalogue
- [22] J. M. O'Hare & V. L. Donlan, 'Crystal field determination for trivalent thulium in yttrium orthoaluminate', Phys. Rev. B, vol. 14, no. 9, 3732 (1976)
- [23] A. A. Kaminskii, 'Laser crystals', 2nd edition, Berlin : Springer-Verlag (1990)
- [24] V. A. Antonov, P. A. Arsenev, K. E. Bienert & A. V. Potemkin, 'Spectral properties of rare earth ions in $YAlO_3$ crystals', Phys. Stat. Sol. A, vol. 19, 289 (1973)
- [25] J. B. Gruber, M. E. Hills, M. D. Seltzer, S. B. Stevens, C. A. Morrison, G. A. Turner & M. R. Kokta, 'Energy levels and crystal quantum states of trivalent holmium in yttrium aluminium garnet', J. Appl. Phys., vol. 69, no. 12, 8183 (1991)
- [26] H. P. Jenssen, A. Linz, R. P. Leavitt, C. A. Morrison & D.E. Wortman, 'Analysis of the optical spectrum of Tm^{3+} in $LiYF_4$ ', Phys. Rev. B, vol. 11, no. 1, 92 (1975)
- [27] N. Karayianis, D. E. Wortman & H. P. Jenssen, 'Analysis of the optical spectrum of Ho^{3+} in $LiYF_4$ ', Phys. Chem. Solids, vol. 37, no. 7, 675 (1976)
- [28] Speirs Robertson product catalogue
- [29] Hamamatsu photomultipliers catalogue
- [30] T. T. Basiev, Y. V. Orlovskii, K. K. Pukhov, V. B. Sigachev, M. E. Doroshenko & I. N. Vorob'ev, 'Multiphonon relaxation in the rare-earth ion doped laser crystals', in OSA Trends in Optics & Photonics, "Advanced Solid-State Lasers", vol. 1, 575 (1996)
- [31] M. J. Weber, 'Multiphonon relaxation of rare-earth ions in yttrium orthoaluminate', Phys. Rev. B, vol. 8, no. 1, 54 (1973)
- [32] M. Falconieri & G. Salvetti, 'Pumping-laser-fluence dependence of the time resolved fluorescence at 2.09 μm in Tm,Ho:YAG crystals', Opt. Materials, vol. 3, no. 2, 157 (1994)

- [33] K. M. Dinndorf & H. P. Jenssen, '*Lack of correlation between Tm,Ho upconversion measurements*', in *OSA Trends in Optics & Photonics, "Advanced Solid-State Lasers"*, vol. 1, 539 (1996)
- [34] S. A. Payne, L. L. Chase, L. K. Smith, W. L. Kway & W. F. Krupke, '*Infrared cross-section measurements for crystals doped with Er³⁺, Tm³⁺ and Ho³⁺*', *IEEE J. Quantum Electron.*, vol. 28, no. 11, 2619 (1992)
- [35] M. Falconieri & G. Salvetti, '*Effects of co-dopant concentrations and excitation conditions on the 2 μm fluorescence dynamics in Tm,Ho:YLF crystals*', *Appl. Phys. A*, vol. 59, no. 3, 253 (1994)
- [36] G. Armagan, A. M. Buoncristiani, A. T. Inge & B. DiBartolo, '*Comparison of spectroscopic properties of Tm and Ho in YAG and YLF crystals*', in *OSA Proceedings on Advanced Solid-State Lasers*, (OSA, Washington, DC), vol. 10, 222 (1991)

Relaxation oscillations

7.1 Introduction

Solid-state lasers are characterised by having an upper laser level lifetime much longer than the cavity decay lifetime; they are class B lasers. In general, excitation of such a class of laser leads to the formation of large amplitude spikes at the leading edge of the laser output, spikes which decrease in amplitude at some characteristic decay rate until steady-state oscillation is achieved. Perturbation of laser operation, for example by fluctuations in the gain or loss experienced by the lasing mode, or by alterations in resonator alignment, also lead to this spiking behaviour. This temporal behaviour is in marked contrast to that of most gas lasers, where the cavity lifetime is much longer than the upper laser level lifetime (class A lasers). In this regime any fluctuations in the laser output intensity are very rapidly damped out, preventing the formation of spiking.

The time evolution of this spiking behaviour can be explained as follows. The photon density in the laser resonator remains at the spontaneous emission level until the population inversion in the gain medium reaches the lasing threshold value (at which value the inversion is clamped during steady-state operation). Continued excitation of the gain medium, with minimal photon density in the resonator, allows the population inversion to grow further. Now the round-trip gain exceeds the loss and so the cavity photon density can begin to build up exponentially from the spontaneous emission level, at a rate determined principally by the cavity decay rate. Once the photon density exceeds its steady-state oscillation value there is sufficient circulating intensity to commence depleting the population inversion, pulling it back to its lasing threshold value. At this point the photon density reaches its peak value, and then begins to decrease. However there is still sufficient intensity to continue depleting the population inversion below its lasing threshold value. Both the photon density and population inversion continue to decrease until the former reaches its steady-state oscillation value. At this point continued excitation of the gain medium allows the population inversion to slowly build up once again, while the photon density falls back towards the noise level.

This large-signal spiking behaviour eventually damps down toward small-signal quasi-sinusoidal relaxation oscillation behaviour which decays exponentially in amplitude to true steady-state oscillation. Since neither the population inversion nor the photon density drop to zero after a spike, successive spikes start from initial conditions tending towards the steady-state conditions, causing the spikes to be damped out.

There have been a number of publications in the open literature dealing with theoretical treatments of this spiking/relaxation oscillation behaviour¹⁻³. Siegman⁴ outlines the analysis for a four-level laser, the simplest case to investigate. This chapter summarises the four-level laser analysis as this provides the basis on which to carry out the corresponding treatment for a three-level laser, then a thulium laser and finally a double-doped thulium,holmium laser.

The rationale behind this work was to explain the markedly different temporal behaviour of cw single-doped thulium and double-doped thulium,holmium lasers observed during the course of the experiments described previously in chapter four. This chapter presents the results of recording this temporal behaviour, before carrying out relaxation oscillation analysis to provide an explanation for the observed behaviour.

7.2 Laser temporal behaviour

The temporal behaviour of the three types of laser investigated, Tm:YAP, Tm,Ho:YAP and Tm,Ho:YLF, was observed and recorded on a digital oscilloscope connected to a fast long wavelength InGaAs photodiode which monitored the time-dependence of the laser output intensity.

For both the double-doped laser crystals similar results were obtained. A typical oscilloscope trace of the Tm,Ho:YAP laser output is shown in figure 7.1.

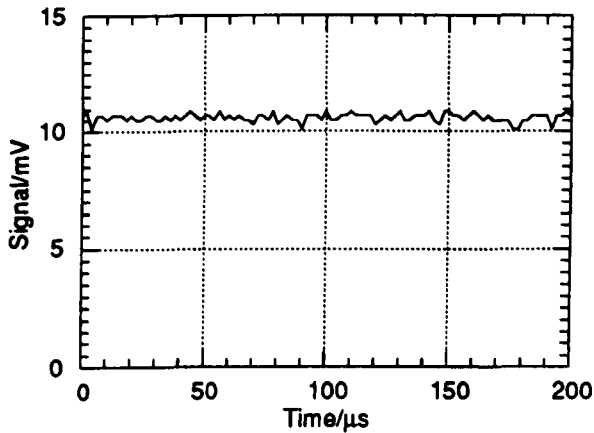


Figure 7.1 Typical temporal behaviour of Tm,Ho:YAP laser

The timescale viewed is not short enough to see any intensity fluctuations in the laser output due to longitudinal mode-beating effects. The observed behaviour is that expected for steady-state operation, with the small fluctuations on the otherwise flat photodiode signal due to detector noise.

Repeating this measurement with the Tm:YAP laser produced a markedly different result, as shown in the three oscilloscope traces comprising figure 7.2. The expected flat photodiode signal is instead swamped by a continuous series of spikes, the amplitude envelope of which varies over time in what appears to be a nonrepeatable fashion. Note that these spikes are smooth in lineshape, as witnessed on an analogue oscilloscope, and that any distortions in the traces shown here are due to the digitisation process in the Tektronix TDS540 oscilloscope used to record them. This spiking behaviour has also been observed in a diode-pumped Tm:YLF laser⁵.

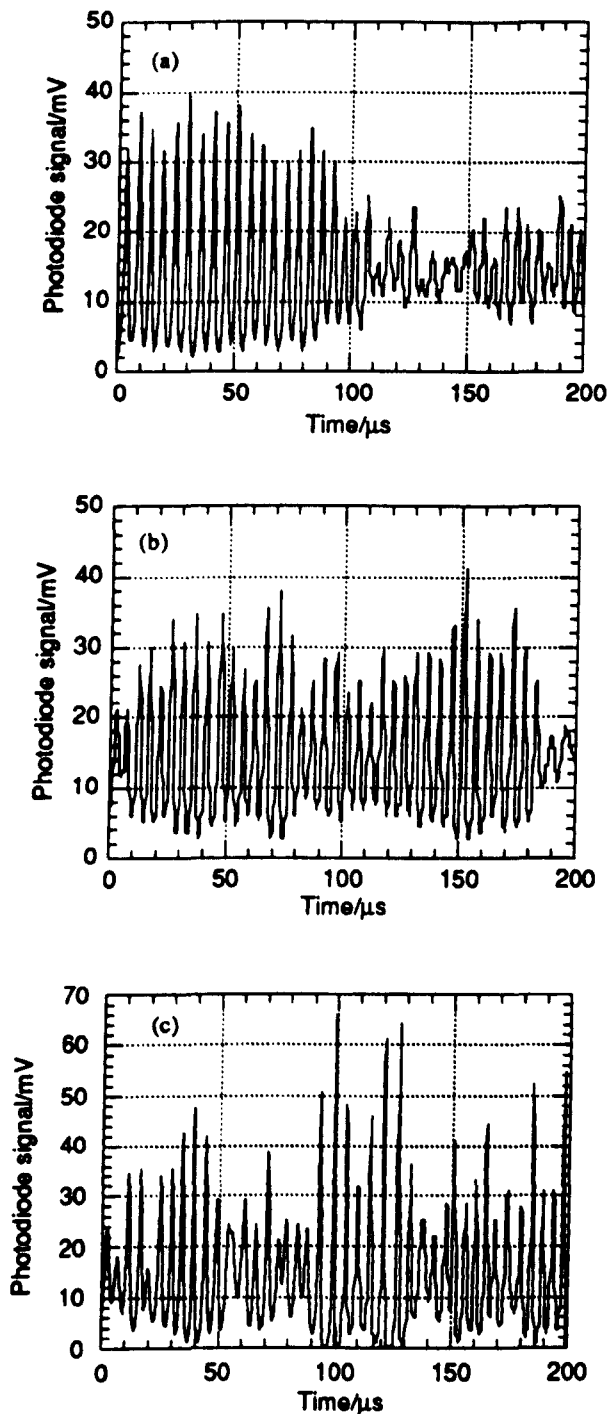


Figure 7.2 Examples of recorded temporal behaviour of Tm:YAP laser

Inspection of these traces shows that large amplitude spiking behaviour can damp down to lower levels, but never decays to small-signal relaxation oscillations or to true cw operation before the spiking amplitude grows again. The recorded traces show that as the spike amplitude decreases the period of the spiking also decreases while the width of the spikes increases, which is characteristic of the spiking/relaxation

oscillation behaviour expected in solid-state lasers⁴. The oscilloscope traces in figure 7.2 were captured with the Tm:YAP laser operating at its maximum output power of 730 mW, 2.8 times above threshold. The period of the large amplitude spikes is approximately 5 μ s. Figure 7.3 is a typical oscilloscope trace with the Tm:YAP laser operating at 1.5 times threshold. Here the period of the largest amplitude spikes is approximately 14 μ s. A decrease in spiking period as the laser is operated further from threshold is another characteristic of the expected spiking/relaxation oscillation behaviour.

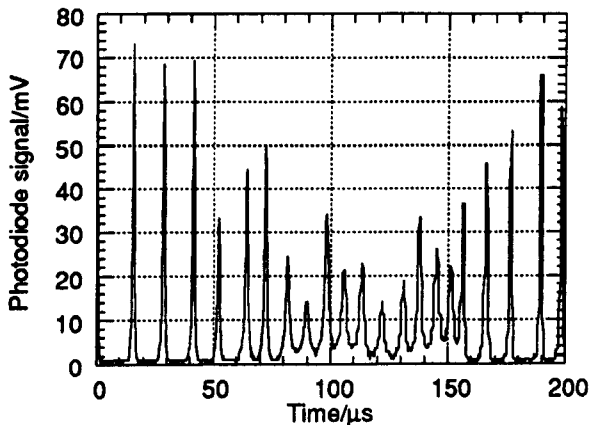


Figure 7.3 Temporal behaviour of Tm:YAP laser operating at 1.5 times threshold

Spiking behaviour dominates the laser output intensity independent of how far the laser is operated above threshold. Just above threshold, the laser output consists of a series of spikes of variable amplitude, each separated by a few tens of microseconds, with no dc level apparent in the photodiode signal between adjacent spikes.

As with the spectral measurements in chapter four, feedback effects were considered as potential sources of this intensity instability. However, use of an optical isolator to prevent feedback of the Tm:YAP laser output back into the resonator made no difference to the observed temporal behaviour. Feedback of diode pump light reflected from the pumped face of the Tm:YAP laser back into the laser diode was effectively suppressed with the insertion of a polariser and quarter-wave plate in the pump optics train. Again, there was no detectable change in the temporal behaviour of the Tm:YAP laser. It was known that feedback into the diode introduced intensity fluctuations onto the pump beam, and although these may have contributed to the resultant instability in the thulium laser output, the observed behaviour meant that this was only a minor effect.

7.3 Relaxation oscillation analysis

The following is the symbol list for this section :

N_{Tm} - total thulium concentration (cm^{-3})

N_{Ho} - total holmium concentration (cm^{-3})

ΔN - population inversion density (cm^{-3})

n - photon number density (cm^{-3})

ΔN_{osc} - small-signal perturbation to population inversion density (cm^{-3})

n_{osc} - small-signal perturbation to photon number density (cm^{-3})

γ_{osc} - damping rate of relaxation oscillations (s^{-1})

σ - stimulated emission cross-section (cm^2)

τ - decay lifetime of upper laser level (s)

γ_c - cavity decay rate (s^{-1})

R_p - pump rate density ($\text{cm}^{-3} \text{s}^{-1}$)

R_{pmin} - minimum pump rate density ($\text{cm}^{-3} \text{s}^{-1}$)

ω_p - pump rate (s^{-1})

$g_u(g_l)$ - degeneracy of upper(lower) laser levels

$f_u(f_l)$ - temperature-dependent fractional occupation of upper(lower) laser level

$k_f(k_r)$ - forward(reverse) excitation transfer parameter ($\text{cm}^3 \text{s}^{-1}$)

7.3.1 Ideal four and three-level lasers

Siegman⁴ provides an analysis of relaxation oscillations for the case of an ideal four-level laser, based on the original work of Dunsmuir¹, Sinnett² and Kleinman³. This involves carrying out a linearised small-signal analysis, and so only applies when the spiking behaviour has damped down to small-signal quasi-sinusoidal fluctuations about the steady-state lasing conditions. The starting equations for this analysis are the rate equations for the population inversion density and the intracavity photon number density, namely

$$\frac{d\Delta N}{dt} = R_p - \Delta N n \sigma c - \frac{\Delta N}{\tau} \quad 7-1$$

and

$$\frac{dn}{dt} = \Delta N n \sigma c - \gamma_c n. \quad 7-2$$

Steady-state solutions for the threshold population inversion density and intracavity photon number density can then be determined. By allowing the instantaneous photon number density and population inversion density to vary by a small amount n_{osc} and ΔN_{osc} from the steady-state values, the rate equations can be reduced to their linearised small-signal form

$$\begin{aligned} \frac{d\Delta N_{osc}}{dt} &= -\gamma_c n_{osc} - \frac{r\Delta N_{osc}}{\tau} \\ \frac{dn_{osc}}{dt} &= (r-1)\frac{\Delta N_{osc}}{\tau} \end{aligned} \quad 7-3$$

where

$$r = \frac{R_p \tau}{\Delta N_{th}} \quad 7-4$$

is the pumping ratio, with ΔN_{th} the steady-state threshold inversion density. From these equations Siegman derives the following expression for the damping rate γ_{osc} of the relaxation oscillations

$$\gamma_{osc} = \frac{r}{2\tau}. \quad 7-5$$

The population inversion will simultaneously have damped fluctuations about its steady-state value such that the peaks in the laser output occur when the population inversion passes through its steady-state value.

It is of interest, and of some value, to derive the equivalent expressions for a true three-level laser. Using similar notation to the four-level laser analysis, the starting equations are

$$\frac{d\Delta N}{dt} = (R_p - R_{p_{min}}) - \left(1 + \frac{g_u}{g_l}\right) \Delta N n \sigma c - \frac{\Delta N}{\tau} \quad 7-6$$

and

$$\frac{dn}{dt} = \Delta N n \sigma c - \gamma_c n \quad 7-7$$

where

$$R_{p_{min}} = \frac{g_u}{g_l} \frac{N_0}{\tau} \quad 7-8$$

is the pump rate needed to achieve the inversion threshold (N_0 being the population density of the lasing ion).

The linearised small-signal form of these equations are

$$\begin{aligned}\frac{d\Delta N_{osc}}{dt} &= -\left(1 + \frac{g_u}{g_l}\right)\gamma_c n_{osc} - \frac{r\Delta N_{osc}}{\tau} \\ \frac{dn_{osc}}{dt} &= (r-1)\frac{\Delta N_{osc}}{\left(1 + \frac{g_u}{g_l}\right)\tau}\end{aligned}\tag{7-9}$$

where now

$$r = \frac{(R_p - R_{pmin})\tau}{\Delta N_{th}}.\tag{7-10}$$

The only difference from the four-level laser case is the bracketed term containing the level degeneracies. Proceeding with the analysis, this bracketed term drops out when the damping rate is derived, yielding an identical expression to the four-level case.

7.3.2 Quasi-three level lasers

Analytical solutions to the rate equations for this class of laser are not trivial to derive in the case where stimulated emission is present. Instead it is proposed to state the starting equations, and then by comparison with the full solutions for both three and four-level lasers obtain the corresponding damping rate.

Figure 7.5 depicts the principal mechanisms that need to be considered for lasing in both thulium and thulium,holmium lasers. Cross-relaxation (referring to section 5.3 the reverse upconversion process is considered negligible here) dominates the distribution of population in the thulium ions with stimulated emission back to the ground state, or, in the case of double-doped materials, excitation transfer and subsequent stimulated emission on the holmium.

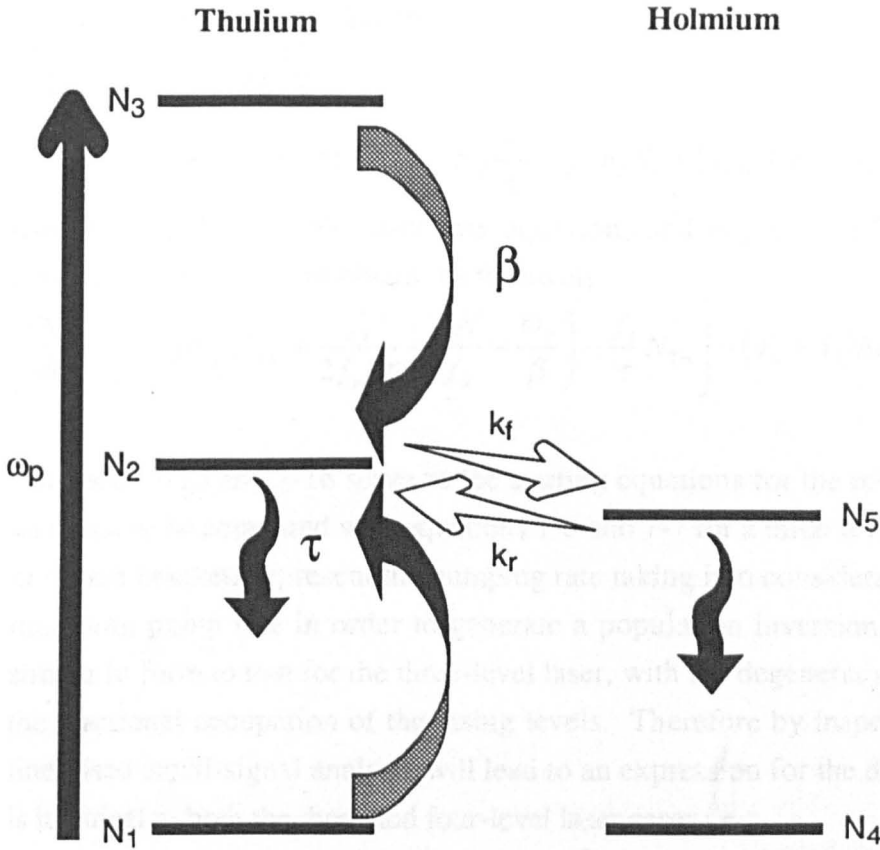


Figure 7.5 Energy level diagram showing principal parameters used in relaxation oscillation analysis

Thulium laser

We assume that the entire thulium population resides in the three levels of figure 7.5 (corresponding to the 3H_6 , 3F_4 and 3H_4 energy level manifolds), yielding equation 7-11

$$N_{Tm} = N_1 + N_2 + N_3. \quad 7-11$$

The rate equations for the level population densities of this system are

$$\begin{aligned} \frac{dN_3}{dt} &= \omega_p N_1 - \beta N_1 N_3 \\ \frac{dN_2}{dt} &= 2\beta N_1 N_3 - \frac{N_2}{\tau} - \Delta N n \sigma c \end{aligned} \quad 7-12$$

with the rate equation for the photon number density as before

$$\frac{dn}{dt} = \Delta N n \sigma c - \gamma_c n. \quad 7-13$$

The population inversion density on the thulium laser transition is defined as

$$\Delta N = f_u N_2 - f_l N_1 \quad 7-14$$

with corresponding rate equation

$$\begin{aligned} \frac{d\Delta N}{dt} &= f_u \frac{dN_2}{dt} - f_l \frac{dN_1}{dt} \\ &= -(f_u + f_l)\Delta N n \sigma c - (f_u + f_l) \frac{N_2}{\tau} + f_l \omega_p N_1 + (2f_u + f_l)\beta N_1 N_3. \end{aligned} \quad 7-15$$

Eliminating N_3 and N_1 from this equation, and expressing N_2 in terms of the population inversion, we obtain the following

$$\frac{d\Delta N}{dt} = \left[2f_u \omega_p \left(N_{Tm} + \frac{f_l}{2f_u \beta \tau} - \frac{\Delta N}{f_u} - \frac{\omega_p}{\beta} \right) - \frac{f_l}{\tau} N_{Tm} \right] - (f_u + f_l)\Delta N n \sigma c - \frac{\Delta N}{\tau}. \quad 7-16$$

Equations 7-13 and 7-16 serve as the starting equations for the relaxation oscillation analysis, to be compared with equations 7-6 and 7-7 for a three-level laser. The terms in square brackets represent the pumping rate taking into consideration the need for a minimum pump rate in order to generate a population inversion. This equation is similar in form to that for the three-level laser, with the degeneracy terms replaced by the fractional occupation of the lasing levels. Therefore by inspection the resulting linearised small-signal analysis will lead to an expression for the damping rate which is identical to both the three and four-level laser cases i.e.

$$\gamma_{osc} = \frac{r}{2\tau}. \quad 7-17$$

Thulium,holmium laser

In this analysis the effects of any upconversion processes are ignored, restricting the holmium population to either the ground or first excited state. The full set of rate equations for the level population densities of this system is

$$\begin{aligned} \frac{dN_3}{dt} &= \omega_p N_1 - \beta N_1 N_3 \\ \frac{dN_2}{dt} &= 2\beta N_1 N_3 - \frac{N_2}{\tau} - k_f N_2 N_4 + k_r N_5 N_1 \\ \frac{dN_5}{dt} &= k_f N_2 N_4 - k_r N_5 N_1 - \frac{N_5}{\tau} - \Delta N n \sigma c \\ &= -\frac{dN_4}{dt} \end{aligned} \quad 7-18$$

with the photon number density rate equation

$$\frac{dn}{dt} = \Delta N n \sigma c - \gamma_c n. \quad 7-19$$

The following definitions are used

$$\begin{aligned} N_{Tm} &= N_1 + N_2 + N_3 \\ N_{Ho} &= N_4 + N_5 \\ \Delta N &= f_u N_5 - f_l N_4. \end{aligned} \quad 7-20$$

The resulting rate equation for the population inversion on the holmium laser transition is

$$\frac{d\Delta N}{dt} = -(f_u + f_l)\Delta N n \sigma c - (f_u + f_l)\frac{N_5}{\tau} + (f_u + f_l)(k_f N_2 N_4 - k_r N_5 N_1). \quad 7-21$$

The final term in the above equation represents the pump rate into the holmium. Explicitly it appears as though it is determined solely by the net excitation sharing rate. Implicitly it depends on the pump rate into the thulium through the N_1 and N_2 terms. Expressing N_4 and N_5 in terms of the population inversion density yields

$$\frac{d\Delta N}{dt} = N_{Ho} \left((f_u k_f N_2 - f_l k_r N_1) - \frac{f_l}{\tau} \right) - (f_u + f_l)\Delta N n \sigma c - \Delta N \left(\frac{1}{\tau} + k_f N_2 + k_r N_1 \right). \quad 7-22$$

Comparing this with previous expressions (equation 7-6 for a three-level laser, equation 7-16 for a thulium laser), the damping rate is given by

$$\gamma_{osc} = \frac{r}{2\tau_d} \quad 7-23$$

where

$$\frac{1}{\tau_d} = \frac{1}{\tau} + (k_f N_2 + k_r N_1). \quad 7-24$$

Comparing equations 7-23 and 7-24 with equation 7-17 reveals the reason for the different temporal behaviour of thulium and thulium,holmium lasers. In the case of the latter, in addition to the fluorescence lifetime of the upper state, the excitation transfer rate between the thulium and holmium needs to be considered when analysing relaxation oscillation phenomena.

From section 6.5 of the previous chapter, the fluorescence lifetime of the thulium 3F_4 first excited state in YAP was measured to be 4.4 ms. This long lifetime results in very weak damping of any spiking in the laser output. For a single set of spikes, it will take of order 40 to 50 ms for the laser output to return to steady-state oscillation. Any further perturbations to the resonator within this period will result in another set of spikes appearing before the initial set have decayed, with the cumulative effect that the expected cw output is instead dominated by large amplitude spiking. It is proposed that the low-gain thulium laser transition is very sensitive to mechanical or

acoustic perturbations to the laser resonator, which occur at frequencies up to a few kilohertz, resulting in the highly unstable temporal behaviour observed.

Pulsed operation of the Tm,Ho:YAP laser allowed the decay rate of the relaxation oscillations to be measured. In this pulsed mode, the laser operated at twice threshold with the diode output at its maximum. Figure 7.4 was generated with the laser operating at maximum output. Neutral density filters were used to attenuate the pump power, allowing the laser to be operated over a range of pumping ratios. Fitting an exponential decay of the form $\exp(-\gamma_{osc}t)$ to the recorded relaxation oscillations, and taking into account how far the laser was from threshold, a value for τ_d of $11.9 \pm 0.8 \mu\text{s}$ was obtained. This value is the sum of the contributions from both the fluorescence decay and the excitation sharing. Referring back to section 6.5 the effective fluorescence lifetime of the coupled thulium and holmium first excited states varies from 2.7 to 4.2 ms, depending on the incident pump intensity on the laser crystal. These values are nearly three orders of magnitude larger than τ_d , and therefore the value of τ_d can be equated to the effective lifetime of the excitation transfer process between thulium and holmium.

Carrying out a similar analysis for Tm,Ho:YLF, which in pulsed mode was operated at up to 1.5 times threshold, a value for τ_d of $14.8 \pm 1.2 \mu\text{s}$ was obtained, of comparable magnitude to the result for Tm,Ho:YAP.

From the open literature, the characteristic lifetime of excitation transfer in Tm,Ho:YAG was calculated as being in the range 10 to 20 μs , where the rare earth concentrations were comparable with the doping levels in both the Tm,Ho:YAP and Tm,Ho:YLF crystals used here⁶. In this case the magnitude of the excitation transfer rate was derived from spectroscopic measurements of the fluorescence of the first excited states of thulium and holmium. Therefore it is proposed that the excitation transfer between thulium and holmium acts as a strong damping mechanism, rapidly quenching any spiking or relaxation oscillations induced by perturbations to the lasing mode. The work of Becker and Huber^{7,8} indicated that in flashlamp-pumped Tm:YAG and Tm,Ho:YAG, the latter exhibited much reduced spiking behaviour, which the authors attributed to the excitation sharing in the double-doped laser crystal.

7.4 Conclusions

In this chapter the markedly different temporal behaviour of the output intensity of single and double-doped two micron lasers was illustrated and analysed. The output of the Tm:YAP laser consisted of continuous fluctuations on the microsecond timescale, characteristic of spiking/relaxation oscillation behaviour, with a randomly varying amplitude envelope. This phenomenon was difficult to analyse quantitatively because of its very unstable nature. However it was possible to eliminate feedback effects, both in the pump diode and thulium laser itself, as well as the multiline output of the thulium laser, as the principal sources of this instability. In contrast, the output intensity of both the Tm,Ho:YAP and Tm,Ho:YLF lasers was truly cw on the same timescales. Perturbation of the resonator induced spiking and relaxation oscillations in the laser output which were damped back down to steady-state operation within 100 μs .

Derivation of the rate equations governing the population inversion density and photon number density allowed this different behaviour to be explained, by comparison with the corresponding rate equations for an ideal four-level laser. Relaxation oscillations in this class of laser have been treated theoretically and experimentally in the open literature. For quasi-three level thulium (and also for true three-level lasers) the small-signal relaxation oscillations are damped exponentially at a rate depending on the number of times threshold the laser operates, and inversely on the upper laser level lifetime. This behaviour is identical to that of an ideal four-level laser. In the case of thulium,holmium lasers the damping rate depends once more on the number of times threshold the laser operates, but now inversely on an effective lifetime obtained by summing the inverses of both the upper laser level lifetime and the characteristic lifetime of the excitation sharing process between the thulium and holmium first excited states.

The experimental results obtained with pulsed operation of Tm,Ho:YAP and Tm,Ho:YLF produced respective values of $11.9 \pm 0.8 \mu\text{s}$ and $14.8 \pm 1.2 \mu\text{s}$ for this effective lifetime. In both cases these are far shorter than the upper laser level lifetimes of several milliseconds, and so can be taken as the values for the excitation sharing lifetime.

Therefore the fundamental difference in the temporal behaviour of single and double-doped lasers can be attributed to the excitation sharing process occurring in the latter,

which is sufficiently rapid to efficiently quench spiking/relaxation oscillations in the output intensity of the laser mode. The long fluorescence lifetime of thulium, 4.4 ms for 4.2% Tm:YAP, results in very weak damping of any intensity fluctuations. The broad gain bandwidth and low gain cross-section inherent to thulium render it very sensitive to perturbations of the lasing mode which, combined with very weak damping of the induced spiking, results in the laser output intensity being dominated by large amplitude spikes even when cw pumped. Careful resonator design is required in order to suppress this behaviour.

This is a major benefit of using double-doping in diode-pumped two micron lasers, as without it the damping of spiking is determined solely by the long fluorescence lifetime of the upper laser level, which as a consequence is very weak, allowing so-called steady-state operation to in fact be very unstable in the time domain.

7.5 References

- [1] R. Dunsmuir, *Theory of relaxation oscillations in optical masers*, J. Electronics and Control, vol. 10, 453 (1961)
- [2] D. M. Sinnott, *An analysis of the maser oscillator equations*, J. Appl. Phys., vol. 33, no. 4, 1578 (1962)
- [3] D. A. Kleinman, *The maser rate equations and spiking*, Bell Sys. Tech. J., vol. 43, 1505 (1964)
- [4] A. E. Siegman, *Lasers*, California: University Science Books (1986) - principally Ch. 25
- [5] K. L. Schepler, Wright Patterson Air Force Base, private communication
- [6] R. R. Petrin, M. G. Jani, R. C. Powell & M. Kokta, *Spectral dynamics of laser-pumped $Y_3Al_5O_{12}:Tm, Ho$ lasers*, Optical Materials, vol. 1, no. 2, 111 (1992)
- [7] T. Becker & G. Huber, *Dynamic properties of 2 μm Tm and Ho lasers*, in *Digest of Conference on Lasers & Electro-Optics*, (OSA, Washington, DC), paper CTuO3 (1991)
- [8] T. Becker & G. Huber, *Optimisation and dynamics of 2 μm Tm and Ho lasers*, J. Phys. IV Coll., vol. 1, no. C7, 353 (1991)

CHAPTER 8

Conclusions

8.1 Summary of the achievements of this work

The work presented in this thesis has detailed an investigation of diode-pumped two micron solid-state lasers, concentrating on a comparison of the cw room temperature operation of three laser crystals, Tm:YAP, Tm,Ho:YAP and Tm,Ho:YLF. Several aspects of their behaviour were investigated in order to explain the observed laser performance. Dopant concentrations (percentage substitution of yttrium) in YAP were 4.2% thulium and 0.28% holmium; in YLF they were 6% thulium and 0.4% holmium.

Thermal modelling was carried out in order to determine the temperature profiles generated by absorption of pump light in these laser crystals. Peak mean temperature rises of 35°C in YLF and 25°C in YAP were calculated, assuming that 50% of the absorbed pump light was converted to heat. The magnitude of the temperature gradient was used to estimate the strength of the thermal lensing. Despite the steeper temperature gradients in YLF, the thermal lensing was weaker because the major contributions to the lensing were of opposite sign. Under lasing conditions, the heat loads in Tm:YAP, Tm,Ho:YAP and Tm,Ho:YLF were estimated to be 500 mW, 850 mW and 780 mW respectively. For the observed laser transitions in these crystals, the corresponding thermal lenses were calculated to be of order 5 cm, 3 cm and 10 cm. Knowledge of the temperature profiles was also important for the quasi-three level thulium and holmium lasers investigated here because temperature-dependent population distributions determined the inversion threshold contribution to the laser threshold and also the excitation sharing between thulium and holmium. Using the calculated temperature rises, it was estimated that the fraction of the ground state population requiring excitation in order to generate an inversion threshold was 5% in Tm:YAP, 7% in Tm,Ho:YAP and 16.5% in Tm,Ho:YLF. For the relative concentrations of thulium and holmium in both the YAP and YLF crystals studied here, it was calculated that excitation was shared approximately equally between the two ionic species at the calculated operational temperatures. The lower thermal

conductivity of YLF made it more susceptible to thermal fracture than YAP, with a factor of three difference in maximum heat loads (5 W versus 15 W).

Laser operation was achieved utilising an end-pumping geometry with a simple two mirror standing wave resonator, relying on thermal lensing in the gain medium to form a stable resonator mode. The pump source for these experiments was a 3 W AlGaAs laser diode. This simple experimental arrangement allowed the laser crystals of interest to be assessed under nominally identical conditions.

Maximum output power was achieved using a 2 mm thick Tm:YAP laser crystal, generating 730 mW of laser output, representing 42% conversion efficiency in terms of absorbed pump power. The conversion efficiency of double-doped laser crystals was hampered by excitation being shared between the thulium and holmium. Upper bounds on the conversion efficiency of a 3 mm thick Tm,Ho:YAP and a 4 mm thick Tm,Ho:YLF laser crystal of 14% and 30% were obtained, with corresponding output powers of 270 and 660 mW. In all three cases, the output beam was approximately Gaussian in profile, and measured to be near diffraction-limited. Thus it was close to TEM₀₀ in nature.

Double-doped laser crystals exhibit significant amounts of upconversion, particularly large phonon energy hosts such as YAP. Visible upconversion fluorescence bands in the green and red were identified in Tm,Ho:YAP and Tm,Ho:YLF, with additional blue emission from the latter, all assigned to transitions on holmium. The principal upconversion mechanisms in these materials all involved the holmium first excited state which, since it also contains the upper laser level, represented a loss to the stimulated emission process.

However, although the conversion efficiency from diode pump light to laser output was superior in Tm:YAP, its spectral and temporal characteristics were far inferior. In terms of wavelength, the output consisted of a comb of lines in the range 1.965 to 2.020 μm , linearly polarised parallel to the YAP a-axis. The nature of the spectral output was very sensitive to perturbations to the resonator. For both the double-doped crystals, the laser output was on a single transition, wavelength 2.120 μm in YAP (c-axis polarised), 2.065 μm in YLF (a-axis polarised). Spatial holeburning effects allowed of order six longitudinal modes to lase in both of these holmium lasers.

In the time domain, the output intensity of the Tm:YAP laser was dominated on a microsecond timescale by large amplitude spiking, characteristic of the spiking/relaxation oscillation behaviour expected in solid-state lasers. It was proposed that the long lifetime of the upper laser level (measured to be 4.4 ms) provided very weak damping of any spiking behaviour initiated by a perturbation to the lasing mode. This effect was found to be independent of the multi-line operation in the spectral domain. On similar timescales, both the double-doped laser crystals exhibited the smooth intensity behaviour expected for cw lasing. By examination of the rate equations governing the stimulated emission process, it was proposed that the excitation sharing between thulium and holmium, with a measured characteristic lifetime in YAP of 11.9 μs and YLF of 14.8 μs , provided strong damping of any spiking behaviour.

This work has shown that although at room temperature more efficient conversion can occur in single-doped thulium laser crystals, there is a price to pay in terms of spectral and temporal quality, brought about by the low gain and broad bandwidth of thulium as compared to holmium. Line-narrowing elements in the resonator can be used to reduce the spectral linewidth; careful design of the laser is necessary in order to minimise or eliminate the intensity fluctuations.

With the double-doped crystals, the principal consideration was the magnitude of the resultant upconversion losses. Initial spectroscopic measurements and thermal modelling highlighted Tm,Ho:YAP as potentially a useful laser crystal, combining the robustness and natural birefringence of YAP with a large stimulated emission cross-section in the holmium (at $7.5 \cdot 10^{-20} \text{ cm}^2$ measured to be twice that of the holmium in YLF laser transition, and an order of magnitude greater than that of thulium in YAP). In addition, its long wavelength transition at 2.12 μm is in a good window for atmospheric transmission, whereas with holmium in YLF the wavelength has to be carefully controlled in order to avoid CO₂ absorption lines, and with thulium in YAP wavelengths shorter than 1.96 μm start to experience strong water absorption. However in terms of optical conversion efficiency Tm,Ho:YAP was far inferior to the other two laser crystals, hampered by the upconversion occurring, particularly the resulting increased levels of nonradiative decay into the host lattice.

In order to calculate the conversion efficiency from diode pump light to laser output measurement of the pump power absorbed in the laser crystals was required. This experiment revealed that with Tm:YAP significant bleaching of the ground state

population was occurring, verified by rate equation analysis. With the double-doped crystals, the presence of upconversion partially compensated for this bleaching by providing additional absorption of the pump light; however the accompanying enhanced nonradiative decay levels temperature-broadened the absorption spectrum, increasing the transmission of pump light through these crystals.

The deleterious effects of upconversion on lasing in the two micron waveband can be reduced by using low phonon energy hosts such as YLF. This crystalline host has the additional benefit of weak thermal lensing due to the two principal contributions being of opposite sign, despite the fact that the temperature gradients are more severe in YLF than in YAP due to the former's lower thermal conductivity.

Therefore, of the three laser crystals assessed here, we can conclude that for low power room temperature operation $T_{m,Ho:YLF}$ offers the best compromise between conversion efficiency, spectral linewidth and temporal stability. Indeed, the more pronounced temperature sensitivity of holmium in YLF will allow a significant enhancement in conversion efficiency for a moderate increase in cooling of the crystal. The major disadvantage of YLF as a laser crystal is its brittle nature, which is the ultimate limiting factor in power scaling of a diode-pumped two micron laser utilising this host.

8.2 Prospects for future work

With the advent of high power laser diode pump sources, there has been a significant amount of effort devoted to investigating a wide range of potential laser hosts, many of which had previously been tested then discarded as being unsuitable for flashlamp pumping e.g. vanadates and fluoroapatites. To date, the bulk of such work has been carried out with neodymium-doped materials, as opposed to the thulium and holmium doped crystals studied here.

The simple experimental set-up employed here can be used to characterise and compare appropriately coated single-doped thulium or double-doped thulium,holmium materials as and when they become available, simply by placing them at the focus of the diode pump beam. If the relevant materials parameters are known, the thermal modelling detailed in this thesis can also be applied to provide a further comparison. Since thermal management is of critical importance in thulium and holmium lasers, validation of the modelling is required. An accurate experimental technique for determining the thermal lensing would be one route to providing a comparison between experiment and theory. One of the unresolved issues related to measurement of the thermal lensing concerns how more significant the end-face curvature becomes to lasing when the pumped face of the laser crystal is also a mirror for the two micron resonator. Another technique to provide validation of the thermal modelling would be accurate calorimetric measurements of the laser crystals upon optical excitation, in order to determine a value for the fractional heat load.

Most of the published work in the open literature on the topic of diode-pumped two micron lasers has dealt with Tm:YAG. Given that thulium in YAP is quoted as having twice the emission cross-section of thulium in YAG, it would be instructive to make a rigorous comparison of the two under identical experimental conditions, in order to ascertain if YAP offers any significant advantages as a laser host. One practical advantage of Tm:YAP over Tm:YAG is the longer pump wavelength (795 nm versus 785 nm) which matches better the spectral band covered by commercially available AlGaAs laser diodes.

The use of laser diodes emitting in the wavelength range 1.8 to 2.0 μm allows pumping directly into the first excited state of either thulium or holmium, reducing the quantum defect between pump and laser output. This would be of interest principally with single-doped holmium, as one route to a diode-pumped holmium laser without the inefficiency of excitation sharing in materials co-doped with thulium.

Upconversion and temporal behaviour could then be compared to double-doped lasers.

High power operation can be investigated using fibre-coupled centimetre bar arrays as the pump source. Power scaling requires issues such as thermal fracture and ground state bleaching effects to be carefully considered. One technique for reducing the thermally induced stresses is to detune the pump wavelength from the absorption peak, and employ a longer length of gain medium. This requires a high power source with reasonable beam quality to achieve the necessary depth of focus, such as that offered by a fibre-coupled diode array. The thermal fracture limit of the gain medium can be increased by raising the thermal conductivity, which is most readily achieved by cooling to cryogenic temperatures. This is of particular interest in brittle materials such as YLF; high power operation utilising YLF almost certainly entails cryogenic cooling of the laser crystal.

Cooling to cryogenic temperatures would allow the temperature dependence of the various excitation and upconversion mechanisms to be investigated. Low temperature operation would "freeze out" phonon-assisted transitions, which may or may not contribute to increasing the lasing efficiency. Operation at reduced temperature decreases the lower laser level population and increases the population of the upper laser level, which has a marked reduction on the inversion threshold.

Measurement of the magnitude of the upconversion events relative to the excitation of the upper laser level needs to be performed in order that the true significance of the upconversion losses to laser operation can be assessed quantitatively, rather than the qualitative results presented here.

The long upper laser level lifetime of thulium and holmium makes them potentially attractive as Q-switched laser sources. Repetitive Q-switching of a cw pumped laser allows operation over a wide range of pulse repetition frequencies. In double-doped crystals the effects of excitation sharing and upconversion once again have to be taken into account in order to determine lasing efficiency. A Q-switched source emitting in the wavelength range 2 to 2.1 μm is an ideal source for pumping an OPO designed to operate in the three to five microns waveband because both signal and idler beams generated are in the desired waveband.

Single frequency operation for coherent remote sensing applications is also of interest. In this case the issues to address include operation at a wavelength offering good atmospheric transmission, ability to tune the output wavelength and ease of obtaining and maintaining stable single frequency operation.

APPENDIX A

Thulium and holmium energy levels

Determination of the energy levels of a lasing ion in a host matrix is usually carried out by analysing absorption spectra measured at low temperatures (either liquid helium or liquid nitrogen temperatures) in order to obtain sharp non-broadened spectra. Excitation and emission spectra are used to determine the Stark levels of the ground state energy level manifold. Combined with knowledge of the symmetry of the site in which the lasing ion resides, group theory can be used to determine the transitions producing the observed spectra. Experimental levels and their symmetry labels can be compared to theoretical levels calculated using the Hamiltonian of the system being studied.

The following tables list published figures of the experimentally derived energy levels of the ground and first excited state energy level manifolds of thulium and holmium in the crystalline hosts YLF and YAP, as well as the thulium 3H_4 diode pump band energy level manifold in these two host crystals. The asterisked energy levels are those involved in laser transition(s) investigated during the course of this work. Levels which are both asterisked and shaded are lasing levels considered to be effectively degenerate at room temperature because their separation is small. Note that these levels are listed in wavenumbers (cm^{-1}).

Kaminskii¹ lists the expected number of Stark levels for each energy level manifold. This number depends on the symmetry of the site the laser ion resides in, and also on the J value of the energy level manifold.

Manifold	Host Lattice	
	YLF ²	YAP ³
³ H ₆	0	0
	31	3
	56	65
	282	144
	310	210
	324	237
	327	271
	374	282
	374	313
	375	440*
	409	574*
		628*
³ F ₄	5605	5622*
	5760	5627*
	5757	5716
	5827	5722
	5944	5819
	5967	5843
	5977	5935
		5965
		5988
³ H ₄	12612	12515
	12619	12574
	12648	12668
	12765	12742
	12826	12784
	12841	12872
	12938	12885
		12910
		12951

Table A-1 Energy levels of thulium in the crystalline hosts YLF and YAP

For YAP the maximum number of Stark levels in an energy level manifold is given by $2J+1$, hence the number is 13 for the ³H₆ manifold and 9 for both the ³F₄ and ³H₄ manifolds. The corresponding numbers for YLF are 11 and 7. Inspection of the tabulated levels above reveals that there is one missing Stark level in the ground state manifold of thulium in YAP. This is assumed to mean that one of the listed levels is in fact doubly degenerate, but no information is available to determine which level.

Manifold	Host Lattice	
	YLF ⁴	YAP ¹
⁵ I ₈	0	0
	7	6
	23	37
	48	48
	56	58
	72	71
	217	100
	270	126
	276	137
	283	193
	290	211
	303*	222
	315*	289
		327
		425
		474*
		499
⁵ I ₇	5153*	5186*
	5157*	5187*
	5164*	5222
	5185	5253
	5207	5255
	5229	5264
	5233	5266
	5291	5268
	5293	5280
	5293	5288
		5318
		5326
		5337
		5346
		5357

Table A-2 Energy levels of holmium in the crystalline hosts YLF and YAP

For YAP the maximum number of Stark levels in an energy level manifold is given by $2J+1$, hence the number is 15 for the ⁵I₇ manifold and 17 for the ⁵I₈ manifold. The corresponding numbers for YLF are 11 and 13. Inspection of the tabulated levels above reveals that there is one missing level in the ⁵I₇ energy level manifold of holmium in YLF. This is assumed to mean that one of the listed levels is in fact doubly degenerate, but no information is available to determine which level.

References

- [1] A. A. Kaminskii, *'Laser crystals'*, 2nd edition, Berlin : Springer-Verlag (1990)
- [2] H. P. Jenssen, A. Linz, R. P. Leavitt, C. A. Morrison & D.E. Wortman, *'Analysis of the optical spectrum of Tm³⁺ in LiYF₄'*, Phys. Rev. B, vol. 11, no. 1, 92 (1975)
- [3] J. M. O'Hare & V. L. Donlan, *'Crystal field determination for trivalent thulium in yttrium orthoaluminate'*, Phys. Rev. B, vol. 14, no. 9, 3732 (1976)
- [4] N. Karayianis, D. E. Wortman & H. P. Jenssen, *'Analysis of the optical spectrum of Ho³⁺ in LiYF₄'*, Phys. Chem. Solids, vol. 37, no. 7, 675 (1976)